DEPARTMENT OF THE INTERIOR
U.S. GEOLOGICAL SURVEY

Tectonic History of the Northern Nabitah Fault Zone, Arabian Shield, Kingdom of Saudi Arabia

James E. Quick and Paul S. Bosch

Open-File Report 90- 316

Report prepared by the U.S. Geological Survey in cooperation with the Deputy Ministry for Mineral Resources, Saudi Arabia

This report is preliminary and has not been reviewed for conformity with U.S. Geological Survey editorial standards and stratigraphic nomenclature.

1/ USGS, Denver, CO

1990

CONTENTS

Page

ABSTRACT..... 1

INTRODUCTION..... 2

GEOLOGY OF SELECTED AREAS..... 2
- Bi'r Tuluhah..... 2
  - Overview..... 5
  - Hulayfah group..... 5
  - Shammar group..... 6
  - Fault-zone rocks 6
    - Metasedimentary rocks..... 6
    - Silicic volcanic rocks..... 6
    - Metabasalt..... 6
    - Amphibolite..... 6
    - Ultramafic rocks, undivided..... 7
    - Marble 8
    - Cumulus gabbro..... 8
    - Quartz diorite and microdiorite. 8
    - Granitic rocks and late gabbro.. 8
  - Nabitah faults..... 8
  - Najd faults..... 8
  - Folding..... 9
  - Lithologic sequence..... 11
  - Geochronology..... 11
  - Synthesis..... 12
- Bi'r Nifazi..... 12
  - Overview..... 12
  - Interlayered ultramafic and mafic rocks..... 13
  - Gabbro..... 13
  - Hypabyssal intrusive rocks..... 13
  - Interbedded pillow basalt and lahar deposits..... 14
  - Jabal Mardah gossans..... 14
  - Interbedded basaltic flows and flow breccia..... 15
  - Interbedded wacke, shale, and tuff.. 15
  - Undivided volcanic rocks..... 15
  - Dacite..... 15
  - Basalt..... 15
  - Carbonate-replaced basalt, diabase, and gabbro..... 16
  - Upper Proterozoic intrusive rocks... 16
  - Structure..... 16
  - Geochronology..... 16
  - Synthesis..... 16
- Wadi Khadra..... 17
  - Overview..... 17
  - Undivided ultramafic tectonite..... 17
  - Interlayered gabbro & peridotite.... 18
  - Gabbro..... 18
  - Basalt and diabase..... 18
  - Metabasalt..... 18
  - Breccia..... 18
  - Wadi Khadra phyllonite (mylonite)... 19
  - Granodiorite..... 19
  - Faulting..... 19
  - Folding..... 19
  - Synthesis..... 24
- Jabal al Qub..... 24
  - Overview..... 26
  - Ultramafic rocks..... 26
  - Amphibolite..... 27
  - Metadiorite..... 27
  - Granodiorite and Rharaba complex.... 28
  - Volcanic and sedimentary rocks..... 28
  - Tonalite and undivided granite..... 29
  - Faulting..... 29
  - Folding..... 29
  - Fault kinematics..... 30
  - Geochronology..... 31
  - Synthesis..... 31

GEOCHEMISTRY..... 31
- Geochemical techniques..... 31
- Geochemical results..... 32
  - Petrogenesis and immobile elements.. 32
  - Darb Zubaydah ophiolite..... 32
  - Bi'r Tuluhah..... 35
  - Spinel analyses..... 38

REGIONAL SYNTHESIS..... 42
- Terranes..... 42
- Nabitah faulting..... 42
- Afif terrane..... 42
  - Nabitah volcanic arc..... 42
  - Rharaba complex..... 42
  - Opiolitic rocks of the western Afif terrane..... 43
  - Amphibolite of the western Afif terrane..... 43
  - Hijaz terrane..... 44
  - Asir terrane..... 44
  - Bi'r Umq suture..... 44
  - Offset of the Asir terrane and the Bi'r Umq suture..... 44

TECTONIC MODEL..... 45
Sumatra..... 45
Kuril Arc..... 45
California..... 46
Applications to Saudi Arabia..... 46

IMPLICATIONS FOR GOLD MINERALIZATION..... 50
Nabitah Zone..... 50
Foothills Fault Zone and the
Mother Lode District..... 51
Conclusions..... 54

DATA STORAGE..... 54

ACKNOWLEDGMENTS..... 55

REFERENCES..... 64

APPENDIX..... 69

ILLUSTRATIONS

[Plates in pocket]

PLATE

1. Geologic map of the Bi'r Tuluhah area.

2. Geologic map of the Hulayfah area.

3. Geologic map of the Bi'r Nafazi area.

4. Geologic map of the Wadi Khadra area.

5. Geologic map of the Jabal al Qub area.

FIGURE

1. Map showing location of Arabian Shield and distribution of major suture zones..... 3

2. Geologic map of the Nuqrah-Mahd adh Dhahab vicinity..... 4

3. Equal-area-projection diagrams showing the orientations of F_1 fold axes and lineations in the Bi'r Tuluhah area organized by lithology..... 9

4. Block diagram showing the shape and orientation of small asymmetric folds in the metatuff unit at Bi'r Tuluhah..... 10

5. Equal-area-projection diagrams showing the orientations of F_2 fold axes and lineations in the Bi'r Tuluhah area organized by lithology..... 11

6. View (from north to south) of the northernmost gossan at Jabal Mardah..... 14

7. An outcrop of polymict breccia in the Wadi Khadrah area..... 20

8. Oblique air photo showing contact between phyllonite and moderately deformed cumulus gabbro and peridotite..... 20

9. Effects of deformation on plagioclase-phyric diabase at Wadi Khadra..... 21

10. Equal-area projection diagrams showing orientations of fold axes and lineations in the Wadi Khadra area..... 22

FIGURE

11. Folded quartz veins on horizontal outcrop surfaces in the Wadi Khadra phyllonite..... 23

12. Outcrop of the Wadi Khadra phyllonite showing F_3 folds..... 25

13. Block diagram of the Wadi Khadra phyllonite..... 26

14. Equal-area-projection diagrams showing orientations of fold axes and lineations in the Jabal al Qub area..... 30

15. AFM diagrams for volcanic rocks and hypabyssal rocks of the Darb Zubaydah ophiolite..... 33

16. Compositional (K_2O-SiO_2) diagrams for volcanic rocks and hypabyssal rocks of the Darb Zubaudah ophiolite..... 33

17. Compositional (Ti-Zr) diagrams for volcanic rocks and hypabyssal rocks of the Darb Zubaydah ophiolite..... 34

18. Zr-Ti-Y ternary diagrams for volcanic rocks and hypabyssal rocks of the Darb Zubaydah ophiolite..... 35

19. AFM diagrams for rocks of the Bi'r Tuluhah area..... 36

20. Compositional (K_2O-SiO_2) diagrams for rocks of the Bi'r Tuluhah area..... 37

21. Compositional (Tr-Zr) diagrams for rocks of the Bi'r Tuluhah area... 39

22. Zr-Ti-Y ternary diagrams for rocks of the Bi'r Tuluhah area..... 40

23. Plot of Cr-value versus Fe-value for the average compositions of primary spinel in serpentinite samples from the Nabitah fault zone..... 41

24. Maps illustrating the modern tectonic elements of Sumatra and Japan north of Hokkaido..... 47

25. Maps illustrating analogous geologic and tectonic features in California and the Arabian Shield..... 48

26. Simplified geologic maps of the northern Sierra Nevada mountains showing the Foothills Fault Zone, the Melones Fault, gold mines, and major lithologies..... 53

TABLES

TABLE

1. Characteristics of ancient gold mines in the vicinity of the Nabitah fault zone..... 56

2. Au-Ag geochemical values for selected samples from ancient mines of the Nabitah fault zone..... 62

TECTONIC HISTORY OF THE NORTHERN NABITAH FAULT ZONE, ARABIAN SHIELD, KINGDOM OF SAUDI ARABIA

By

JAMES E. QUICK AND PAUL S. BOSCH

ABSTRACT

Geologic mapping combined with structural, petrographic, and geochemical investigations were used to evaluate the motion and paleogeographic setting of the northern Nabitah fault zone. The orientation and asymmetry of small structures in three areas along the fault zone suggest that motion was primarily left-lateral strike slip. East of the fault zone, the Afif terrane is underlain by a north-trending granodioritic batholith that is interpreted to be the plutonic core of a volcanic arc (herein named the Nabitah arc) whose activity was coincident with Nabitah faulting. Available geochronologic data indicate that the Nabitah fault zone and arc were active at 710 Ma and that activity may have continued until about 670 Ma. Relicts of a prebatholithic island-arc ophiolite crop out as roof pendants and septa east of the fault zone. Analysis of petrologic, geochemical, and geochronologic data suggests that these rocks may have formed a terrane older than 800 Ma that was continuous from the Nabitah fault zone to the Nuqrah belt. These rocks may have been moved northward by Nabitah faulting from an original position opposite the Asir terrane.

Scale-model comparisons with Recent and Phanerozoic volcanic arcs suggest that the Nabitah fault zone may have been a transform fault that developed as a result of sinistral oblique subduction east of the Al Amar fault. According to this model, the Abt schist would have formed in an accretionary prism and the Murdama group would have been deposited in a fore-arc basin. Analogs for thrust faults in the northern Arabian Shield are found in modern arcs developed behind oblique subduction zones. The orientations of the Najd faults may reflect initial formation as normal faults in the fore-arc region of such an arc system.

Based on the presence of similar lithologies, similar structure, and analogous tectonic setting, the Mother Lode District in California is reviewed as a model for gold occurrences near the Nabitah fault zone in this report.

INTRODUCTION

This report presents an integrated structural and geochemical study of selected areas located along the northern extension of the Nabitah fault system (Gonzalez, 1974) between lat 23°30'30" and 26°00' N. (fig. 1). Identified by a locus of north-trending, fault-bounded serpentinite bodies, the Nabitah fault system can be traced for more than 900 km along the axis of the Arabian Shield (Schmidt and others, 1978). The Nabitah fault system and an associated belt of foliated grano-dioritic plutonic rocks have been collectively termed the Nabitah suture zone. The observation that this fault system approximates the boundary between two lead-isotopic provinces (Stacey and Stoeser, 1983) has resulted in speculation that it may be a major "suture zone" or plate boundary (Stoeser and others, 1984; Stoeser and Camp, 1984; Stacey and Agar, 1985).

Despite growing awareness that the Nabitah fault system is a significant tectonic element of the Arabian Shield, there is no consensus on its precise role, and it has been variously interpreted as (1) a relic of a west-dipping subduction zone (Stoeser and others, 1984), (2) a relic of an east-dipping subduction zone in the south and a west-dipping subduction zone in the north (Stoeser and Camp, 1984), (3) a relic of a composite of two subduction zones--one east-dipping and the other west-dipping (Stacy and Agar, 1985), and (4) a strike-slip fault (Gonzalez, 1974; Caby, 1982). These hypotheses carry significantly different implications for both the tectonic evolution of the Arabian Shield and the recognition of metallogenic provinces therein. Therefore, the present study was initiated to develop structural and petrochemical evidence to better define the tectonic role of this important fault system.

Palinspastic histories of fault systems can only be determined in the Arabian Shield by detailed mapping and gathering of structural, geochemical, and geochronologic data. Paleomagnetism, which has been used with success to delineate exotic terranes in western North America, is difficult to apply in the Arabian Shield due to regional obliteration of the Precambrian remnant magnetism by a 600-Ma thermal event (Kellogg and Beckmann, 1984). Regional correlation of rocks is hampered by a lack of fossils, and in the absence of tight radiometric age constraints, regional correlations must depend strongly on geochemical and petrographic criteria.

The present study was conducted between January, 1985 and August, 1986. Four areas (fig. 2; pls. 1-5) were mapped at scales ranging from 1:20,000 to 1:50,000 in order to more accurately determine structural relations and tie structural and geochemical data to the regional geology. Two-hundred-fourteen whole-rock analyses were determined (appendix A) and about 500 orientations of fold axes and lineations were measured. Due to the scope of the structural and petrologic information, these data are presented by area. Geochemistry is presented in a single summary section followed by a tectonic synthesis that attempts to tie the different data together. The implications for mineral exploration are discussed in the final section of this report.

GEOLOGY OF SELECTED AREAS

Bi'r Tuluhah

The Bi'r Tuluhah study area (fig. 2; pls. 1 and 2) was mapped during four weeks in the Spring of 1985 and two weeks in the Spring of 1986. The structurally complex area in the center of plate 1 was mapped in detail at a scale of 1:20,000 and compiled at a scale of 1:50,000. The area north of lat 25°45' N. (plate 2) was mapped at 1:50,000 scale and compiled at a scale of 1:100,000. Representative fold axes are shown on plates 1, 2, and 4, and geochemical sample sites appear in plate 2.

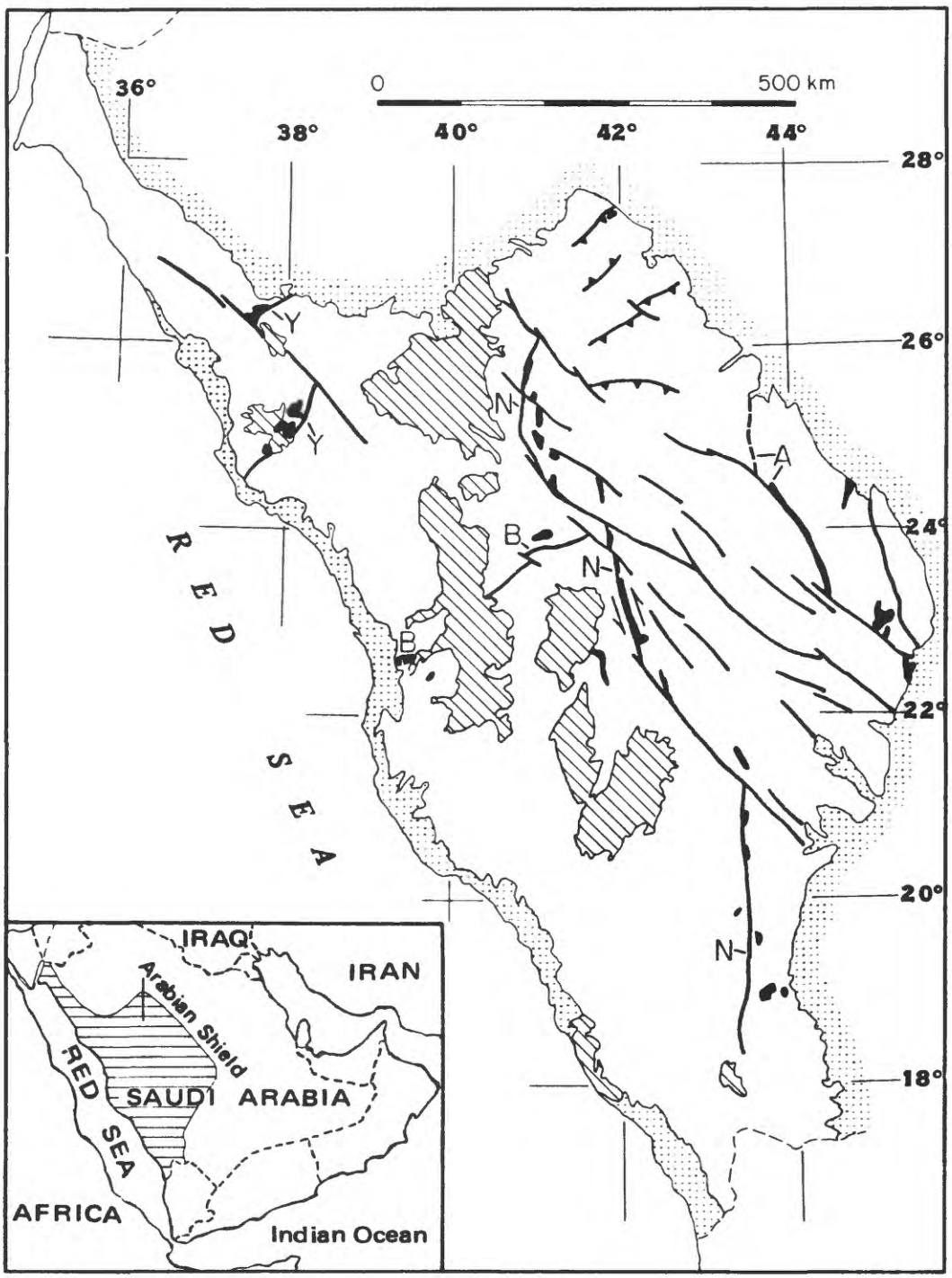

Figure 1--Map showing the location of the Arabian Shield (hachured area on inset index map) and the distribution of major suture zones: Y, Yanbu suture; B, Bi'r Umq Suture; N, Nabitah suture; and A, Al Amar suture. Stippled pattern indicates cover rocks; Quaternary-Tertiary basalts are indicated by hachured diagonal pattern; and ophiolites shown as black spots.

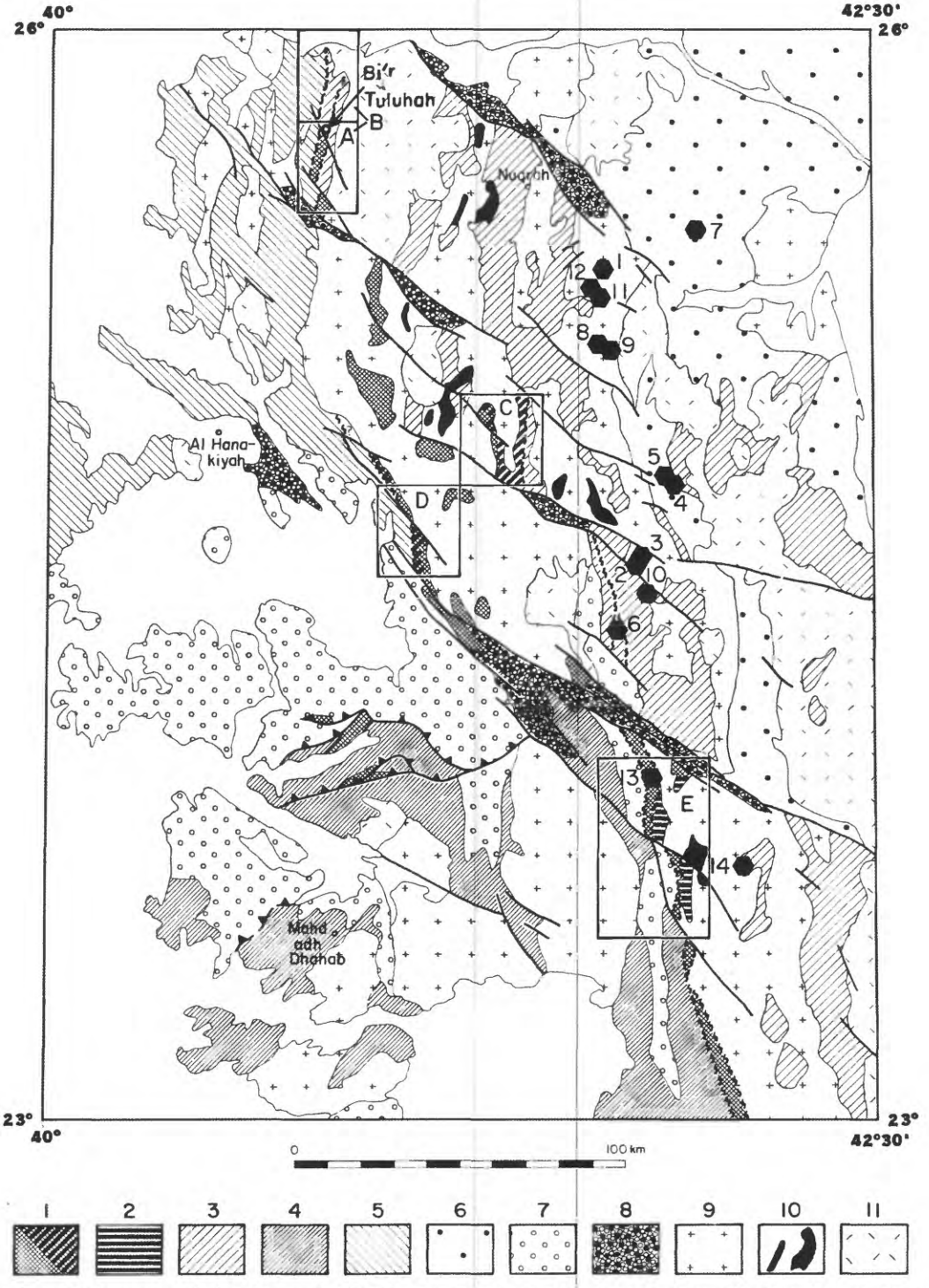

Figure 2--Geologic map of the Nuqrah-Mahd adh Dhahab vicinity showing distribution of precambrian rocks (patterns) and areas covered by Plates 1-5 (areas A-E in figure), and locations of gold prospects (solid hexagons) discussed in Table 1. Plates 1-5 are as follows: area A, plate 1, Bi'r Tuluhah; area B, plate 2, Hulayfah; area C, plate 3, Bi'r Nifazi; area D, plate 4, Wadi Khadra; and area E, plate 5, Jabal al Qub. Geology is modified from Johnson (1983) based on the present study. Patterns are: (1) ophiolitic serpentinite (grid) and gabbro/diabase (grid + inclined bars); (2) amphibolite; (3) volcanic and sedimentary rocks of the Nuqrah belt; (4) volcanic and sedimentary rocks older than 800 Ma; (5) volcanic and sedimentary rocks younger than 800 Ma; (6) Murdama group; (7) sedimentary and volcanic rocks of the Furayh group; (8) sedimentary and volcanic rocks of the Jibalah group; (9) granodiotite, tonalite and diorite; (10) Rharaba complex; (11) undivided granitic rocks. Faults are depicted as follows: wavy lines, (~~), Nabitah faults; heavy lines, (——), Najd faults; and barbed lines, (▲▲), north-dipping thrust faults of the Bi'r Umq suture.

Relationships depicted in plates 1 and 2 are based on this work, although parts or all of the area were mapped previously by other investigators (Delfour, 1977; Le Metour and others, 1983; Kattan, 1983).

Overview

The western third of the Bi'r Tuluhah area is underlain by volcanic and sedimentary rocks of the Hulayfah group (Delfour, 1977), and the eastern third of the area is underlain by alkali granite and volcanic rocks of the Shammar group (Brown and others, 1963; Delfour, 1977). These units are resistant to weathering and form steep-sided mountains. The central third of the study area is a broad, north-northeast-trending valley underlain by tectonic slivers of serpentinite, amphibolite, metabasalt, metatuff, and metasedimentary rocks collectively referred to in this report as "fault-zone rocks" because they are juxtaposed against each other and the Hulayfah group by a swarm of north-northeast-trending strands of the Nabitah fault system. Delfour (1977) assigned the serpentinite, amphibolite, and some of the metabasalt to the Urd ophiolite. All of the fault-zone rocks have been more intensely recrystallized, faulted, and deformed relative to the Hulayfah and Shammar-group rocks. Diorite and quartz diorite intrude the fault-zone rocks, but intrusion appears to have been coincident with Nabitah faulting. Granitic rocks intrude most of the lithologies listed above and crosscut the Nabitah fault system. These intrusive rocks are in turn crosscut by a northwest-trending set of faults recognized as part of the Najd fault system (Delfour, 1977).

Hulayfah Group

Rocks of the Hulayfah group (Delfour, 1977) crop out within the map area in a north-north-east-striking, west-facing steeply dipping (>60°) homocline. In this report, it is subdivided into informal lithologic units that, in order of stratigraphic succession, are composed of basaltic breccia (hb), poorly sorted sandstone (hw), andesitic tuff (ht), and undivided basalt and andesite (hu). Lenses of blue marble are common, but not confined to any single stratigraphic horizon within the Hulayfah group.

The basaltic breccia is composed of abundant subrounded clasts of vesicular basalt that are as much as 0.3 m across and contained in a very fine grained lavender tuffaceous matrix. Bedding is massive, but the attitude is inferred from the preferred orientation of flattened clasts and ing-plane foliation in the matrix. The basalt clasts are fine-grained subophitic intergrowths; the plagioclase grains are fresh, but matrix pyroxenes are altered to chlorite and green amphibole. Clinopyroxene phenocrysts are partially to completely altered to opaque minerals and calcite. Vesicles are filled with calcite.

The poorly sorted sandstone is composed of thick-bedded volcanic wacke with subrounded to subangular mineral and lithic fragments mixed with a poorly sorted tuff-rich matrix. This rock type grades laterally and vertically into tuff. Cross-bedding indicates that the section is oriented upward to the west. Clasts are angular to subangular and rarely exceed 1 cm in diameter. Plagioclase forms the most abundant mineral clasts; clasts of green-brown amphibole and opaque minerals are locally abundant. Lithic clasts are subrounded to subangular fragments of light-gray andesite, dark gray-green vesicular basalt and aphanitic basalt, fine-grained recrystallized hornblende-gabbro, and sandstone. Plagioclase grains are moderately saussuritized and the tuffaceous matrix is recrystallized to a fine-grained intergrowth of chlorite and feldspar.

The andesitic tuff is composed of about 5 percent angular fragments of light-gray andesite contained in dark-gray matrix. Both the fragments and the matrix are composed of abundant (40-50 percent) plagioclase crystals set in an aphanitic matrix. Locally, the rock is a true crystal tuff, composed of more than 70 percent plagioclase crystals and less than 30 percent interstitial tuff. The plagioclase crystals range from being completely unaltered to being about 50 percent saussuritized. The tuffaceous matrix is replaced by an intergrowth of chlorite, feldspar, and opaque minerals. Locally, the rocks are intensely epidotized along narrow northeast-trending zones.

The undivided basalt and andesite map unit is composed of massively bedded medium- to dark-gray volcanic flows. Bedding is indistinct, except where interbedded sedimentary rocks crop out. Flow breccia crops out locally, but pillow structures are completely absent. Some flows contain calcite-filled vesicles. Plagioclase forms the most abundant phenocrysts, followed by equant

opaque minerals and clinopyroxene. Most flows are epitaxic with large (0.3-2 cm), blocky plagioclase phenocrysts set in a matrix of oriented plagioclase laths, equant opaque minerals, and a fine-grained groundmass of secondary minerals. Clinopyroxene-phyric flows tend to have subordinate amounts of plagioclase phenocrysts. Interstitial glass and groundmass minerals are completely replaced by a fine-grained intergrowth of chlorite, actinolite, and feldspar. By contrast, phenocrysts and smaller laths of plagioclase are remarkably fresh, alteration being restricted to saussuritization along fractures. Clinopyroxene phenocrysts are partially uralitized in most rocks but relics are present within green amphibole pseudomorphs; pyroxene is virtually unaltered in about 20 percent of the pyroxene-phyric rocks.

Shammar Group

The Shammar group is mapped as three informal lithologic units. Conglomerate (cgl) overlying a basal basalt unit (b) is poorly indurated, crops out on low hills, and is stratigraphically the lowest unit. It is composed of rounded clasts (1-50 cm) of mostly hypabyssal and plutonic rocks of intermediate to granitic composition in a matrix of poorly sorted sandstone. The clast lithologies are hornblende-quartz diorite, alkali-feldspar granite, syenogranite, microdiorite, granophyre, diabase, and minor granodiorite. The conglomerate is overlain by red-weathering rhyolitic volcanic rocks (sv). Although the base of the Shammar group is not exposed, the areal extent of the conglomerate suggests that it is a basal conglomerate overlying a major unconformity. Deformation in the conglomerate and volcanic rocks is limited to gentle homoclinal tilting to the east.

Fault-Zone Rocks

Metasedimentary Rocks--Metawacke (mw) crops out northeast of Bi'r Tuluhah, where it overlies metabasalt. It is composed of interbedded volcanogenic sandstone, shale, and blue marble. The sandstone is poorly sorted and contains fragments of volcanic rock partly derived from the underlying basalt.

Silicic Volcanic Rocks--This unit (mt) is composed of interbedded felsic tuff and minor basalt. All of the rocks are foliated and, in many places, lineated. Quartz phenocrysts and volcanic lithic clasts are locally abundant in the tuff, and albite forms phenocrysts in about 10 percent of the rocks. These clasts and phenocrysts are flattened and rotated parallel to the foliation. The rocks are significantly more deformed and recrystallized than those of the Hulayfah or Shammar groups. Quartz phenocrysts are highly deformed with undulatory extinction in the cores and mosaic-textured rims. The groundmass is recrystallized to a fine-grained intergrowth of quartz, feldspar, muscovite, epidote, and calcite. Interbedded basalt is completely recrystallized to an intergrowth of acicular actinolite, equant opaque minerals, albite, chlorite, and epidote.

Metabasalt--The metabasalt (mb) is composed of massively bedded, gray-green aphanitic basalt interbedded with minor amounts of fine-grained sandstone and keratophyre. The unit has a distinctive topographic expression, typically underlying long, low northeast-trending ridges. The rocks are highly fractured and cut by an anastomosing foliation that is present on ridge flanks but is less well developed or absent near ridge crests. Lineation and small folds are present locally on ridge flanks. The rocks are devoid of phenocrysts. Quartz-filled vesicles are present in some rocks. Pillow structures are preserved locally but in most places intense fracturing of the rock obscures them. Recrystallization is more pronounced than in the rocks of the Hulayfah and Shammar groups. Although relics of primary intersertal textures are preserved in most rocks, plagioclase laths are highly saussuritized and primary pyroxene has been completely uralitized. Calcite- and zoisite-filled veins are ubiquitous. On the microscopic scale, the foliation is defined by anastomosing ribbons of crushed plagioclase and uralite, flattened vesicles, and chlorite-filled interstices. Lensoidal relics between these ribbons preserve an undeformed intersertal texture and spherical vesicles. Therefore, the foliation appears to be a localized cataclastic feature rather than a product of regional metamorphism.

Amphibolite--Amphibolite (a) is poorly exposed and typically confined to valley floors. The rock is black weathering and bimodal in grain size. Fine-grained (<0.5 mm) amphibolite is schistose, folded, and lineated. Coarse-grained (>1 mm) bolite is massive to weakly gneissic; folds and lineation are locally present but indistinct. Sparse relics with

igneous textures and mineralogy indicate that the protolith of the coarse-grained amphibolite was gabbro and diabase. The transition between the coarse- and fine-grained amphibolites is abrupt but difficult to delineate due to poor exposure. Coarse-grained amphibolite is typically sandwiched between serpentinite to the west and fine-grained amphibolite to the east.

The maximum grade of metamorphism was at least epidote-amphibolite. The primary metamorphic minerals of both types of amphibolite are plagioclase, hornblende, ± epidote, quartz, opaque minerals, and, in some rocks, minor biotite. In the coarse-grained amphibolite, a weak foliation is defined locally by the orientation and tration of euhedral amphibole grains. Interstices between amphibole grains are filled with a mosaic of smaller grains of plagioclase and other minerals. The composition of plagioclase is uniform within individual samples but ranges from An_{23} to An_{65} from sample to sample. The presence of labradorite and bytownite is consistent with, but does not require, almandine-amphibolite-grade metamorphism. A previous report (Le Metour and others, 1983), which mentions the presence of garnet in these rocks, is not substantiated by this study.

The primary metamorphic mineralogy and texture have been affected by at least one major deformational event at temperatures lower than epidote-amphibolite facies. The effects are not uniform and some rocks show no evidence of recrystallization or deformation. In moderately affected rocks, the primary metamorphic assemblage is cut by anastomosing bands of crushed primary minerals set in a mosaic of extremely fine-grained plagioclase, quartz, and chlorite. The fine-grained amphibolites appear to be the result of even more extreme cataclasis. These rocks are mostly composed of a very fine-grained, foliated intergrowth of plagioclase, quartz, chlorite, and opaque minerals, but locally contain deformed amphibole porphyroclasts, rock fragments, and lenses that preserve coarse-grained primary metamorphic mineralogy and texture.

Ultramafic rocks, undivided--Ultramafic rocks (un) are composed of massive to foliated serpentinite. Unfoliated serpentinite, which preserves relict primary texture, occurs as lenses within highly foliated serpentinite. These lenses range from less than a meter to hundreds of meters in size. Chromium-spinel is the only surviving primary mineral. It occurs in most rocks as randomly distributed equant to euhedral grains and does not define the classic spinel foliation of mantle tectonites. Locally, however, a poorly developed foliation is defined by flattened spinel grains and trails of spinels. Chromium-spinel rims are replaced by magnetite, but cores preserve primary chromium-spinel compositions. Pyroxene and olivine are completely replaced by serpentine, magnetite, minor talc, and calcite. X-ray diffractometer analysis indicates that the serpentine polymorph is lizardite.

Complete serpentinization in these rocks prevents unequivocal identification of the primary lithologies. In many places, serpentinized dunite weathers to a buff color. Serpentinized pyroxene-bearing peridotite tends to weather dark brown to dark green, but the mineralogy of the primary pyroxenes cannot be determined with certainty. Therefore, in the absence of clear cumulus textures, it is uncertain if the protoliths of these rocks were mantle tectonites or ultramafic cumulates. The general lack of a well-developed, pervasive spinel foliation suggests the latter origin, and the local poorly developed spinel foliation could be explained by the deformation in a deep crustal environment. Indeed, foliation is locally developed in the cumulus gabbro of the Troodos ophiolite (George, 1978). Le Metour and others (1983) divided the ultramafic rocks into subequal amounts of ultramafic cumulate and mantle tectonite. Although both may be present, the uncertainties mentioned above and the deformation of the serpentinite make subdivision tentative at best.

The serpentinite is cut by dikes of diabase, gabbro, plagiogranite, and diorite. These dikes are disrupted and recrystallized to various degrees, indicating that they were emplaced over a significant span of time. Diabase and gabbro dikes crop out as discontinuous trails of boudins with a moderately to well-developed black-wall reaction zone that formed during serpentinization of the peridotite wall rocks. The interiors of some preserve primary igneous mineralogy, but others are completely recrystallized to rodingite. Compared to the diabase and gabbro dikes, the plagiogranite dikes are less boudined, surrounded by thinner black-wall reaction zones, and preserve more primary mineralogy. Diorite dikes are undeformed and show little evidence of black-wall

reaction or rodingitization, suggesting that they were emplaced after serpentinization of the peridotite wall rocks was virtually complete. The range in deformation and alteration of the dikes suggests that dike emplacement and presumably volcanism overlapped with the deformation and serpentinization of the peridotite.

The overall appearance of the disrupted dikes in serpentinite is suggestive of a melange. Unlike a true accretionary melange, however, there are no exotic blocks and no petrologic evidence of high-pressure metamorphism, and the boudinage is most intense at the margins of the ultramafic outcrops where the serpentinite is highly "foliated and folded".

Marble--Fault-bounded slivers of marble are abundant near Bi'r Tuluhah and along the eastern contact of the Hulayfah group. Chromium-spinel grains and serpentinite fragments are present in the northwest-trending sliver located northwest of Bi'r Nifazi. These features suggest that this particular marble is actually listwaenite (carbonate-replaced peridotite). However, chromium-spinel and serpentinite fragments are not present in the other slivers. Furthermore, some of the slivers are bedded. These two observations suggest that most of the marble slivers are sedimentary in origin rather than formed by carbonate replacement of peridotite.

Cumulus gabbro--Slivers of layered gabbro (cg) are faulted into the serpentinite southwest of Bi'r Tuluhah. The primary mineralogy is clinopyroxene, magmatic amphibole, olivine, plagioclase, and opaque minerals. Although not observed in the present investigation, orthopyroxene-bearing assemblages were reported by Le Metour and others (1983). Pyroxene-rich rocks exhibit good cumulus texture with interstices between tabular pyroxene filled with olivine and plagioclase. Alteration of the primary mineralogy is extensive. Plagioclase is highly saussuritized, pyroxene and hornblende are replaced by actinolite, and olivine is replaced by serpentine.

Quartz diorite and microdiorite--A small quartz-diorite (qd) pluton south of Bi'r Tuluhah contains xenoliths of amphibolite. The quartz-diorite pluton is medium grained, undeformed in most places, and appears to be the source of fine-grained diorite dikes that intrude serpentinite. Similar microdiorite (d) forms dikes intruded along the Nabitah faults. The interiors of these dikes are undeformed and contain relatively unaltered igneous texture and mineralogy. Locally, the diorite clearly intrudes adjacent rocks, but in many places the contact is sheared. Similarly, the quartz-diorite pluton crosscuts several north-trending faults, but a small stock of quartz diorite about 2 km to the north is crosscut by a north-trending fault and is pervasively foliated. These relations suggest that quartz diorite and diorite emplacement chronologically overlapped Nabitah faulting.

Granitic rocks and late gabbro--Fine- to medium-grained alkali granite (ga), granophyre (gph), and undivided granite (g) intrude all of the lithologies listed above, and gabbro stocks and dikes in the eastern Bi'r Tuluhah area intrude the Shammar group. The intrusions cut Nabitah faults, but are offset by Najd faults.

Nabitah Faults

The central third of the Bi'r Tuluhah area may be thought of as a collage of tectonic slivers that are juxtaposed by strands of the Nabitah fault system. Outcrop patterns in plates 1 and 2 suggest that rock distributions are controlled by north-northeast-trending Nabitah faults. Contacts between the Hulayfah group, serpentinite, cumulus gabbro, amphibolite, metabasalt, and metatuff are invariably sheared and locally intruded by fine-grained diorite. Cataclasis is most intense and foliation best developed at the edges of the tectonic slivers; both decrease toward the slivers' interior. Therefore, although displacements cannot be demonstrated, the contacts are clearly tectonic. The attitudes of cataclastic foliation and fault traces are subvertical (dip >70°) in most places. Collectively, the different strands of the Nabitah fault system define a fault zone that is about 7 km wide.

Najd Faults

The Bi'r Tuluhah area is cut by several northwest-trending Najd faults. Displacements of the Hulayfah group rocks, serpentinite, diorite, and quartz diorite suggest that movement on these faults involved a left-lateral component. The intersections of the Najd faults and the Nabitah faults are not exposed but differences in age relative to granitic intrusions and left-lateral offsets

of the Nabitah faults by the Najd faults suggest that the two fault orientations are separate systems and not splays or conjugates of a single fault system.

Folding

The folding history of the rocks of the Bi'r Tuluhah area is complex and intimately tied to the faulting history. Two fold orientations are recognized, F_1 and F_2, which may represent pre-Nabitah- and Nabitah-age events, respectively.

F_1 folds (fig. 3) are defined by deformed bedding. These folds typically have subhorizontal, northeast-trending axes and range from a few centimeters to hundreds of meters in amplitude. A lineation locally parallels the fold axes. F_1 folds are found in the interiors of the lithologic slivers and are scarce near the Nabitah faults. Two kilometers northeast of Bi'r Tuluhah, a large F_1 anticline is truncated by a Nabitah fault, suggesting that the F_1 event predated Nabitah faulting. Southeast of Bi'r Tuluhah, a strong asymmetry is developed in F_1 folds in the metatuff unit (fig. 4). The sense of asymmetry and associated boudinage suggests that overthrusting from the west to the east may have occurred, at least locally, during the F_1 event.

F_2 folds (fig. 5) are defined by deformed foliation. These folds typically have steeply dipping axes and amplitudes on the order of centimeters to several meters. A well-developed lineation typically parallels F_2 fold axes. Unlike F_1, F_2 folds are most abundant near Nabitah faults where they deform foliated and cataclastic rocks. This suggests that F_2 folds were produced during Nabitah faulting. The steep plunge of F_2 fold axes and lineations suggests that the motion on the Nabitah faults in this area was primarily strike slip, and well-developed drag folds in foliation along both east and west margins of the large serpentinite body southeast of Bi'r Tuluhah suggest that the motion was left-lateral.

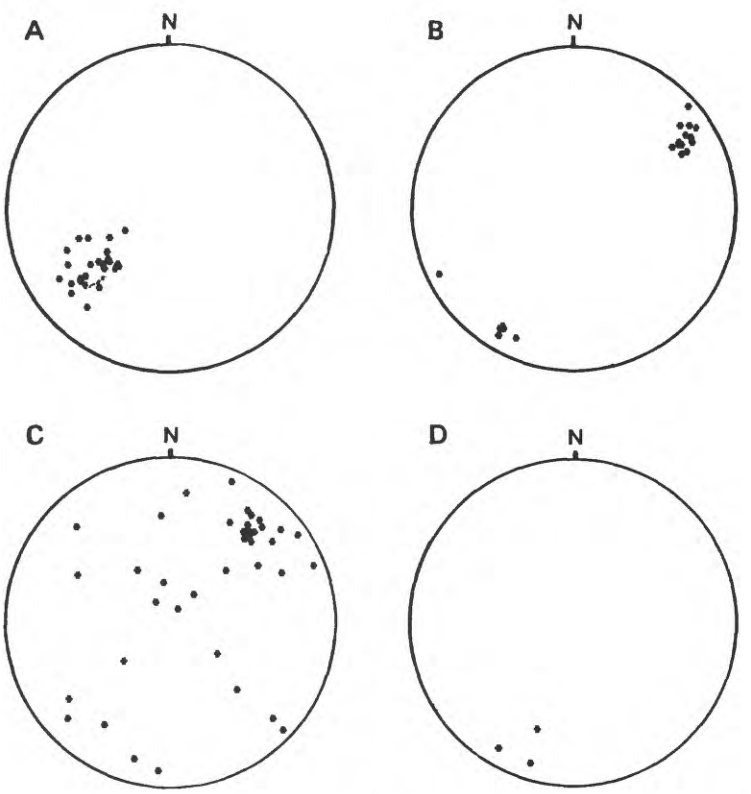

Figure 3—Equal-area-projection diagrams showing the orientations of F_1 fold axes and lineations in the Bi'r Tuluhah area organized by lithology: (A) metasedimentary rocks, (B) metatuff, (C) coarse-grained, and amphibolite, (D) serpentinite.

Several lines of evidence suggest that F_2 folding was produced by a significantly younger deformational event than that which produced F_1 folding: 1) F_1 folds appear to be cut by Nabitah faults and F_2 folds appear to be genetically related to Nabitah faults; 2) F_1 folding is recognized in bedding whereas F_2 folding is recognized in foliation that cuts bedding, and 3) one example of an F_1 fold that is deformed by F_2 was observed in the fine-grained amphibolite.

Fold orientations in the coarse-grained amphibolite are somewhat problematic. The orientation of fold axes (fig. 3C) ranges from subvertical to subhorizontal but no simple relationship with the Nabitah faults is evident. In fact, most of the subhorizontal fold axes are located near fault contacts with the serpentinite. Perhaps strain was concentrated in the less-competent serpentinite during Nabitah faulting so that older structures were preserved in the coarse-grained amphibolite. The fine-grained amphibolite was apparently produced by cataclasis of the coarse-grained amphibolite during Nabitah faulting and, consequently, contains abundant, steeply plunging F_2 folds but preserves little or no evidence of folding along subhorizontal axes remains (fig. 5D).

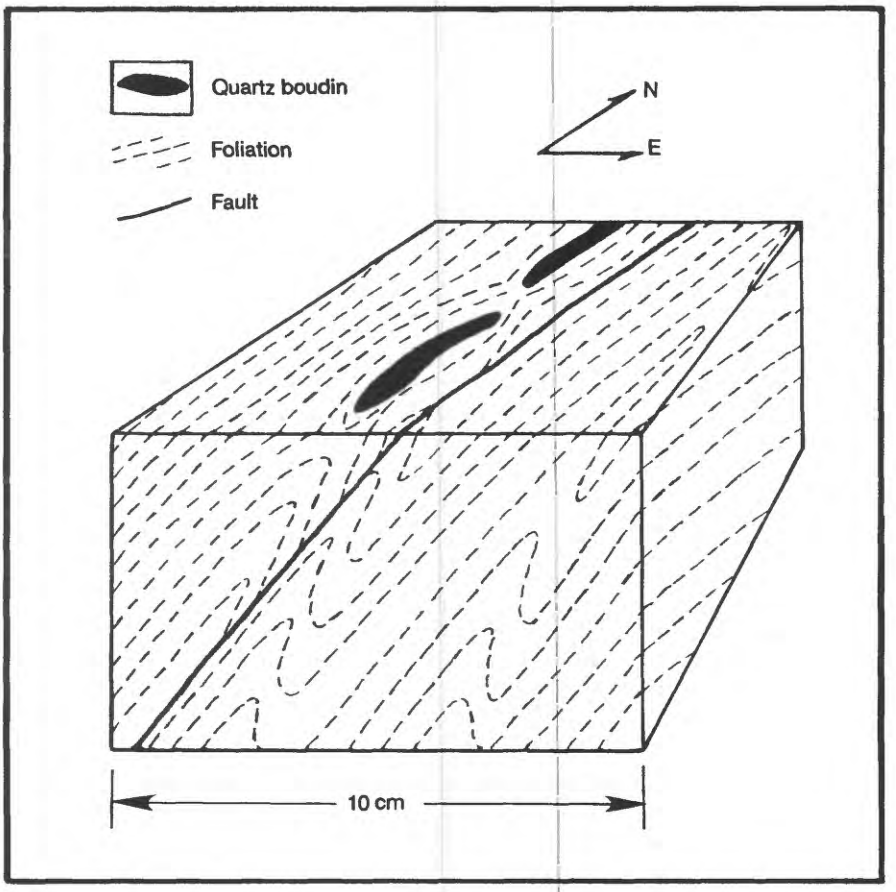

Figure 4—Block diagram showing the shape and orientation of small asymmetric folds in the metatuff unit at Bi'r Tuluhah.

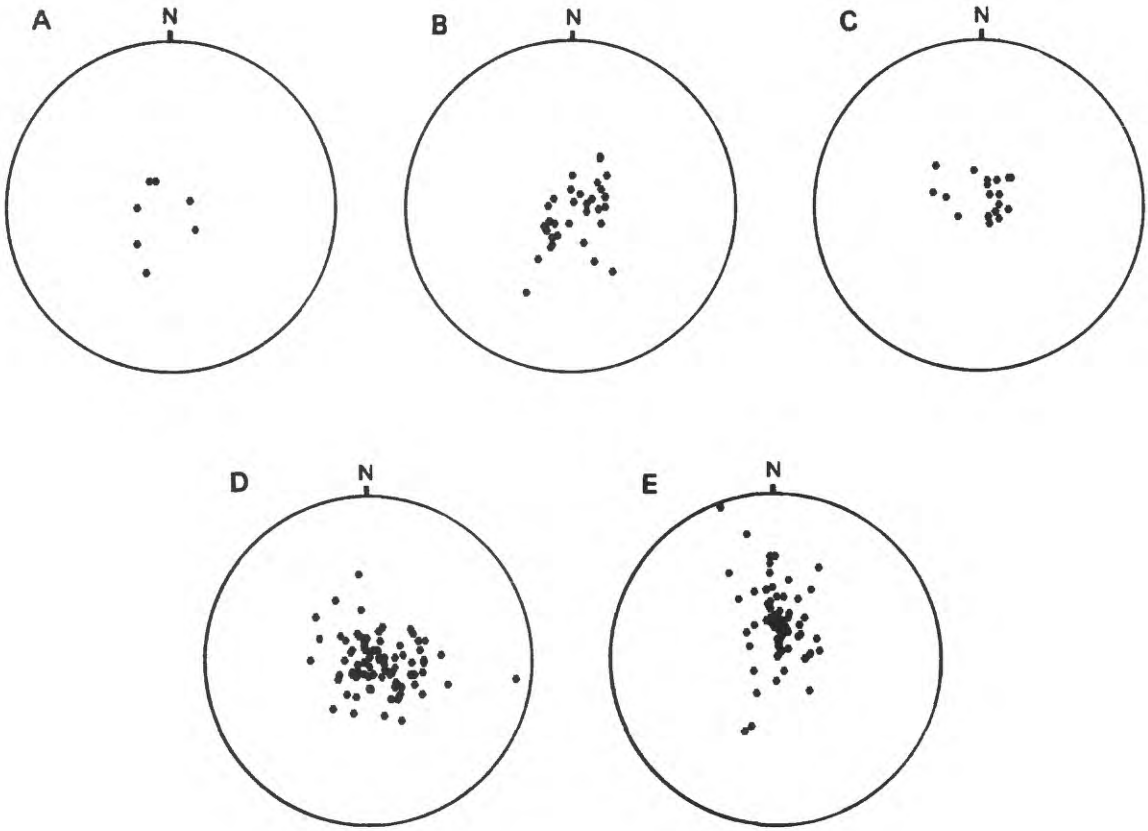

Figure 5—Equal-area-projection diagrams showing the orientations of F_2 fold axes and lineations in the Bi'r Tuluhah area organized by lithology: (A) metasedimentary rocks, (B) metatuff, (C) metabasalt, (D) fine-grained amphibolite, and (E) serpentinite.

Lithologic Sequence

The fault-zone rocks commonly crop out from west to east in the sequence serpentinite, amphibolite, and metabasalt. The contacts between these units are invariably steeply dipping faults and the sequence is disrupted in many places. Nevertheless, the sequence is repeated sufficiently to suggest that there is a decrease in metamorphic grade from west to east away from the serpentinite bodies. This metamorphic gradient has been cited as evidence that the serpentinite was thrust over (obducted) the amphibolite and metabasalt (Pallister and others, 1987). This would be consistent with evidence from F_1 folds suggesting east-west compression and overthrusting from the west. Although this must be considered a strong possibility for the early deformational event in these rocks, it is emphasized that insufficient structural evidence exists to prove it due to the profound effects of later Nabitah faulting.

Geochronology

Four radiometric ages are available from rocks in the Bi'r Tuluhah area. Pallister and others (1987) report U-Pb model ages of 823 ±11 Ma and 847 ±14 Ma for zircons from plagiogranite dikes that intrude the serpentinite south of Bi'r Tuluhah (pls. 1 and 2). These two ages are barely equivalent within the stated precision but do establish a lower age limit for the serpentinite protolith. Extensive boudinage of and blackwall reaction around the plagiogranite dikes indicates that significant serpentinization and deformation occurred after 823/847 Ma. Delfour (1977) interprets K-Ar isotopic data for the Hulayfah group at Jabal at Tin to indicate primary crystallization at 740 Ma (pls. 1 and 2), with isotopic reequilibration at 577-563 Ma. Although the 740-Ma K-Ar age must be considered a minimum age in view of the metamorphic history of the rocks, it is in general agreement with the existence of 800-700-Ma volcanic rocks further to

the east (Camp, 1984). J. S. Stacey (personal commun., 1985) reports a U-Pb age of 710 Ma for zircons from the quartz diorite south of Bi'r Tuluhah (pls. 1 and 2), which is also a minimum age for the formation of the amphibolite, metabasalt, and metatuff and for the initiation of Nabitah faulting. However, this age is not interpreted to mark the end of Nabitah faulting because emplacement of the quartz diorite and fine-grained diorite apparently overlapped with Nabitah faulting in time (see above). Delfour (1977) reports an age of 570 Ma for a small granophyre plug northwest of Bi'r Tuluhah (pl. 2). This age is interpreted to be a lower limit for the cessation of Nabitah faulting because strands of the Nabitah fault system are truncated by granitic rocks of similar composition throughout the area.

Synthesis

Previous interpretations of the structure of the Bi'r Tuluhah area are contradictory. Delfour (1977) assigned the serpentinite, amphibolite, and some of the metabasalt and metasedimentary rocks to the Urd ophiolitic complex. He considered the Hulayfah group to be an island-arc sequence deposited unconformably on the ophiolite, and the gross structure was considered to be a gently plunging, overturned isoclinal antiform with Hulayfah-group rocks cropping out to the east and west of the ophiolite. Le Metour and others (1983) concluded that (1) the protoliths of the serpentinite were ultramafic cumulates, (2) the ultramafic rocks and amphibolite probably represent fragments of subcontinental mantle and deep crustal metamorphic rocks, and (3) the tectonic history was dominated by vertical motion on subvertical faults. Based on observations within and south of the Bi'r Tuluhah area, Caby (1982) concluded that (1) the ultramafic rocks are not part of a classical ophiolite but were hot peridotite diapirs emplaced along vertical Nabitah faults, (2) Nabitah faulting involved a left-lateral, strike-slip component of motion, and (3) that east-west shortening was minor. Pallister and others (1987) model the structure of the Bi'r Tuluhah area as a west-dipping ophiolitic nappe obducted during the closure of an oceanic basin and rotated to high angles during formation of the Nabitah suture.

The conclusion of this report is that the dominant structure of the Bi'r Tuluhah is a 7-km-wide, north-northeast-trending subvertical fault zone that marks the eastern limit of the Hulayfah group. Within the fault zone, tectonic slivers of deformed, medium-grade metamorphic rocks are juxtaposed by strands of the Nabitah fault system. To the east, the fault zone is intruded by granitic and gabbroic rocks and may be unconformably overlain by rocks of the Shammar group. The rocks within the fault zone are of a higher metamorphic grade than the adjacent rocks of the Hulayfah and Shammar groups and preserve evidence of a significantly more complex deformational history. The dominant fold system (F_2) within the fault zone is characterized by subvertical fold axes and proximity to the Nabitah faults. The geometry of these folds suggests that the dominant motion on the Nabitah faults was left-lateral strike slip. A subordinate and older fold system (F_1) within the fault zone is characterized by northeast-trending subhorizontal fold axes and is best preserved in the interiors of the tectonic slivers. The F_1 folding was produced by compression in a northwest-southeast direction accompanied by local and possibly regional overthrusting from the west. The sense of lithologic repetition within the fault zone could have been the result of obduction produced during this compressional event. Geochronologic data suggest that Nabitah faulting began after about 823 Ma and before 710 Ma, and ceased prior to 570 Ma. Crosscutting relationships suggest that emplacement of mafic and intermediate intrusive rocks overlapped with Nabitah faulting. The Nabitah faults were offset by left-lateral strike-slip motion on the Najd faults after 570 Ma.

Bi'r Nifazi

The Bi'r Nifazi area (fig. 2; plate 3) was mapped at a scale of 1:50,000 during four weeks in the late winter, 1986. Earlier geologic maps that include the Bi'r Nifazi area in their coverage were published by Duhamel and Petot (1972) and Delfour (1981).

Overview

The Bi'r Nifazi area is located in the southern Nuqrah belt, which is the most extensive exposure of old (>800 Ma) volcanosedimentary rocks east of the Nabitah fault zone. These rocks are significant for both their mineral potential (Delfour, 1977; Smith and Johnson, 1986) and the

information they convey about the geologic environment before and during Nabitah faulting. The Bi'r Nifazi area is underlain by an east-dipping section of ophiolitic rocks, herein referred to as the Darb Zubaydah ophiolite, that has been extensively intruded by quartz diorite, granodiorite, and granitic rocks. The ophiolite is exposed in an east-dipping homocline that contains, from west to east, serpentinite, gabbro, hypabyssal intrusive rocks, interbedded pillow basalt, lahar deposits, gossan, and interbedded volcanic and sedimentary rocks. This is considered to be the true "stratigraphic sequence" of the ophiolite because preliminary mapping suggests that tectonic disruption was minor.

Interlayered Ultramafic and Mafic Rocks

Mixed ultramafic rocks, gabbro, and diabase crop out along the western limit of the Darb Zubaydah ophiolite. The ultramafic rocks (um) are completely serpentinized dunite and pyroxene-bearing peridotite. Intense alteration makes identification of the protolith difficult. However, a cumulus origin is suggested by (1) the absence of well-developed spinel foliation, (2) the equant, subhedral morphology of spinel grains, (3) the morphology of bastitized pyroxene, and (4) the composition of the spinel grains (see Geochemistry section). Outside the study area, a clear example of ultramafic tectonite with well-developed spinel foliation crops out about 15 km southwest of the Darb Zubaydah serpentinite. These observations suggest that the exposed base of the Darb Zubaydah ophiolite is composed of altered cumulus rock and that the boundary with true mantle assemblages, or "petrologic moho", lies west and southwest of the study area. X-ray diffraction analysis indicates that lizardite is the dominant serpentine polymorph in the Bi'r Nifazi area.

The serpentinite contains north-striking layers of gabbro and diabase that are boudined and enveloped by black-wall reaction zones. The appearance is reminiscent of the deformed dikes in the Bi'r Tuluhah area except that mafic layers comprise 30 to 50 percent of the exposed rock in the Bi'r Nifazi area. It is not possible to state with certainty the relationship between these mafic layers and the serpentinite because of alteration and deformation. The mafic layers may represent deformed dikes and sills or, alternatively, deformed cumulus layers.

Gabbro

Massive, medium-grained gabbro (gb) crops out immediately east of the mixed ultramafic and mafic rocks. The western contact of the gabbro is gradational with the ratio of serpentinite to gabbro increasing to the west. Although this gradation may reflect the magmatic evolution of a single differentiating pluton, it appears to be due, in part, to tectonic interleaving.

The primary mineralogy of the gabbro has been extensively altered. The rocks are cut by quartz- and epidote-filled veins. Pyroxenes(?) are completely replaced by green amphibole, plagioclase is replaced by a very fine-grained mosaic of albite, quartz, and zoisite, and the only surviving primary minerals appear to be equant, euhedral magnetite grains. However, the primary cumulus texture is preserved. Textures and alteration are similar to those in the cumulus gabbros of the Bi'r Tuluhah area.

Hypabyssal Intrusive Rocks

A complex unit (db) mapped as hypabyssal intrusive rocks crops out to the east of the gabbro. This unit is mostly composed of a mixture of fine- to medium-grained intrusive rocks. Volcanic screens between intrusions are present in the eastern half of the unit and become increasingly abundant up section to the east. Observed intrusive rocks are gabbro, diabase, fine-grained diabase, and diorite. Intrusion shapes are difficult to delineate because of intense fracturing of the rocks and poor exposure. However, randomly oriented dike forms are locally visible from the air.

The hypabyssal rocks, like the underlying gabbro, are profoundly altered. In diabase bodies, the pyroxene is completely replaced by blue-green amphibole, plagioclase is completely recrystallized to a very fine-grained mosaic of quartz, feldspar, and zoisite, and the rocks are cut by quartz- and epidote-filled veins. Although primary igneous textures are preserved in most places, amphibole defines a weak foliation in some rocks. This is particularly true near the contact with the underlying gabbro, suggesting that the contact could be tectonic. These foliated rocks are mineralogically similar to the lower grade amphibolites in the Bi'r Tuluhah area. In dioritic rocks, the primary minerals are replaced by sparse

clusters of blue-green amphibole needles set in a very fine grained, mosaic-textured matrix of quartz, feldspar, and opaque minerals. Some dioritic rocks contain highly saussuritized relicts of blocky plagioclase phenocrysts.

Interbedded Pillow Basalt and Lahar Deposits

Interbedded pillow basalt, lahar deposits, minor marble, and volcanic wacke (bl) are faulted against the eastern side of hypabyssal rocks. The pillow basalts are medium gray to green, highly fractured, locally vesicular, and contain abundant pillows. In outcrop, the rock is identical to the pillow basalts of the Bi'r Tuluhah area. The lahar deposits are composed of rounded to angular fragments of volcanic rock and marble in a fine-grained, poorly sorted sandy matrix. The clasts are predominantly basalt and completely matrix supported. The matrix is carbonate rich, foliated, and ranges in grain size from a fine-grained sandstone to a shale. Both the volcanic wacke and lahar deposits decrease in abundance relative to pillow basalt toward the north, suggesting that the source for these sediments was to the south.

The basalts were originally composed of subophitic intergrowths of plagioclase, pyroxene, olivine (?), and opaque minerals. However, the primary mineralogy of the pillow basalt has been obscured by extensive greenschist-facies recrystallization. Plagioclase is highly saussuritized and pyroxene is completely uralitized. The effects of carbonate metasomatism are similar to those observed in metabasalt of the Bi'r Tuluhah area but are locally more intense; in moderately affected rocks, calcite and epidote form veinlets, fill vesicles, and replace patches of the groundmass. The abundance of calcite and epidote increase dramatically near north-northeast trending faults.

Jabal Mardah Gossans

Gossan crops out in the upper third of the interbedded pillow basalt and lahar deposits. They are composed of rusty-red-weathering ironstone and range in size from a few meters

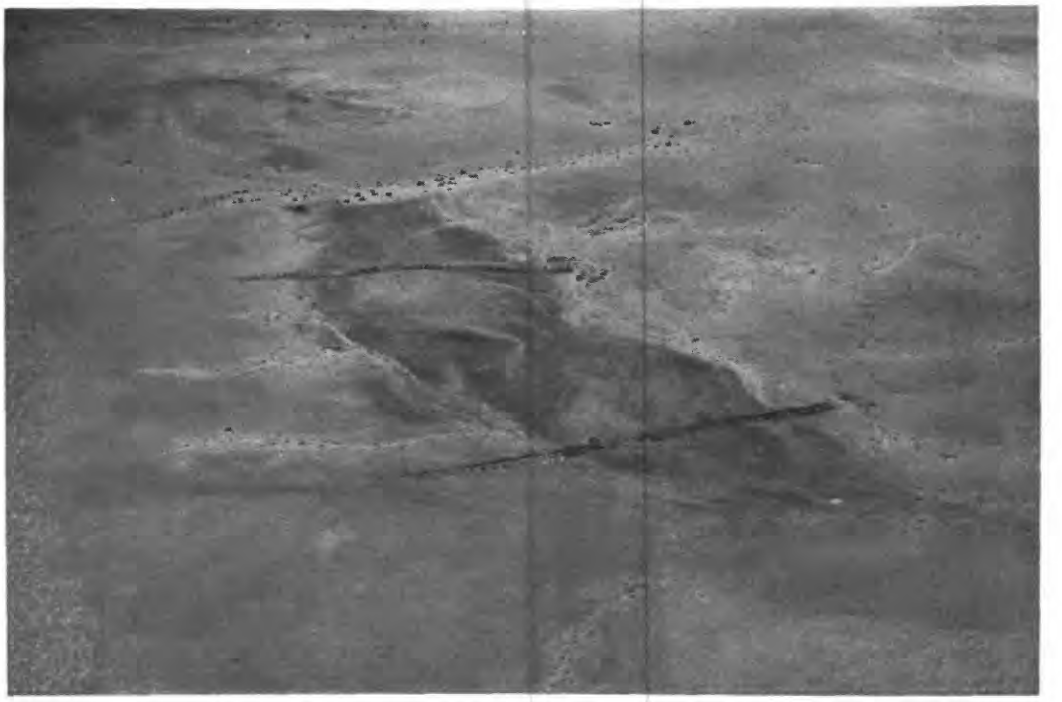

Figure 6--View (from north to south) of the northernmost gossan at Jabal Mardah. The trench in the foreground is approximately 130 m long.

across to 0.4 km long (fig.6). The size of these features suggests that large massive-sulfide deposits are present at depth. Chemical data indicates that some gossans contain horizons with anomalous nickel concentrations (1,000-11,000 ppm), suggesting that associated massive-sulfide deposits may be like the Hadbah ore body (Blain, 1978).

The Jabal Mardah gossans appear to be unrelated to the Nuqrah ore bodies to the north. The Jabal Mardah gossans are nickel rich, whereas mineralization in the Nuqrah area is copper-, lead-, zinc- and gold-rich (Delfour, 1977). The Jabal Mardah gossans are interbedded with pillow basalt and lahar deposits that are located near the base of the volcanosedimentary pile. In contrast, the Nuqrah ore bodies are associated with low-potassium rhyolites that are presumably located high in the volcanosedimentary pile (Shanti, 1985). These differences suggest that there are two types of sulfide deposits in the Nuqrah belt.

Interbedded Basaltic Flows and Flow Breccia

In the south, the stratigraphic horizon of the interbedded pillow basalt and lahar is occupied by a sequence of basaltic flow breccia interbedded with keratophyre, volcanic wacke, basaltic tuff, dacite, andesite, and andesitic breccia (bb). These rocks are deposited directly on hypabyssal diabase and microdiorite. Basaltic flow breccia, the dominant rock type, forms numerous recognizable flow units composed of massive basalt capped by breccia and, locally, basaltic tuff. Vesicles are locally abundant in these rocks but pillows are scarce. Crossbedding in the basaltic tuff indicates that stratigraphic up is toward the east. Interbedded andesite and andesitic breccia contain abundant angular fragments of volcanic rock.

Interbedded Wacke, Shale, and Tuff

A thick sequence of volcanic wacke is in gradational contact with the underlying basaltic-breccia unit. The unit(s) is composed of volcanic wacke and smaller amounts of mudstone, shale, and minor ferruginous marble. These clastic rocks crop out in a wedge that increases in thickness to the north. Graded bedding indicates that stratigraphic up is toward the east.

Undivided Volcanic Rocks

A thick sequence of interbedded volcanic and sedimentary rocks (vu) conformably overlies the pillow basalt and lahar deposits in the north and the volcanic wacke in the south. There is considerable lithologic variation in this unit from north to south. In the north, the rocks are composed of interbedded basalt, fine-grained volcanogenic sandstone, marble, and flows and tuffs that range in composition from andesite to rhyolite. To the south, sedimentary rocks and volcanic breccias become progressively more abundant, and clasts in andesitic tuffs become significantly larger, suggesting that the source area and volcanic center was to the south.

Dacite

Massive dacite (da) crops out within the interbedded volcanic and sedimentary rocks to the north. The dacite is composed of plagioclase phenocrysts, opaque microphenocrysts and fine-grained, biotite-rich segregations in a very fine-grained mosaic-textured groundmass of feldspar, quartz, opaque minerals, and biotite. Plagioclase is strongly saussuritized and biotite appears to be a replacement of the primary mafic minerals. An intrusive origin for this unit cannot be ruled out. However, on the basis of its lenticular shape, it is inferred to have formed as an eruptive dome similar to those extruded late in the evolution of an Aleutian-type volcanic center (Marsh, 1982).

Basalt

Massive basalt (b) interfingers with and overlies the interbedded volcanic and sedimentary rocks to the south; the basalt pinches out to the north. The rocks are massive, pyroxene-phyric basalt and the general absence of plagioclase phenocrysts contrasts with plagioclase-phyric basalts lower in the section. The presence of rounded, cordierite-cummingtonite-bearing xenoliths near the base of the unit suggests that the eruptive vent was nearby. Pillow structures are absent, suggesting that the basalt was deposited subareally.

Carbonate-Replaced Basalt, Diabase, and Gabbro

Carbonate metasomatism is pronounced near north-northeast-trending fault zones. A separate unit (cr) is mapped to indicate areas where replacement of the primary mineralogy by carbonate is extreme. The best example is located along the northern fault contact between the volcanic and hypabyssal rocks. For a distance of 1.5 km, pillow basalt has been almost completely replaced by buff-weathering carbonate minerals. Rounded, pillow-like structures are locally preserved, although the rocks are almost completely replaced by carbonate that contains small (<10 cm) relicts of gray-green basalt.

These replacement zones demonstrate that carbonate-replaced rocks along fault zones need not be listwaenite (carbonate-replaced peridotite). Instead, it is possible that the protolith may have been basaltic in composition.

Upper Proterozoic Intrusive Rocks

Two-pyroxene gabbro (gb2) intrudes the serpentinite and dacite along the western and eastern margins of the ophiolite, respectively. The western margin of the ophiolite is also intruded by a granodiorite batholith (gd). The intrusive nature of this contact is indicated by serpentinite xenoliths in the granodiorite, dikes of granodiorite cutting serpentinite, and fining of grain size in the granodiorite toward the serpentinite. The eastern margin of the ophiolite is extensively intruded by granitic rocks (g) that range in composition from syenogranite to alkali-feldspar granite. The intrusive nature of this contact is indicated by granite dikes cutting volcanic rocks and granite crosscutting structural trends in the volcanic rocks. Plutons of granodiorite and quartz diorite (qd) intrude the center of the ophiolite, cutting ophiolite structures and containing roof pendants of ophiolitic rocks. Alkali-feldspar granite (ga) intrudes the ophiolite along a pre-existing north-northeast-trending fault zone.

No evidence for a pre-ophiolitic, crystalline basement (Delfour, 1981) was observed. To the contrary, crystalline rocks are either clearly part of the ophiolite sequence or intrude it.

Structure

The Darb Zubaydah ophiolite is exposed as a simple, east-dipping to subvertical homocline. The lithologic sequence and sedimentary structures in tuff and sandstone indicate that stratigraphic up is toward the east, which is consistent with the direction indicated by the ophiolitic "stratigraphy" (see above). A pervasive foliation parallels the bedding in all units and is well developed in tuffs and fine-grained clastic rocks, but there is no evidence of folding other than homoclinal tilting.

The boundary between hypabyssal rocks and volcanic rocks is disrupted by north-northeast-trending, anastomosing faults. A "melange" composed of rafts of hypabyssal, volcanic, and sedimentary rock in a matrix of carbonate-rich cataclasite is locally present along the faults. Sense and magnitude of displacement is unknown, but fold axes in the "melange" zones are subvertical, suggesting that the faults are strike slip and probably belong to the Nabitah fault system.

The ophiolite is cut by two stands of the Najd fault system. Sedimentary rocks of the Jabalah group (j) crop out along the southern strand. These faults are clearly younger than the Nabitah faults as they truncate alkali-feldspar granite along the Nabitah fault. The ophiolite is also cut by northeast-trending faults whose relationship to the Najd and Nabitah fault systems is uncertain.

Geochronology

No radiometric-age data is available for the Bi'r Nifazi area. However, rhyolitic tuff from the Nuqrah belt near the village of Nuqrah has been dated at 839 ±23 Ma by the uranium-lead method and 821 ±48 Ma by the rubidium-strontium method (Calvez and others, 1983). These dates are considered to be a reasonable first approximation for the age of the Darb Zubaydah ophiolite because the Nuqrah belt is a north-south-trending section of volcano-sedimentary rocks that is continuous from Nuqrah to Bi'r Nifazi.

Synthesis

A nearly complete ophiolitic section, the Darb Zubaydah ophiolite, is preserved in the Bi'r

Nifazi area. The section is composed of mixed serpentinite, of probable cumulus origin, overlain in turn by gabbro, hypabyssal mafic and intermediate intrusive rocks, pillow basalt, lahar, interbedded sedimentary rocks, and basaltic to rhyolitic volcanic rocks. Gossans, presumably formed by the weathering of massive-sulfide deposits, are interbedded with the pillow basalt and lahar. Stratigraphic up is to the east. Although tectonized peridotite is not present at the base of the ophiolite, roof pendants of tectonized peridotite are present in the granodiorite batholith to the west.

The abundance of pillow basalt, volcanic wacke, and coarse-grained andesitic to rhyolitic volcanoclastic rocks, and the absence of pelagic, sediments suggest that this section formed near an island-arc volcanic center rather than at a spreading ridge or back-arc basin; it is, therefore, an example of the type D ophiolite of Leitch (1984). Facies changes in the volcanic rocks suggest that, to the north, the section was submarine and distal to the volcanic center, and to the south, emergent and proximal to the volcanic center.

The Darb Zubaydah ophiolite appears to comprise the oldest rocks in the area; all observed plutonic rocks are either part of the ophiolite or intrude it. Reports of the presence of pre-ophiolitic basement rocks in the Bi'r Nifazi area (Delfour, 1981) were not supported by the results of this investigation.

The Darb Zubaydah ophiolite is possibly an analogue for the source terrane of the tectonic slivers in the Nabitah fault zone of the Bi'r Tuluhah area. All ophiolitic lithologies found in the fault zone of the study area, except the amphibolites, are represented in the Darb Zubaydah ophiolite. Radiometric ages obtained from Nuqrah belt rocks north of Bi'r Nifazi are the same (within stated errors) as zircon age dates obtained from the ophiolitic rocks in the study area.

Wadi Khadra

The Wadi Khadra area (fig. 2, pl. 4) was mapped during Spring, 1986 to collect structural data. Maps covering the area were done by Delfour (1981) and Le Metour and others (1983).

Overview

The geology of the Wadi Khadra area is dominated by a 5-km-wide, north-trending belt of mylonitic rocks that is interpreted to represent the Nabitah fault zone. The east side of the fault zone is underlain by peridotite tectonite, cumulus peridotite, and gabbro. Deformation in these rocks increases progressively to the west until primary mineral assemblages, textures, and structures are completely obliterated by extreme cataclasis. To the east, the peridotite and gabbro are intruded by a granodiorite batholith. The west side of the fault zone is underlain by relatively undeformed basalt and massive breccia. Structural data indicate that the intense cataclasis occurred during left-lateral, strike-slip motion along subvertical north-trending faults of the Nabitah system. Two additional deformations are recognized, one that predates and one that postdates Nabitah faulting.

Undivided Ultramafic Tectonite

Tectonized peridotite comprises serpentinized ultramafic rocks (um) that preserve a relatively well-defined spinel foliation. The peridotite is composed of mostly harzburgite and(or) lherzolite, recognized by the presence of bastitized pyroxene. Pyroxene-free dunite crops out as tabular and irregular bodies and swarms of northeast-trending metadiabase dikes cut the peridotite. Locally, the peridotite is strongly sheared and the diabase dikes are boudined.

Pyroxene and olivine are completely replaced by serpentine, talc, and calcite so that specific pyroxene-bearing protoliths are often impossible to infer. However, all of these rocks are cut by a northeast- to east-striking foliation defined by trails of spinel and the orientation of individual flattened spinel grains. This foliation is much better developed than at Bi'r Nifazi and Bi'r Tuluhah, and suggests that the protoliths were deformed mantle rocks, rather than ultramafic cumulates. X-ray diffraction analysis indicates that lizardite is the dominant serpentine polymorph, although antigorite was also identified in two samples.

The metadiabase dikes are composed of undeformed to weakly foliated intergrowths of green hornblende, quartz, and plagioclase. A foliation

defined by the preferred orientation of amphibole is developed in diabase boudins. The mineralogy and textures of these rocks is the same as those of the amphibolites in the Bi'r Tuluhah area.

Interlayered Gabbro and Peridotite

The tectonized peridotite is overlain by a complex unit that is interpreted to be cumulus peridotite and gabbro (gbp). These rocks are composed of interlayered gabbro and highly serpentinized ultramafic rocks that are similar in appearance to the undivided ultramafic and mafic rocks of the Darb Zubaydah ophiolite. The gabbro and serpentinite layers range in thickness from a few centimeters to 10 m and parallel the contact with the underlying tectonized peridotite. Locally, this layering drapes over irregularities in the contact, suggesting a cumulus origin. The contact is interpreted as the "petrologic moho" of the ophiolite; it truncates the metadiabase dike swarms in the underlying tectonite, indicating that it marks a significant hiatus.

As in the tectonized peridotite, the ultramafic protolith is often impossible to identify with certainty. Nevertheless, in many places, bastite after extremely coarse-grained, euhedral pyroxene (0.25-3 cm) is surrounded by interstitial serpentine after olivine. By analogy to less altered clinopyroxene-rich peridotite dikes and cumulus peridotite (for example, Quick, 1981), the relict pyroxene morphology suggests that the dominant pyroxene was clinopyroxene and that the protolith was cumulus wehrlite. Spinel in these rocks tends to be equant, subhedral, and without preferred orientation, which is also consistent with a cumulus origin. X-ray diffraction analysis indicates that lizardite is the dominant serpentine polymorph.

Gabbro

The cumulus peridotite and gabbro grades upward into a thick section of layered to massive gabbro (gb). Cumulus textures are locally developed in these rocks but become less distinct upward in the section. Primary igneous texture is preserved but the igneous minerals are highly altered. Green to green-brown amphibole envelopes sparse relicts of unaltered clinopyroxene. Primary plagioclase has been completely replaced by a mosaic of albite, quartz, and zoisite.

Basalt and Diabase

Basalt and diabase (b), significantly less deformed and recrystallized than the rocks to the east, crop out at the western edge of the Wadi Khadra area. The diabase is weakly plagioclase phyric. The basalt overlies the diabase and is highly vesicular. Vesicle trails parallel the contact, suggesting that the basalt was deposited on the diabase, but formation of the diabase as a sill cannot be ruled out. The relationship of this unit to the metabasalt is unclear, but the low degree of deformation and recrystallization suggests that they are younger.

Metabasalt

Metabasalt (mb) crops out in the southwest corner of the Wadi Khadra area; it is foliated, but contains recognizable vesicles and plagioclase phenocrysts. The rocks are cut by quartz veins that appear to be confined to conjugate joint sets.

Breccia

Massive breccia (br) crops out in a long, north-trending, east-dipping belt at the western edge of the Wadi Khadra area. The breccia overlies and is interbedded with the undeformed vesicular basalt. Well-bedded (0.3-1 m) fine-grained sandstone, siltstone, and shale are also exposed near the base of the unit, but bedding is indistinct. The breccia contains poorly sorted subangular clasts 1 mm-3m in diameter (fig. 7). Observed clast lithologies are gray aphanitic volcanic rock, phyllonite, fine-grained gabbro, quartz, plagiogranite, and vesicular basalt. The breccia is poorly foliated in its easternmost outcrops. It appears that, from east to west, the foliation dies out, clast size decreases, and clasts appear to become rounder.

The immaturity of the breccia suggests that it was deposited near its source area, and probably at the base of a steep slope. The linear outcrop pattern suggests that deposition may have occurred along a fault-controlled mountain front. Variations in clast size and angularity suggest that the source terrane was located to the east; indeed, the clast population could have been derived from lithologies within the Wadi Khadra area.

Wadi Khadra Phyllonite (Mylonite)

The Wadi Khadra phyllonite (m) is named (in this report) for exposures of highly mylonitized rock in the center of the Wadi Khadra area. The rock is buff to gray weathering, aphanitic, and well foliated. A sheen is typically present on the foliation surface. The rocks are cut by locally abundant quartz veins, and both the foliation and the quartz veins are deformed by small, steeply plunging isoclinal to open folds. A steeply plunging lineation is well developed in most places. X-ray diffraction analysis of two phyllonite samples determined that they were composed of chlorite, quartz, calcite, albite, muscovite, and(or) paragonite.

The Wadi Khadra phyllonite appears to have been formed by extreme cataclasis of at least two different lithologies. To the east, the phyllonite grades into gabbro and cumulus peridotite with decreasing deformation (fig. 8). In many places, deformed gabbroic or basaltic textures are preserved in elongate lenses that parallel the foliation (figs. 8 and 9). These lenses appear to be relicts of the protolith that have survived the deformation. The phyllonite is mapped as "m(mb)" or "m(gb)" where basalt or gabbro relicts are preserved.

Granodiorite

The tectonized peridotite, cumulus peridotite, and gabbroic rocks are cut by granodiorite dikes and are metamorphosed at their contacts with a granodiorite batholith (gd). The interior of the granodiorite is composed of plagioclase, microcline, biotite, and sphene. Muscovite and dark-green hornblende are present in some rocks. A primary hypidiomorphic-granular texture is slightly overprinted by a weak protoclastic texture and a foliation that is defined by preferred orientation of biotite. Near the contact of the batholith, biotite is replaced by chlorite, a protoclastic texture is well developed, and a pronounced foliation is defined by preferred orientation of biotite and amphibole grains.

Faulting

Two orientations of strike-slip faults and one orientation of shallow, normal faults were recognized in the study area.

The Nabitah fault system is represented by north-trending faults that are spatially associated with the Wadi Khadra phyllonite. The phyllonite is broken by north-trending, anastomosing faults that are too numerous to map, and the phyllonite appears to have formed by intense cataclasis. Therefore, faults were mapped only where major breaks in lithology and(or) some degree of deformation occur. The entire Wadi Khadra phyllonite is interpreted to be a 5-km-wide tectonic zone of intense deformation produced by Nabitah faulting.

Najd faults crosscut all lithologies in the Wadi Khadra area. Offsets of map units consistently indicate that the system was dominated by left-lateral strike-slip faulting. One outcrop of Jabalah-group sedimentary rocks is bounded by the southernmost Najd fault.

West-dipping low-angle faults cut the Wadi Khadra phyllonite but are not shown on the map because they appear to have limited extent along strike.

Folding

Three generations of folding are recognized in the Wadi Khadra area (fig.10). Two fold orientations, F_1 and F_2, are similar to the F_1 and F_2 orientations in the Bi'r Tuluhah area. A third orientation, F_3, is unique to the Wadi Khadra area and could be related to emplacement of the granodiorite batholith to the east.

F_1 folds (fig. 10D) are scarce and are only recognized in the layered gabbro where they are defined by deformed layering. As at Bi'r Tuluhah, these folds are discernable in rocks that are distant from Nabitah faults.

The folds are open and typically have amplitudes of less than 2 m. Fold axes plunge gently and have a north-to-northwest bearing in contrast to the northeast bearing of F_1 in the Bi'r Tuluhah area. Also included in figure 10D are five northeast-bearing fold axes reported by Delfour (1981) in the vicinity of Jabal Sanam, which is located midway between the Wadi Khadra and Bi'r Nifazi areas (fig. 2). The F_1 folding also appears to have deformed the contact between the tectonite and cumulus peridotite. Outcrop pattern and attitudes of cumulus layers in the layered gabbro suggest that the tectonite peridotite occupies the core of an open anticline that plunges gently (about 30°) to the north.

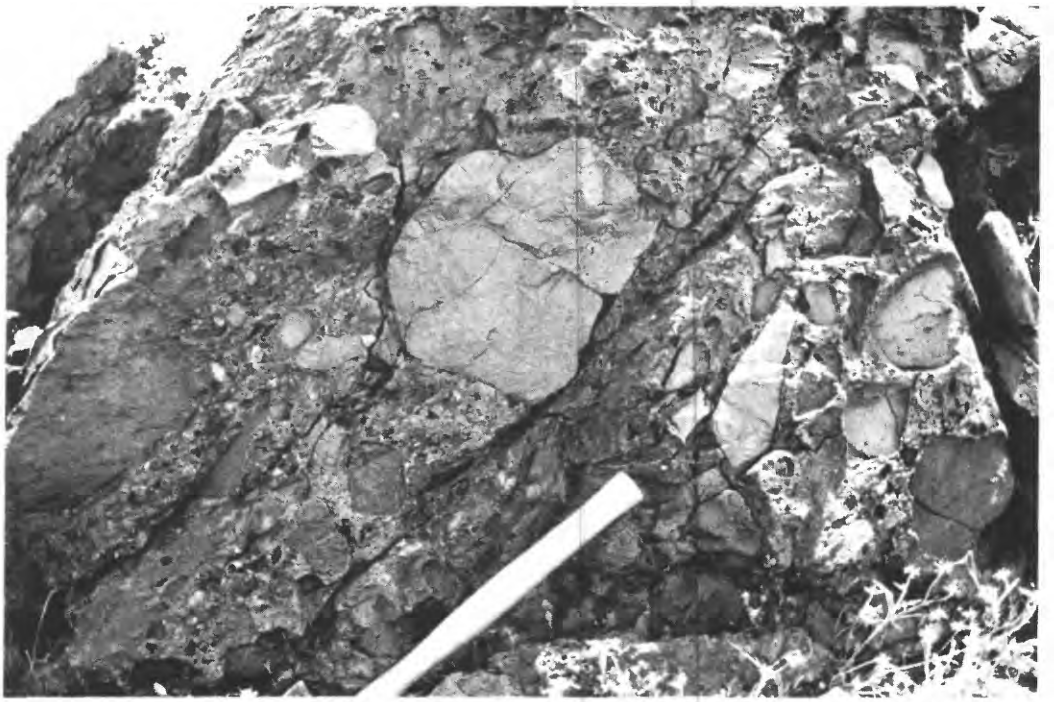

Figure 7--An outcrop of polymict breccia in the Wadi Khadra area. The large boulder in the center of the photo is about 30 cm in diameter.

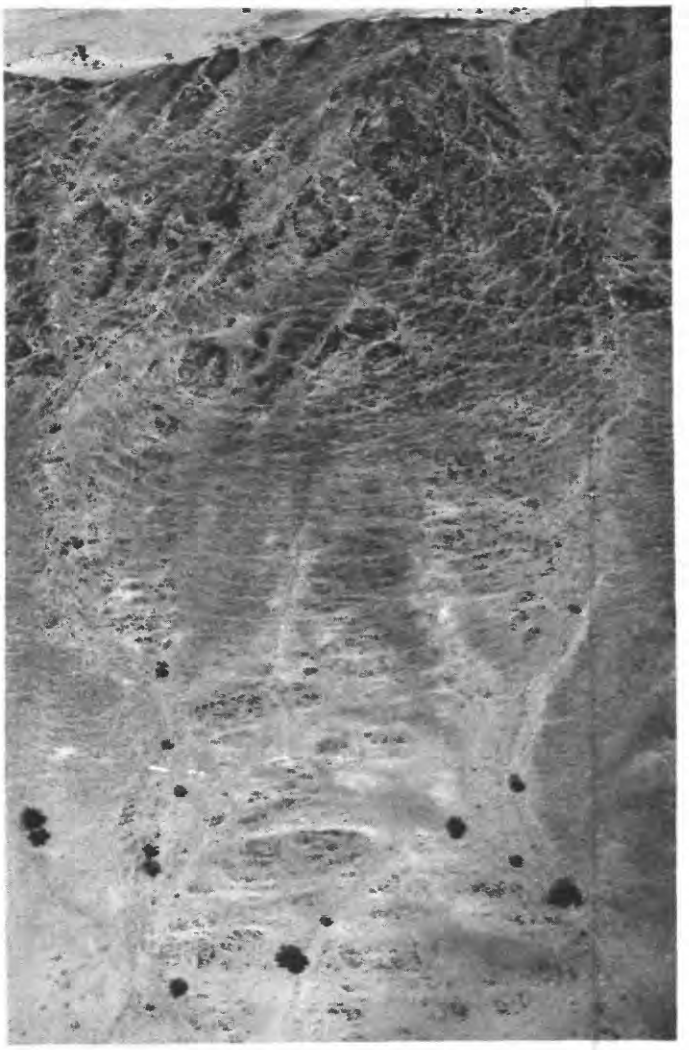

Figure 8--Oblique air photo showing contact between phyllonite (bottom two-thirds of slope) and moderately deformed cumulus gabbro and peridotite (upper third of slope). Outcrop relief decreased into the phyllonite. Lenses of less-deformed rock stand out as rocky patches at the bottom of the slope. Rock between these lenses is nonresistant phyllonite.

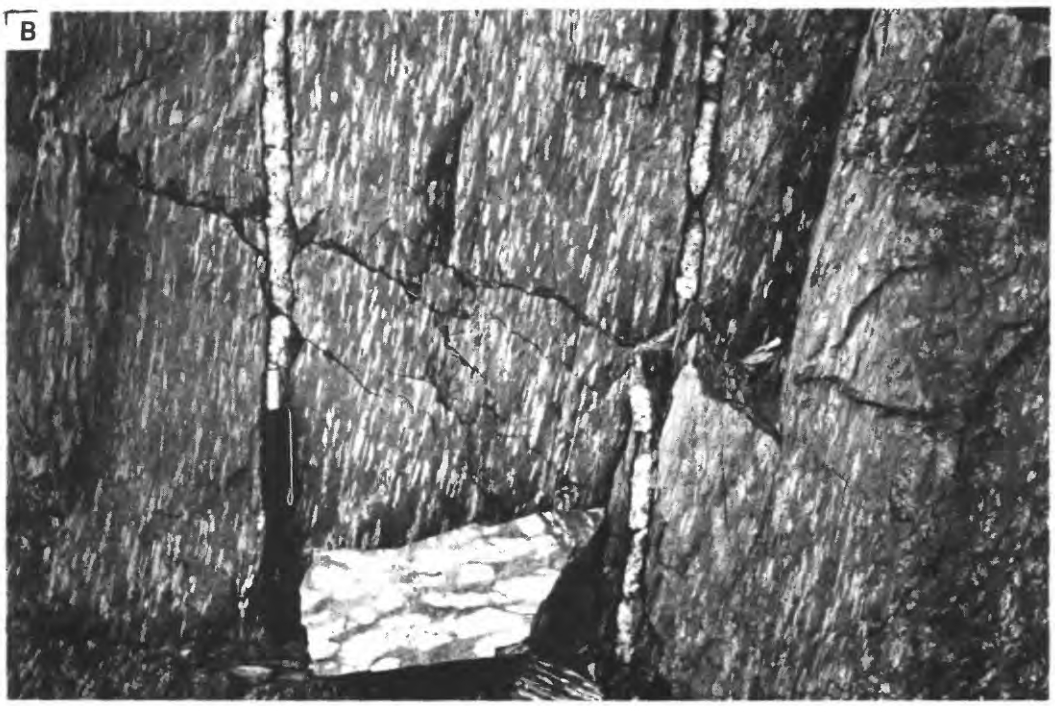

Figure 9–Effects of deformation on plagioclase-phyric diabase at Wadi Khadra. (A) Relatively undeformed plagioclase-phyric diabase dike intruding peridotite east of Wadi Khadra phyllonite. (B) Relicts of plagioclase-phyric texture preserved in a less-deformed lens within the Wadi Khadra phyllonite. Note that the plagioclase is rotated and flattened. The outcrop is cut by two relatively undeformed quartz veins. Small rock at bottom of picture shows the extreme flattening of plagioclase in foliation plane; long axis of the plagioclase grains parallels the lineation in the rock.

The F_2 folds are defined by deformed foliation in the Wadi Khadra phyllonite, metabasalt, and gabbro by deformed quartz veins in these rocks and by large-scale drag folding of gabbro layers near Nabitah faults. Lineation is typically associated with F_2 folding and invariably parallels the F_2 fold axes.

The spatial association of F_2 folds, the Nabitah faults, and the foliation in the metabasalt, gabbro, and phyllonite suggest that all of these features were produced during the same deformational event. Figures 10A through 10C demonstrate that lineations and F_2 folds plunge steeply, which suggests that they were formed by transcurrent motion. Within 1 km of the easternmost Nabitah fault, gabbro layering is rotated counter-clockwise into an orientation parallel to the fault. Foliation increases with proximity to the fault, suggesting that folding and deformation of the gabbro was produced by left-lateral motion on the fault. This interpretation is

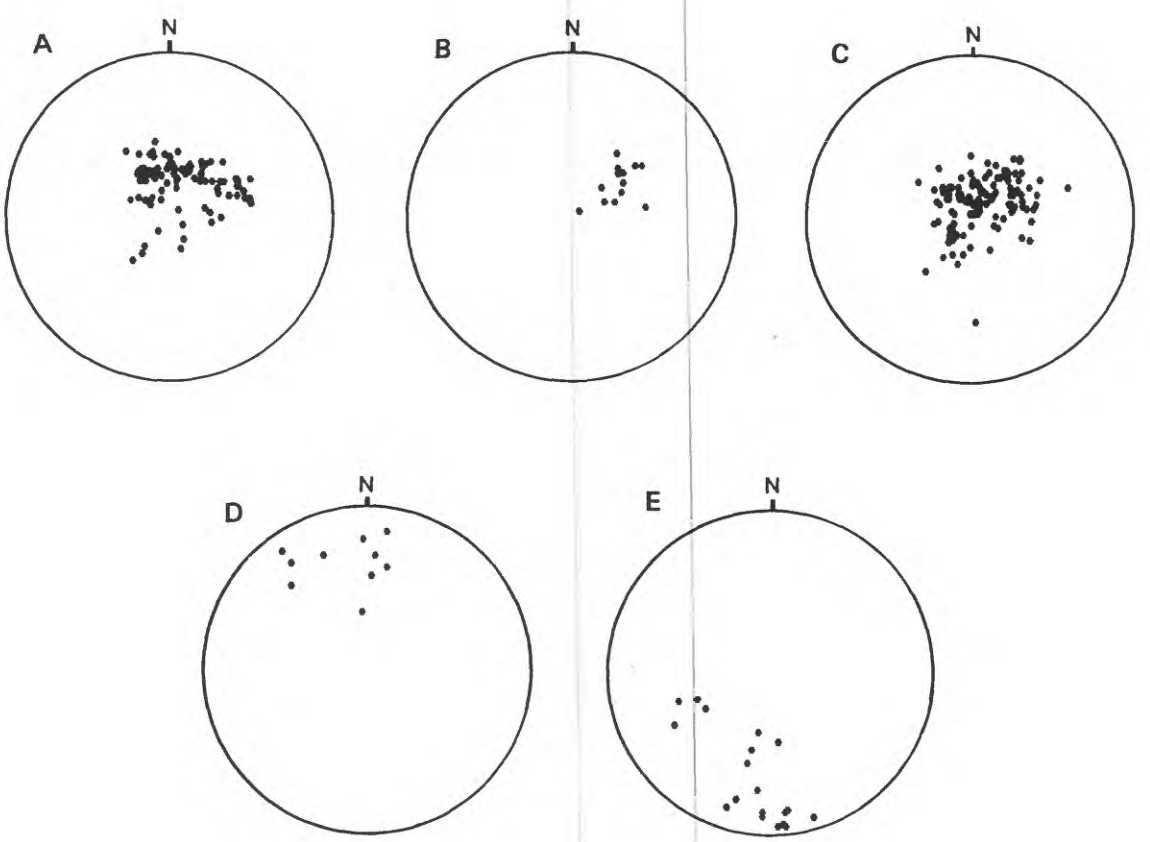

Figure 10--Equal-area-projection diagrams showing orientations of fold axes and lineations in the Wadi Khadra area: (A) F_2 fold axes and lineations in metagabbro, (B) F_2 fold axes and lineations in metabasalt, (C) F_2 fold axes and lineations in mylonite, (D) F_1 folds in gabbro and folds reported by Delfour (1981), and (E) F_3 folds in mylonite.

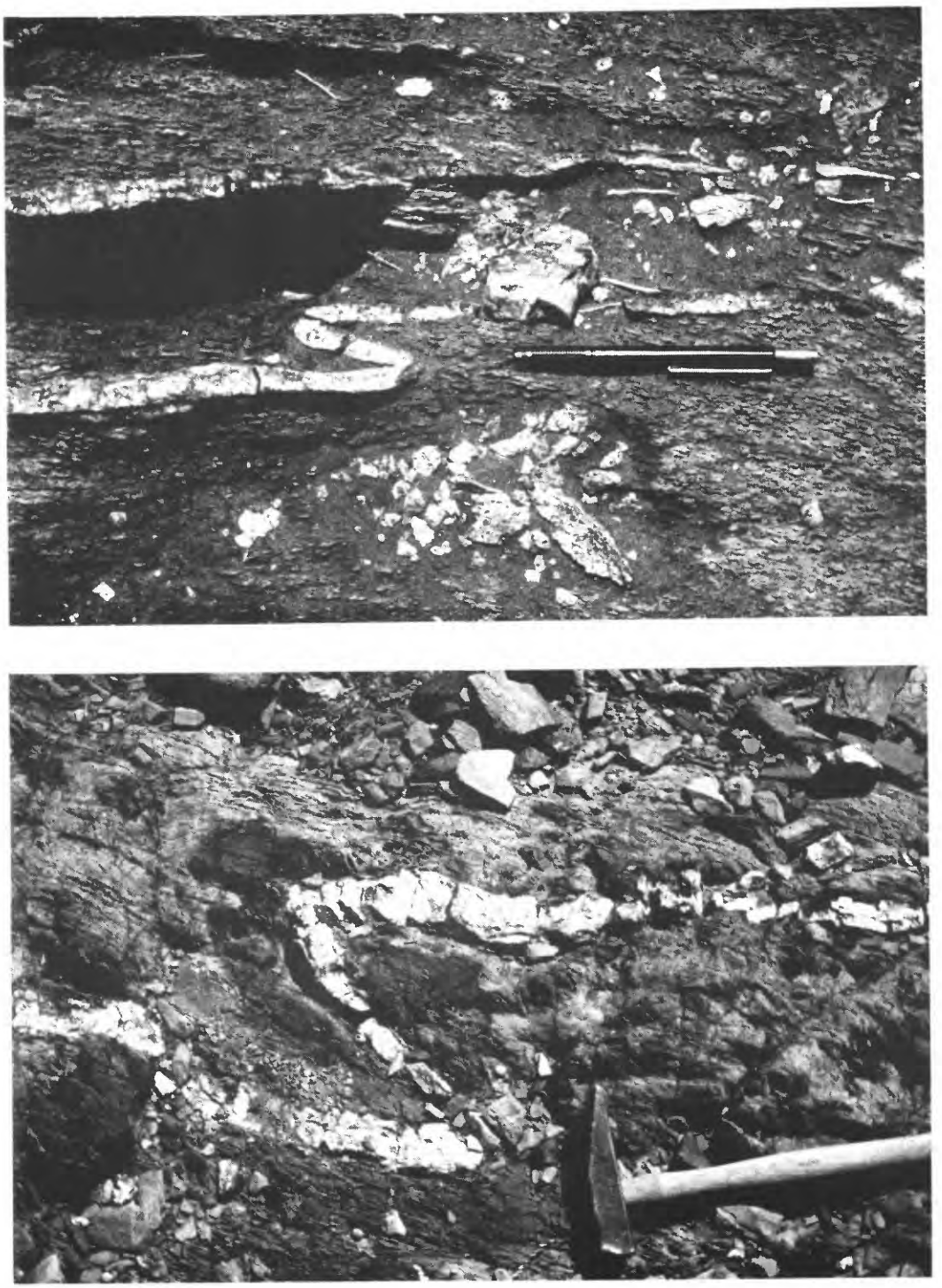

Figure 11--Folded quartz veins on horizontal outcrop surfaces in the Wadi Khadra phyllonite. North is to the left. Axial planes of folds parallel the foliation.

reinforced by the orientation and deformation of quartz veins in the Wadi Khadra phyllonite. The most common quartz-vein orientations in the phyllonite are parallel to the foliation and inclined to the foliation about 15-20° counter-clockwise. The second orientation could have formed in tension gashes related to left-lateral, strike-slip motion in the foliation plane of the phyllonite. Indeed, the inclined veins are commonly deformed by tight folds, the asymmetry of which also suggests left-lateral, strike-slip motion in the plane of the phyllonite foliation (fig. 11).

The F_3 folds (figs. 10E and 12) are defined by gentle warps, crenulations, and drag folds in the phyllonite foliation. The warps and crenulations are invariably monoclines with axes that plunge at shallow angles to the south and southwest. The effect of F_3 folding on older structures is asymmetric. Lineations and F_2 fold axes are rotated from their primary steep plunges to more shallow, easterly plunges (fig. 13). This is seen in figures 10 A and C as a smearing out of points to the right of center of the projections. The F_3 folds are commonly developed as drags on the hanging wall of low-angle faults that dip gently to the west. The sense of the direction of drag invariably indicates that the hanging wall moved downward to the west. This sense of shear is supported by the asymmetry of the crenulations and warps even where faulting is not developed.

F_3 folding is inferred to have been produced during the intrusion of the granodiorite batholith to the east. It is possible that rocks overlying the granodiorite were uplifted and slid off the flanks of the batholith during its emplacement. The direction of transport of these rocks in the Wadi Khadra area would have been to the west, which is consistent with the sense of asymmetry in F_3 folds.

Synthesis

The Wadi Khadra phyllonite is the dominant feature of the Wadi Khadra area. Formed by extreme cataclasis of basaltic and gabbroic rocks, the phyllonite crops out in a 5-km-wide, north-trending band. Spatial association with north-trending Nabitah faults suggests that the cataclasis occurred during Nabitah faulting. Drag folds on Nabitah faults and tension gashes and folds in the phyllonite both suggest that deformation was dominated by left-lateral, strike-slip motion: therefore, the phyllonite was probably generated by intense deformation within the Nabitah fault zone. The deformation of the phyllonite is significantly greater than observed in the Bi'r Tuluhah area to the north, suggesting that the Nabitah fault zone is exposed to a deeper level at Wadi Khadra. This could be explained by uplift during emplacement of a large granodiorite batholith to the east.

A folded west-dipping section of tectonized peridotite, cumulus peridotite, and gabbro is exposed on the western side of the Wadi Khadra phyllonite. The composition and sequence of these lithologies is appropriate for the base of an ophiolitic section; it is suggested that they are related to the Darb Zubaydah ophiolite and, therefore, represent an outlier of the Nuqrah belt. Identification of an ophiolitic section in the Wadi Khadra area is consistent with the interpretations of Delfour (1981), but is in disagreement with the conclusions of Le Metour and others (1983), who interpreted the same rocks to be part of a peridotite-gabbro-tonalite intrusive complex. This ophiolitic section is progressively more deformed to the west until the rocks grade into the Wadi Khadra phyllonite with increasing development of foliation and destruction of primary igneous textures and structures. These observations and the occurrence of gabbro and metabasalt relicts in the phyllonite suggest that the phyllonite was formed by cataclasis of the ophiolite.

An east-dipping section of diabase, basalt, and massive breccia is exposed on the western side of the Wadi Khadra phyllonite. The lower metamorphic grade, lower degree of deformation, and clast population of the breccia suggest that this section is younger than the gabbro, metabasalt, and phyllonite to the east. The breccia may have been deposited along a steep, fault-controlled mountain front, and the weak foliation along its eastern margin suggests that it was, in fact, deposited beside the active Nabitah fault zone. Alternatively, the breccia may have been deposited during unroofing of the granodiorite batholith to the east.

Jabal Al Qub

The Jabal al Qub area (fig. 2, pl. 5) is located along the Nabitah fault zone and south of the Bi'r Umq suture (Stoeser and Camp, 1984).

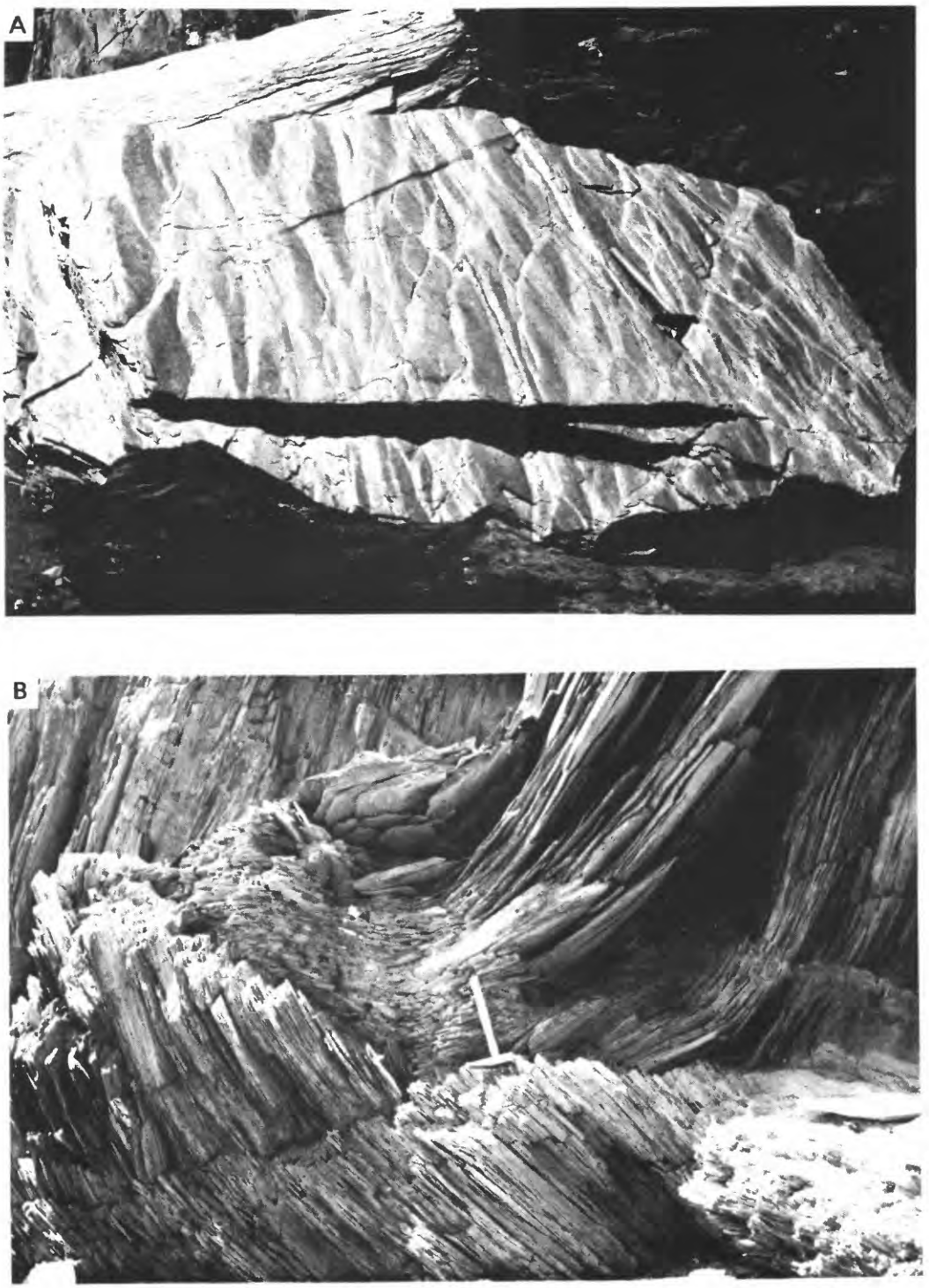

Figure 12–Outcrop of the Wadi Khadra phyllonite showing F_3 folds: (A) crenulations in a float block, and (B) Drag folds along a low-angle, west-dipping (to the right) fault.

The geology on plate 5 is derived from the 1:250,000-scale map of the Mahd Adh Dhahab quadrangle (Kemp and others, 1982) with modifications based on two weeks of reconnaissance in the spring, 1986.

Overview

The Jabal al Qub area is cut by a set of north-trending faults that are spatially associated with serpentinized peridotite and that are interpreted to be strands of the Nabitah fault system. East of these faults, the area is underlain by amphibolite, syntectonic metadiorite, and granodiorite and gabbro of the Rharaba complex. West of these faults, the area is underlain by the Dhukhr tonalite, undivided granitic and granophyric rocks, interbedded volcanogenic sedimentary rocks, and intermediate to felsic volcanic rocks. As in the Bi'r Tuluhah and Wadi Khadra areas, the steep plunge of fold axes near the Nabitah faults suggests that faulting on that system was dominated by strike-slip movement. Rocks located more than about 1-2 km from the Nabitah faults preserve shallow plunging folds that suggest a pre-Nabitah, east-west compressional event.

Ultramafic Rocks

Most of the ultramafic rocks(serpentinite) (um) of the Jabal al Qub area crop out in a narrow, north-trending, fault-controlled zone. Except for disruption by Najd faults, this serpentinite forms a continuous belt that varies from 5 m to 3 km in thickness. To the east, small outliers of serpentinite crop out in association with amphibolite.

The rocks are completely altered to serpentinite and listwaenite, in which no primary silicate minerals are preserved. In the serpentinite,

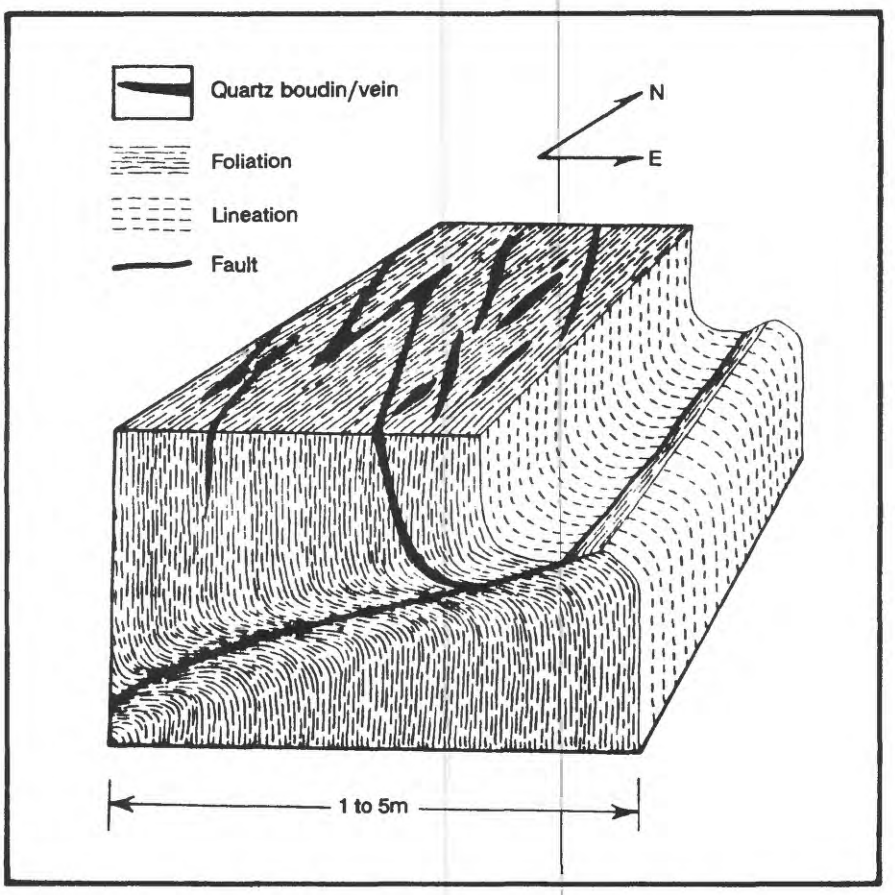

Figure 13--Block diagram of the Wadi Khadra phyllonite illustrating (1) the orientation of quartz boudins relative to the foliation, (2) the sense of folding of quartz veins, and (3) deformation of the phyllonite by low-angle faults resulting in F_3 folds and rotation of lineation.

olivine is replaced by serpentine, pyroxene is replaced by serpentine, talc, and carbonate, and chromium-spinel grains are mantled by magnetite but retain primary chromium-spinel in their cores. X-ray diffraction analysis of three samples determined that the serpentine polymorphs were lizardite and chrysotile. These rocks are cut by anastomosing bands of listwaenite in which silicate minerals are replaced by magnesite, quartz, and talc. As in the other study areas, the composition of the peridotite protolith is uncertain because of the extreme alteration.

The center of the serpentinite belt appears to be relatively undeformed. The rocks are massive and devoid of schistosity except in narrow anastomosing, north-trending shear zones. The peridotite is cut by relatively undeformed mafic dikes that have been altered to amphibolite composed of green amphibole and plagioclase. The serpentinite is composed of equant spinel and bastitized pyroxene grains that are randomly disseminated in a matrix of serpentine replacing olivine. Although spinel trails are developed locally, there is no evidence of a pervasive spinel foliation, suggesting that the rocks were not mantle tectonites.

A well-developed north-trending schistosity is present near the margins of the serpentinite belt. The schistosity cuts both serpentinite rock and listwaenite and is locally deformed by small folds and cut by northwesterly trending, quartz-filled tension gashes. Mafic dikes are rotated to parallel the schistosity and are boudined. In places of extreme deformation, the boudins are flattened into lenticular layers of chlorite-rich schist. The mafic boudins are completely replaced by chlorite, albite, epidote, magnetite, and carbonate. Blackwall reaction zones completely envelope the boudins.

Amphibolite

Black-weathering amphibolite (a) underlies broad areas east of the serpentinite belt and occurs as slivers that are tectonically interleaved with serpentinite. In most places, the contact between the amphibolite and serpentinite is a subvertical north-trending fault of the Nabitah system. The amphibolite is cut by a steeply dipping foliation that strikes from north-northwest to north-northeast. Near the serpentinite, the foliation in the amphibolite parallels the faulted contact.

The amphibolite is composed of an intergrowth of green-brown zoned hornblende, plagioclase, epidote, and opaque minerals. Quartz and garnet are present in some assemblages. The foliation is defined by the preferred orientation of hornblende. Electron microbeam analysis indicates that the garnet is Ca-rich and, therefore, not indicative of almandine-amphibolite-grade metamorphism. Near contacts with the serpentinite, the primary metamorphic assemblage is partially replaced by chlorite and actinolite, plagioclase is saussuritized, and plagioclase and hornblende grains are broken and polygonatized. The paragenesis is identical to that of the amphibolites at Bi'r Tuluhah. Epidote amphibolite, or upper greenschist, is the maximum metamorphic grade attained by the amphibolite and localized deformation of the maximum-grade assemblages was accompanied by partial recrystallization to lower greenschist facies.

Structural relations at two locations suggest that the serpentinite may have been tectonically emplaced above the amphibolite prior to Nabitah faulting. An outlier of garnet amphibolite and serpentinite is located in the middle of a metadiorite pluton near the northern limit of the study area. Foliation in the amphibolite is truncated by the contact with the serpentinite and, although exposures are poor, rock distributions suggest that the amphibolite is overlain by serpentinite. The second location is an inlier of amphibolite too small to show on plate 5 but is located near the center of the serpentinite belt at lat 23°50.5' N. The amphibolite crops out as a north-trending lenticular body. To the west, the amphibolite clearly dips under serpentinite. Near this contact, foliation and compositional layering are parallel and folded (F_1); the asymmetry of folding suggests overthrusting from west to east. The amphibolite is bounded on the east by a subvertical fault that juxtaposes serpentinite. Amphibolite near this contact is cut by a steep axial-plane foliation that parallels the fault and crosscuts the compositional layering.

Metadiorite

Foliated metadiorite (md) crops out on the east side of the serpentinite belt. The foliation

attitude is somewhat variable but has a northward strike on the average. Contacts with the serpentinite belt are faulted. Lenses of blackwall-enveloped metadiorite are tectonically interleaved with talc-serpentine schist. Near the serpentinite the foliation in the metadiorite changes strike in such a way that it parallels the serpentinite-metadiorite contact. In contrast, metadiorite contacts with the amphibolite and serpentinite outlier to the east appear to be intrusive. Amphibolite occurs as xenoliths and roof pendants within metadiorite, and dikes of metadiorite intrude the serpentinite in the outlier.

The metadiorite is composed of green-brown secondary hornblende, saussuritized plagioclase, quartz, epidote, opaque minerals, sphene, and variable amounts of biotite and microcline. No traces of the primary mafic silicates remain. Textures range from weakly protoclastic to stongly porphyroclastic. In weakly protoclastic rocks, hypidiomorphic-granular textured hornblende, feldspar, and quartz are cut by bands of mosaic-textured quartz and feldspar that apparently formed by crushing of primary grains. Quartz and feldspar have undulatory extinction, and biotite is oriented parallel to the mosaic-textured bands, defining a weak foliation. Graphic intergrowths of quartz and feldspar in the interstices of the crushed bands suggest that the rock was still partially molten at the time of deformation. In strongly porphyroclastic rocks, abraded porphyroclasts of plagioclase and microcline are surrounded by a very fine-grained mosaic of quartz, feldspar, epidote, and chlorite. A well-developed foliation, defined by trails of crushed grains and the orientation of chlorite plates, wraps around the porphyroclasts. The textural evidence for synmagmatic cataclasis and the northerly trend of the foliation suggest that emplacement of the metadiorite may have been contemporaneous with Nabitah faulting.

Granodiorite and Rharaba Complex

Undeformed granodiorite (gd), cumulus peridotite (r1), and gabbro (r2) of the Rharaba complex crop out east of the serpentinite belt. Unfoliated granodiorite crosscuts the foliation in the metadiorite and amphibolite, indicating that the granodiorite intrudes the latter lithologies. The Rharaba complex is composed of layered plagioclase olivine-pyroxenite, websterite, troctolite and two-pyroxene gabbro. The rocks are undeformed and only moderately altered to serpentine, chlorite, and epidote. Preliminary electron-microbeam studies of samples from several exposures of the Rharaba complex (fig. 2) indicate that, in many of the rocks, anorthite-rich (typically $An_{>80}$) plagioclase coexists with relatively Fa-rich (Fa_{20}) olivine. Kemp and others (1982) interpreted the Rharaba complex to be the same age as the granodiorite (their monzogranite) based on spatial association and mutually crosscutting relationships. A consanguinous relationship with granodiorite or tonalite, the presence of two-pyroxene gabbros, and coexisting fayalitic olivine and anorthitic plagioclase are characteristics of layered gabbro/peridotite complexes in the western cordillera of North America (James, 1971; Irvine, 1974; Snoke and others, 1981; Burns, 1985). Converging evidence suggests that these complexes formed as cumulates in magma chambers beneath island-arc volcanic centers (Snoke and others, 1981; Burns, 1985); that interpretation is adopted for the Rharaba complex by analogy. The absence of deformation in the Rharaba complex suggests that the layered gabbro and peridotite were emplaced relatively late in the history of the Jabal al Qub area.

Volcanic and Sedimentary Rocks

Interbedded volcanic and sedimentary rocks (vs) and rhyolite (rhy) crop out in a wide band west of the serpentinite belt. Basalt and andesite are more abundant in the west and volcanic sandstone and conglomerate appear to be more abundant in the east. The basalt and andesite locally contain epidote-filled vesicles, and some flows are plagioclase phyric. The volcanogenic sandstone is a poorly sorted wacke that grades into conglomerate. The conglomerate contains clasts of gray aphanitic volcanic rock, rhyolite, and welded rhyolitic tuff; amphibolite clasts where identified at one site. A single belt of rhyolite crops out within the metasedimentary rocks. The rhyolite contains well-developed flow foliation, but fiamme and other structures diagnostic of volcanic origin are absent. Although an intrusive origin is possible, the rhyolite is thought to be volcanic because of its concordance with surrounding sedimentary rocks.

The volcanic and sedimentary rocks are locally foliated. These rocks weather to low,

north-trending ridges, and in general, a north-striking foliation is best developed in the valleys. In contrast, the rocks of the ridge crests are less foliated. This suggests that the terrane is crosscut by numerous, poorly exposed, anastomosing faults. The foliation is steeply dipping, suggesting that the faults are subvertical. In these foliated areas, basalt vesicles and sandstone clasts are flattened into the plane of the foliation.

The rocks show signs of intense deformation near the serpentinite belt. A foliation is pervasive within about 1-4 km of the serpentinite. Within 0.5-1 km of the serpentinite, the rock is phyllonitic with a well-developed schistosity; the primary sedimentary and volcanic textures have been obliterated by cataclasis. Within 20 m of the serpentinite, the schistosity is intensely deformed into tight, steeply dipping disharmonic folds. A lineation parallels the fold axes.

Kemp and others (1982) subdivide the volcanic and sedimentary rocks into the Ghamr group and the Mahd group, which are separated by an unconformity. The younger Ghamr-group rocks are interpreted to occupy the core of a large syncline. In this study, no evidence of unconformity or a major syncline was found and, indeed, available attitudes do not support the existence of either structure. In view of the evidence for extensive faulting, subdivision of this unit into groups should await detailed mapping.

Tonalite and Undivided Granite

Tonalite (dt) and undivided granite (g) underlie the southwest corner of the Jabal al Qub area. Kemp and others (1982) show the Mahd and Ghamr groups unconformably overlying the tonalite (their Dhukr tonalite) in this area. They show the undivided granite (their Bari granodiorite) intruding the Mahd group but unconformably overlain by the Ghamr group. These hypotheses were tested in this investigation because the tonalite is the only isotopically dated rock in the Jabal al Qub area. The results suggest that both the tonalite and undivided granite invariably intrude, or are in fault contact with, rocks corresponding to the Mahd and Ghamr groups of Kemp and others (1982). No evidence of a basal conglomerate exists at the contact between the volcanic and sedimentary rocks and the tonalite or undivided granite contacts. Conglomerate lenses, where present at the contact, are devoid of tonalite and granodiorite clasts. Instead, an intrusive contact is indicated by crosscutting relationships. Unfoliated tonalite cuts bedding and foliation in the interbedded volcanic and sedimentary rocks along the northern 10-15 km of its exposure in the study area (pl. 5). In this area, the tonalite contains xenoliths of andesite and roof pendants of foliated basalt and andesite. Tonalite dikes intrude the roof pendants. To the south, a small septum of volcanic and sedimentary rock is trapped along the contact between the tonalite and undivided granite, and the undivided granite crosscuts bedding in the adjacent volcanic and sedimentary rock.

Faulting

The Nabitah fault system is represented in the Jabal al Qub area by a narrow zone of north-trending anastomosing faults that are spatially associated with serpentinite outcrops. Serpentinite, amphibolite, metadiorite, and interbedded volcanic and sedimentary rocks were deformed by the Nabitah faults. The steep dips of these foliations suggest that the faults are subvertical. The ages of the tonalite, undivided granite, granodiorite, and the rocks of the Rharaba complex relative to Nabitah faulting are uncertain.

Several northwest-trending strands of the Najd fault system were mapped in the Jabal al Qub area. Sedimentary and volcanic rocks of the Jibalah group (j) are exposed along the two northernmost Najd faults. The other Najd faults clearly offset the serpentinite belt and the Nabitah faults.

Folding

Two fold orientations (fig. 14) are recognized in the Jabal al Qub area, and as at Bi'r Tuluhah, the spatial distribution of these orientations is related to the Nabitah faults.

The F_1 folds (fig. 14E) have gently plunging axes and are found some distance from strands of the Nabitah fault system. The best examples of F_1 folds are in the southeastern corner of the Jabal al Qub area where parallel foliation and compositional layering in amphibolite is folded into a tight north-plunging antiform with an amplitude

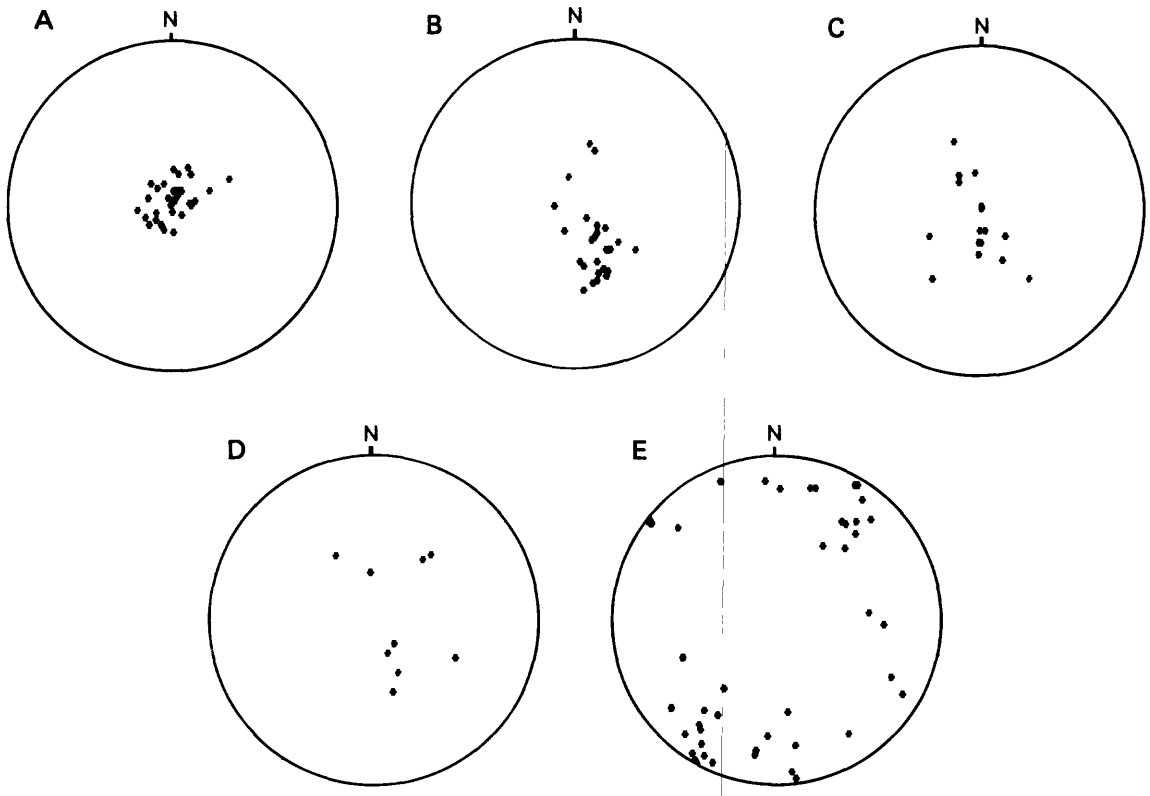

Figure 14--Equal-area-projection diagrams showing orientations of fold axes and lineations in the Jabal al Qub area: (A) F_2 fold axes and lineations in phyllonite along east side of Nabitah fault system, (B) F_2 fold axes in foliated volcanic and sedimentary rocks east of Nabitah fault system, (C) F_2 fold axes and lineations in amphibolite within 100 m of Nabitah faults, (D) F_2 fold axes in foliated serpentine near Nabitah faults, and (E) F_1 fold axes in amphiolite well removed from Nabitah faults.

of several kilometers. The limbs of the antiform contain numerous parasitic folds. Another example of F_1 folding is found in the amphibolite inlier (see Amphibolite, above) within the serpentinite belt. Folds along the western side of the inlier are defined by deformed compositional layering and plunge gently to the northeast or southwest.

The F_2 folds (figs. 14 A-D) are defined by deformations in foliation and schistosity. Most of these folds are located near strands of the Nabitah fault system and are characterized by steeply plunging axes (figs. 14 A, C, and D). F_2 orientations also appear to be developed in the foliated zones that crosscut the interbedded volcanic and sedimentary rocks (fig. 14B).

Fault Kinematics

The Nabitah fault system appears to have been dominated by left-lateral strike-slip motion in the Jabal al Qub area. Fold axes located near the faults are steep, suggesting that motion was strike slip. A left-lateral sense of motion is suggested by (1) the sense of drag folding in the phyllonite near Nabitah faults, (2) asymmetry in small folds in the amphibolite near the Nabitah faults, and (3) the orientation of quartz-filled tension gashes in foliated serpentinite.

Geochronology

Stoeser (1986) reports an age of 815 ±9 Ma for the tonalite in southwestern corner of the Jabal al Qub area. This age is significant because it suggests that the interbedded volcanic and sedimentary rocks are older and belong to a terrane that may be similar in age to the Nuqrah belt.

Synthesis

The Jabal al Qub area is cut by north-trending strands of the Nabitah fault system. Structural evidence suggests that motion on these faults was left-lateral strike slip. A horst of serpentinite may have been tectonically emplaced along these faults. East of these faults, the area is underlain by interbedded andesite, basalt, rhyolite, volcanogenic sedimentary rocks, and marble, all of which are intruded by tonalite and undivided granite (815 Ma). The abundance of volcanic wacke in the section suggests that the rocks were deposited near an island arc. East of the Nabitah faults, the area is underlain by amphibolite, minor serpentinite, and metadiorite, all of which are intruded by granodiorite and gabbroic cumulus rocks. Structural evidence suggests that, prior to Nabitah faulting, the serpentinite may have been thrust over the amphibolite from west to east. Structural and petrographic evidence suggests that subsequent intrusion of the metadiorite may have been synchronous with Nabitah faulting.

GEOCHEMISTRY

GEOCHEMICAL TECHNIQUES

Whole-rock analyses were performed by electron microbeam analysis (EMA) of glasses for major elements and X-ray fluorescence (XRF) spectroscopy of compacted powder for trace elements. Each sample was crushed and ground to 200 mesh. A split of the resulting powder was melted to form a glass bead for EMA and a second split was compacted for XRF analysis. Glass beads were manufactured by melting powder suspended on platinum loops in a vertical furnace open to the atmosphere. Basalts and andesites were heated to approximately 1,300^{o} C for 3 hours. Rhyolites were heated to approximately 1,100^{o} C for 3 hours to minimize alkali loss. Quenching was performed with a compressed-air gun. Glasses were ground and remelted to optimize their homogeneity. Volatiles (H_2O and CO_2) are lost during glass preparation so that EMA's are the "anhydrous" equivalent of the original sample composition. Sodium and potassium do not appear to be affected by glass preparation.

EMA was performed on mineral grains and polished glass mounts using a JEOL T300 scanning electron microscope (SEM) equipped with a Tracor Northern Si(Li) energy-dispersive X-ray detector (EDA). Operating conditions were 15 kV accelerating potential and a take-off angle of 25 degrees. X-ray spectra were analyzed using Bence-Albee correction factors and modified Tracor Northern software. Calculated abundances and precisions were automatically transferred to an IBM XT microcomputer for storage and subsequent manipulation.

XRF analysis was performed using a Kevex 7000 X-ray fluorescence analyzer interfaced to an IBM-PC. Samples were irradiated at atmospheric pressure using ^{109}Cd and ^{241}Am radioactive sources. X-ray spectra were collected using a Kevex Si(Li) EDA and transferred to an IBM-PC for analysis and storage. Spectral analysis was performed using XAP, a least-squares spectral-deconvolution program (Quick and Helaby, 1988).

The data presented in Appendix A are considered to be fully quantitative for major elements determined by EMA and semiquantitative for trace elements determined by XRF. True accuracy for the EMA results was found to be 2 to 5 percent of the abundance for elements present in greater than 1 percent abundance based on analysis of rock standards with published compositions (Quick and Hussein, unpub. data). For the XRF, accuracy depends on the abundance of the element and which X-ray lines (K, L, or M) are measured; in general, the best accuracy is obtainable at 5 to 15 percent of the abundance on this system at present

(Quick and Helaby, 1988). Appendix A also contains 20 major- and trace-element analyses for the Hulayfah group reported by Kattan (1983).

Geochemical Results

The EMA and XRF data are presented graphically in terms of AFM, K_2O-SiO_2, titanium-zirconium, and titanium-zirconium-yttrium diagrams in figures 15-22. All diagrams for the Hulayfah group include 15 analyses from Kattan (1983). Results of over 1,000 spinel analyses are presented graphically in figure 23.

Whole-rock analyses are used primarily to better understand the possible relationships that may exist between the various rock types in the Bi'r Tulubah and Bi'r Nifazi areas. The formation of these rocks in island-arc environments is considered beyond dispute based on petrology and field relations. Spinel analyses, however, are used to investigate the petrogenesis of the serpentinite.

Petrogenesis and Immobile Elements

The extensive greenschist-facies alteration and local carbonate metasomatism of the rocks analyzed in this study suggests that the original rock compositions may have been modified significantly. To minimize this effect, rocks with obvious metasomatism were not analyzed and rocks with greater than 13 weight percent CaO, a conservative upper limit for unaltered volcanic rocks, were discarded from the diagrams. Nevertheless, sodium and potassium concentrations are particularly susceptible to modification by low-grade metamorphic processes, and conclusions drawn from them in greenschist terranes must always be suspect. Therefore, figures 15, 16, 19, and 20 are used mainly to compare the present compositions of different groups of rocks; it should be emphasized that petrogenetic speculations based on these diagrams are tentative.

To avoid the above uncertainties, some geochemists focused on "immobile elements" (for example, Pearce and Cann, 1973) that are considered to be relatively insoluble under conditions of greenschist-and amphibolite-grade metamorphism. The relative abundances of these elements should be more diagnostic of the original rock compositions. Figures 17, 18, 21, and 22 are examples of these diagrams and are divided into "tectonic fields" defined by Pearce and Cann (1973). However, recent exploration (for example, Stern and Bibee, 1984) of active island arcs revealed volcanic compositions that do not conform to these "tectonic fields". Therefore, these diagrams are used mainly to compare rocks analyzed in this study with each other and with those of other arc terranes; the original fields of Pearce and Cann (1973) are included for reference. Figures 17, 18, 21, and 22 contain data for basalt to rhyolite in composition, whereas the fields of Pearce and Cann (1973) were defined solely on the basis of basalt compositions. Rocks with SiO_2 greater than 60 weight percent are included in diagrams where they constitute a significant part of the data and(or) influence the distribution of points.

Darb Zubaydah Ophiolite

Figure 15 presents AFM diagrams for the volcanic and hypabyssal rocks of the Darb Zubaydah ophiolite. The volcanic rocks plot in an elongate field that crosses from the tholeiitic region to the calc-alkali region of the diagram. Compared to AFM diagrams for circum-Pacific arc-related volcanic rocks (Ewart, 1982), this field is similar in position and extent to the fields for low-K and calc-alkali rocks of the western Pacific island arcs. In contrast, most of the hypabyssal rocks plot in the tholeiitic region and define a field with a modest Fe-enrichment trend among the low-alkali rocks. It is uncertain if the differences between figures 15A and 15B are attributable to differences in late differentiation or to the differences in alteration between the volcanic and the dike rocks.

Diagrams showing variations in K_2O and SiO_2 for the volcanic and hypabyssal rocks appear in figure 16. Both the volcanic and hypabyssal rocks display wide ranges in K_2O and SiO_2 abundances, with K_2O generally increasing with increasing SiO_2 content. Both groups of rocks display a compositional gap between 60 and 65 percent SiO_2, indicating that volcanism was bimodal in the Darb Zubaydah ophiolite. The volcanic rocks appear to have two branching differentiation trends above 65 weight percent SiO_2. Although the effects of post-magmatic alteration (such as metasomatism) are unknown in the Darb Zubaydah ophiolite, it is interesting to note that branching differentiation trends are also described in the

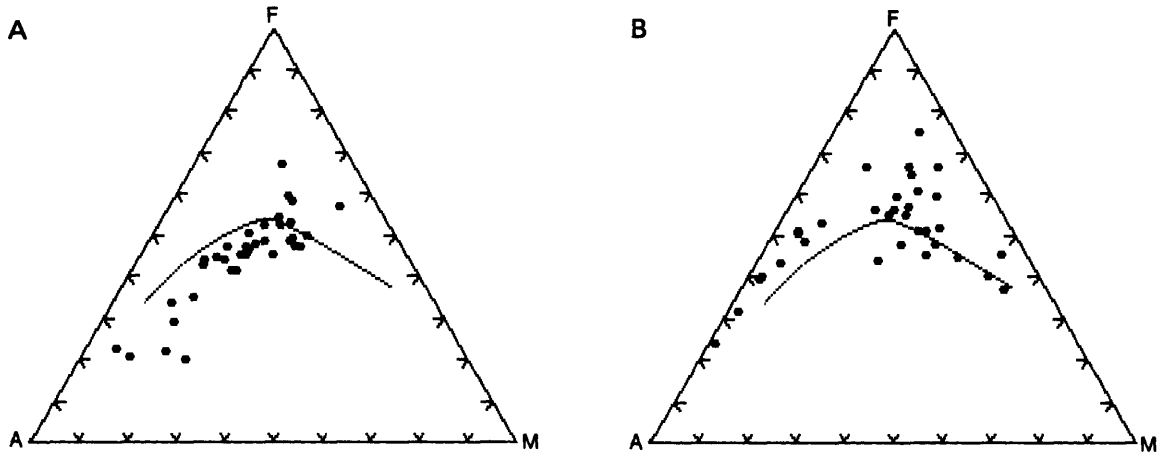

Figure 15--AFM diagrams for (A) volcanic rocks and (B) hypabyssal rocks of the Darb Zubaydah ophiolite. Axes are defined as follows: A, $Na_2O + K_2O$; F, $FeO + 0.9\ Fe_2O_3$; M, MgO. Curve in center of diagram marks boundary between tholeiitic (upper) and calc-alkaline (lower) regions of Irvine and Baragar (1971).

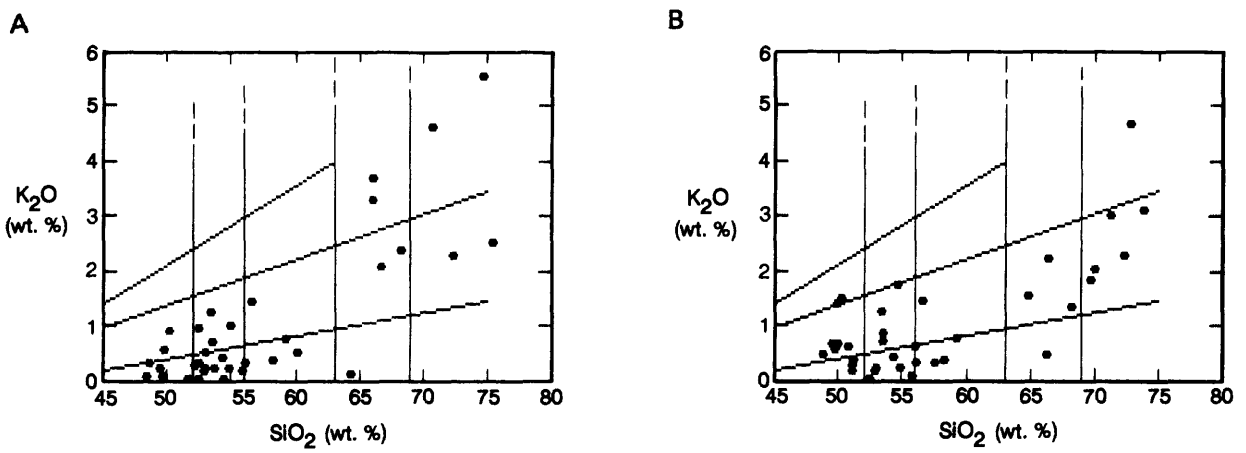

Figure 16--Compositional (K_2O-SiO_2) diagrams for (A) volcanic rocks and (B) hypabyssal rocks of the Darb Zubaydah ophiolite. Fields are described by Ewart (1982) and are listed from left to right: bottom row, low-K tholeiite, low-K basaltic andesite, low-K andesite, low-K dacite, low-K rhyolite; second row, calc-alkali basalt, calc-alkali basaltic andesite, calc-alkali andesite, calc-alkali dacite, calc-alkali rhyolite; third row, high-K basalt, high-K basaltic andesite, high-K andesite, high-K dacite, high-K rhyolite; top row, absarokite, shoshonite, banakite.

Aleutian islands by Marsh (1982) who attributes them to two styles (open and closed) of near-surface magmatic behavior.

The Darb Zubaydah basalts and andesites plot on a titanium-zirconium diagram (fig. 17A) in the fields A, B, and D and in the low-Zr end of field C. A similar pattern is defined by the data for the basaltic- and andesitic-composition hypabyssal rocks (fig. 17B). Taken at face value, the fields of Pearce and Cann (1973) would assign mid-ocean ridge origins to the basalts. However, Stern and Bibee (1984) describe high-titanium/zirconium volcanic rocks of Esmeralda Bank a volcanic center that is located in the back-arc region of the Mariana volcanic arc, that also plot in the mid-ocean ridge basalt field. Furthermore, the volcanic basalts and andesites are interbedded with abundant rhyolitic rocks that must have formed in the same tectonic setting. Perhaps the Darb Zubaydah ophiolite could have formed near a volcanic center similar to Esmeralda Bank. Note that the rhyolitic rocks of the Darb Zubaydah ophiolite plot within or near field C.

The volcanic and hypabyssal rocks that have basaltic to andesitic compositions plot within field B and the high-titanium end of field C on the zirconium-titanium-yttrium plot (on figure 18). This distribution suggests a calc-alkaline affinity (Pearce and Cann, 1973), which would be consistent with formation in an island-arc environment. Note that the rhyolites plot at the low-titanium end of the diagram and are mostly outside the defined fields.

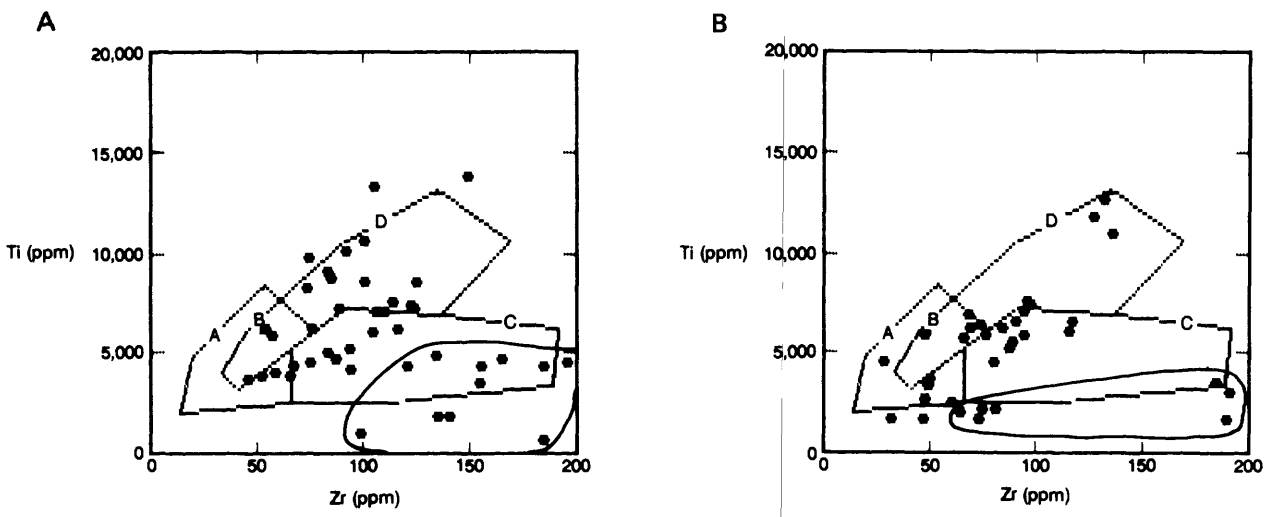

Figure 17--Compositional (Ti-Zr) diagrams for (A) volcanic rocks and (B) hypabyssal rocks of the Darb Zubaydah ophiolite. Fields are defined by Pearce and Cann (1973) as follows: Ocean-floor basalts (MORB), fields D and B; low-K tholeiites, fields A and B; calc-alkali basalts, fields C and B. Rhyolitic compositions are encircled to distinguish them from basalts and andesitic compositions.

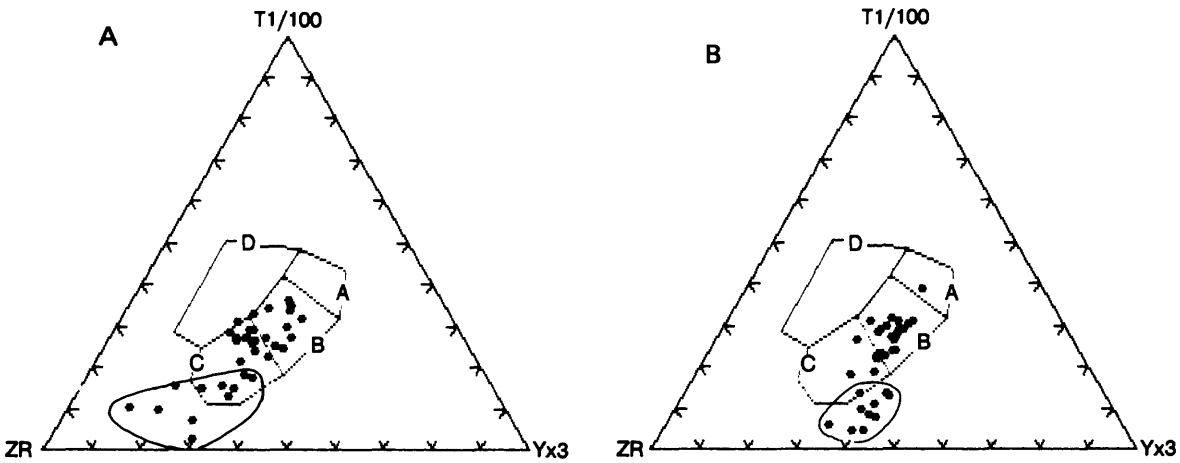

Figure 18--Zr-Ti-Y ternary diagrams for (A) volcanic rocks and (B) hypabyssal rocks fo the Darb Zubaydah ophiolite. Fields are defined by Pearce and Cann (1973) as follows: oceanic-island basalts, field D; ocean-floor basalts, field B; low-K tholeiites, fields A and B; calc-alkali basalts, fields C and B. Rhyolitic compositions are encircled to distinguish them from basalts and andesitic compositions.

Bi'r Tuluhah

Using AFM diagrams (fig. 19), two groups of volcanic rocks are discernable in the Bi'r Tuluhah area. The metabasalt and metatuff (fig. 19A) show more spread than the Darb Zubaydah ophiolite, perhaps reflecting a greater degree of alteration attending deformation in the Nabitah fault zone. Nevertheless, the metabasalt and metatuff compositions define a field that, like the Darb Zubaydah volcanic rocks, extends from the tholeiitic region to the calc-alkali region of the diagram and does not display an Fe-enrichment trend within the low-alkali rocks. In contrast, almost all of the Hulayfah volcanic rocks plot within the calc-alkali region and display a weak Fe-enrichment trend in the low-alkali rocks. The amphibolite, mafic dikes in serpentinite, and fine-grained diorite (figs. 19B-D) plot as relatively tight clusters within the calc-alkali region. This projection sheds little light on the affinities of the amphibolite and mafic dikes. However, the fine-grained diorite cluster falls within the field defined by the Hulayfah volcanic rocks (fig. 19E) and overlaps only slightly with the field defined by the metabasalt and metatuff. This suggests (but does not prove) that the fine-grained diorite could be the hypabyssal equivalent of the Hulayfah volcanic rocks.

The metabasalt and metatuff are also distinguishable from the Hulayfah group on a K_2O-SiO_2-variation diagram (fig. 20). Like the Darb Zubaydah volcanic and hypabyssal rocks, the metabasalt and metatuff (fig. 20A) show wide ranges in K_2O and SiO_2 abundances, extending from low-K tholeiites to calc-alkali rhyolites. There is a suggestion of bimodal volcanism with a compositional gap in the range of about 56 to 67 percent SiO_2; compared to the Darb Zubaydah ophiolite, however, the spread of data points is more like that of the hypabyssal rocks than the volcanic rocks. Compared to the metabasalt and metatuff of the Darb Zubaydah ophiolite, SiO_2 contents of the Hulayfah volcanic rocks are restricted to a small range (50-60 percent) and K_2O concentrations are higher in rocks of similar SiO_2 content. Figure 20 does not clarify the relationships of the amphibolite or the fine-grained diabase with respect to either group of volcanic rocks. The dikes in serpentine (fig. 20C) do, however, display a bimodal spread of compositions that is similar to the metabasalt and metatuff.

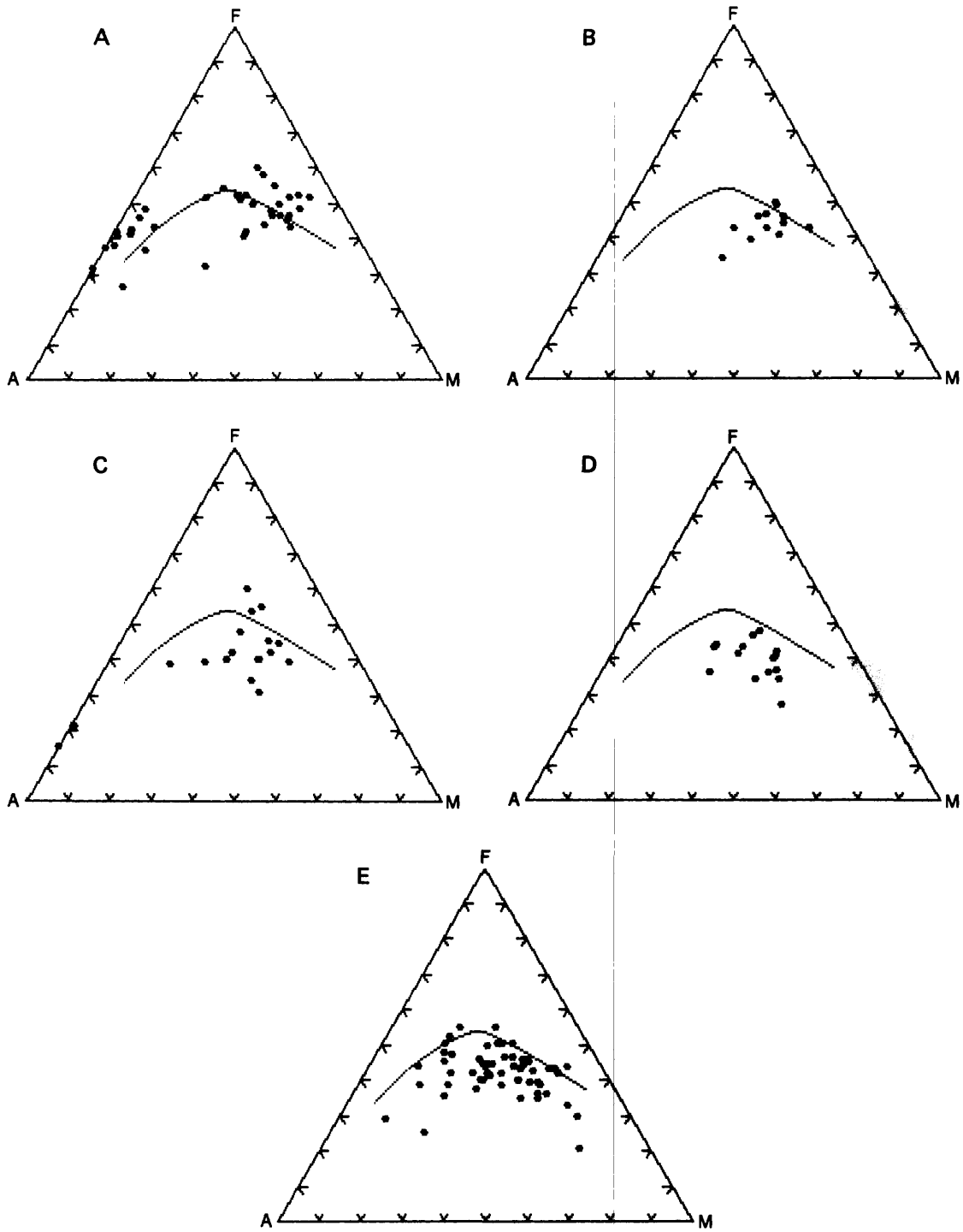

Figure 19—AFM diagrams for rocks of the Bi'r Tuluhah area: (A) metabasalt and metatuff, (B) amphibolite, (C) mafic dikes in serpentinite, (D) fine-grained diorite, and (E) Hulayfah group volcanic rocks. Axes are defined as follows: A, $Na_2O + K_2O$; F, $FeO + 0.9\ Fe_2O_3$; M, MgO. Curve in center of diagram marks boundary between tholeiitic (upper) and calc-alkaline (lower) regions of Irvine and Baragar (1971).

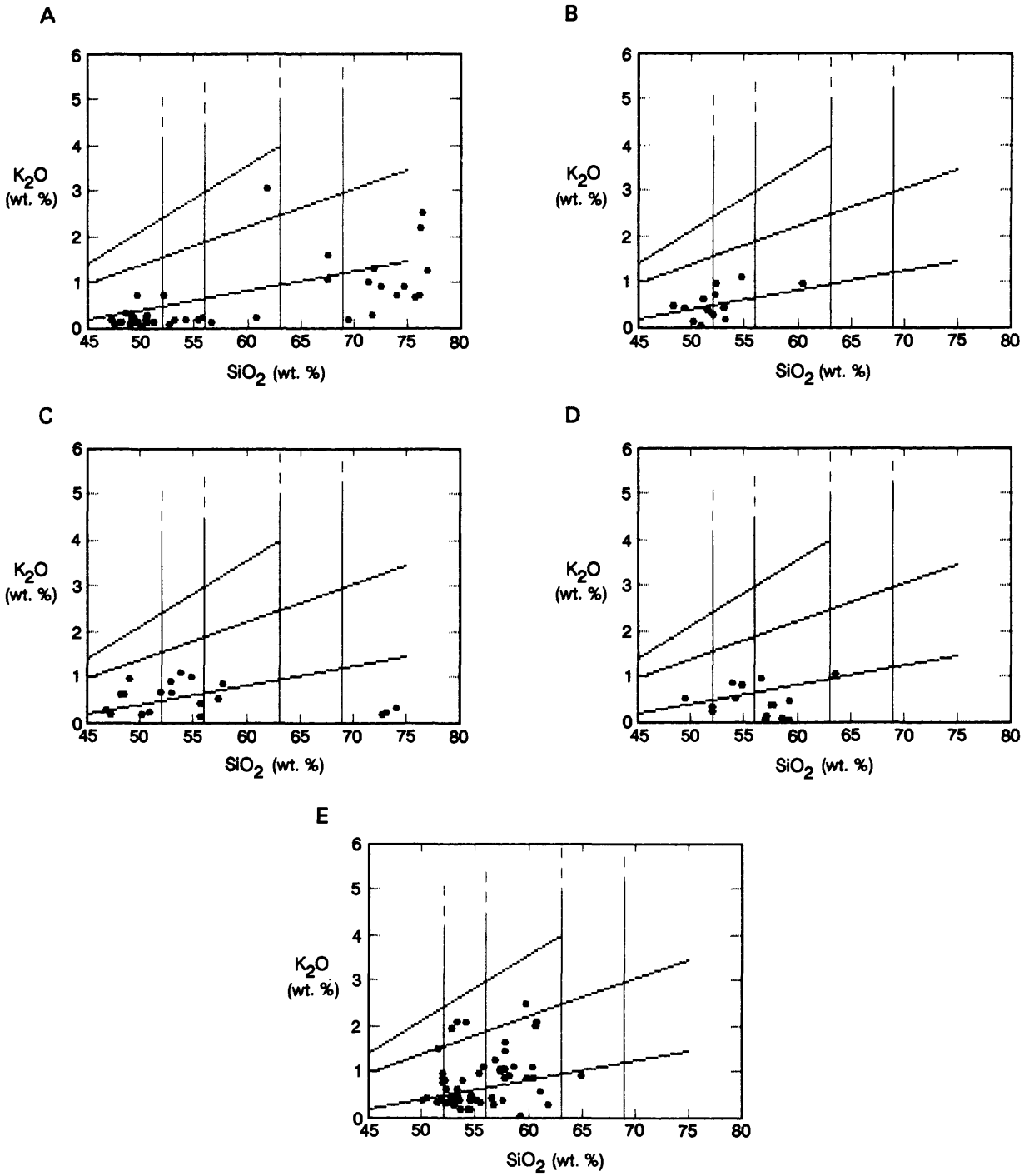

Figure 20--Compositional (K_2O-SiO_2) diagrams of rocks of the Bi'r Tuluhah area: (A) metabasalt and metatuff, (B) amphibolite, (C) mafic dikes in serpentinite, (D) fine-grained diorite, and (E) Hulayfah group volcanic rocks. Fields are described by Ewart (1982) and are listed from left to right: bottom row, low-K tholeiite, low-K basaltic andesite, low-K andesite, low-K dacite, low-K rhyolite; second row, calc-alkali basalt, calc-alkali basaltic andesite, calc-alkali andesite, calc-alkali dacite, calc-alkali rhyolite; third row, high-K basalt, high-K basaltic andesite, high-K andesite, high-K dacite, high-K rhyolite; top row, absarokite, shoshonite, banakite.

The titanium-zirconium variation diagrams (see figure 21) also distinguish the metabasalt and metatuff from the rocks of the Hulayfah group. The basalt and andesite from the metabasalt and metatuff units (fig. 21A) plot in fields A, B, and D and the low-zirconium end of field C; this distribution is strikingly similar to the distribution defined by the Darb Zubaydah volcanic rocks. Furthermore, these units contain rhyolitic rocks that have low titanium and high zirconium concentrations similar to the rhyolite of the Darb Zubaydah ophiolite. In contrast, the fah compositions (fig. 21E) define a single trend that falls midway between the ocean-floor and calc-alkali fields of Pearce and Cann (1973). The compositions of the amphibolite and the mafic dikes in serpentinite (figs. 21B and 21C) both define patterns similar to those of the basalts and andesites of the metabasalt and metatuff. The data for the fine-grained diorite (fig. 21D) is less definitive and does not distinguish between a possible cogenetic relationship with the Hulayfah group or with the metabasalt and metatuff.

Ternary plots for the Bi'r Tuluhah area (fig. 22) corroborate the above observations. The basalts and andesites from the metabasalt and metatuff units (fig. 22A) plot primarily in field B, which is a similar distribution to that of the basalts and andesites of the Darb Zubaydah ophiolite (fig. 18A). The interbedded rhyolites plot at the low-titanium end of the diagram, outside the fields defined by Pearce and Cann (1973), and define a field that is again similar to analogous rocks of the Darb Zubaydah ophiolite (fig. 18A). In contrast, the Hulayfah compositions define a tight cluster in field C and the low-titanium end of field B. The scatter of data points for the mafic dikes in serpentinite (fig. 22C) is like that of the metabasalt and metatuff. The amphibolite data plot mainly in field B, with higher titanium values than the Hulayfah data; these data are like the higher-titanium compositions of the metabasalt and metatuff. The fine-grained diorite defines a field almost identical to that of the Hulayfah group, strongly suggesting that these rocks are related.

Spinel Analyses

Figure 23 presents the average spinel compositions of 56 samples of serpentinized peridotite. Each datum represents the average of 15 to 20 analyses of unaltered cores of spinel grains in a single rock. The data range in chromium-value [100 x Cr/(Cr + Al)], from about 40 to 90, with a clear compositional gap in the range of 60 to 65. The compositional range, taken as a whole, is similar to the range in spinel composition to the Type-II peridotites of Dick and Bullen (1984). These authors pointed out that spinel compositions in abyssal peridotite from oceanic fracture zones (Type-I spinel) rarely exceed chromium values of 60, and that, therefore, spinels with chromium values greater than 60 are indicative of petrogenetic processes not active at midocean ridges. In contrast, chromium values of spinel obtained from island-arc-related volcanic rocks, xenoliths, and xenocrysts range from 38 to almost 90. Cumulate peridotite from southeast Alaskan intrusions (which are inferred to represent the magma chambers of an ancient island arc) contains spinel with chromium values in excess of 60. On the basis of these observations, Dick and Bullen (1984) have suggested that spinel with chromium values in excess of 60 (Type II) are indicative of an island-arc environment, and that Type III spinels, which show a wide range in composition, are indicative of upper-mantle lithosphere that was generated at a mid-ocean ridge but modified by extraction of partial melt beneath an island arc. However, the compositional gap at the 60-65 chromium value in the Nabitah spinels does not fit the Type-III concept because partial melting would produce a continuum in spinel compositions. Instead, the gap suggests that a significant amount of serpentinite along the Nabitah fault zone was produced by alteration of cumulus peridotite formed in magma chambers beneath an ancient island arc. Rocks with high-chromium-value spinels would have crystallized in these magma chambers, and rocks with the low-chromium-value spinels may be altered samples of subarc mantle. It is significant that, on the basis of petrography and whole-rock chemistry, Hariri (1985) has inferred that the Zalm ultramafic complex, which lies along the Nabitah fault zone south of the Jabal al Qub area, was originally an olivine-websterite cumulate.

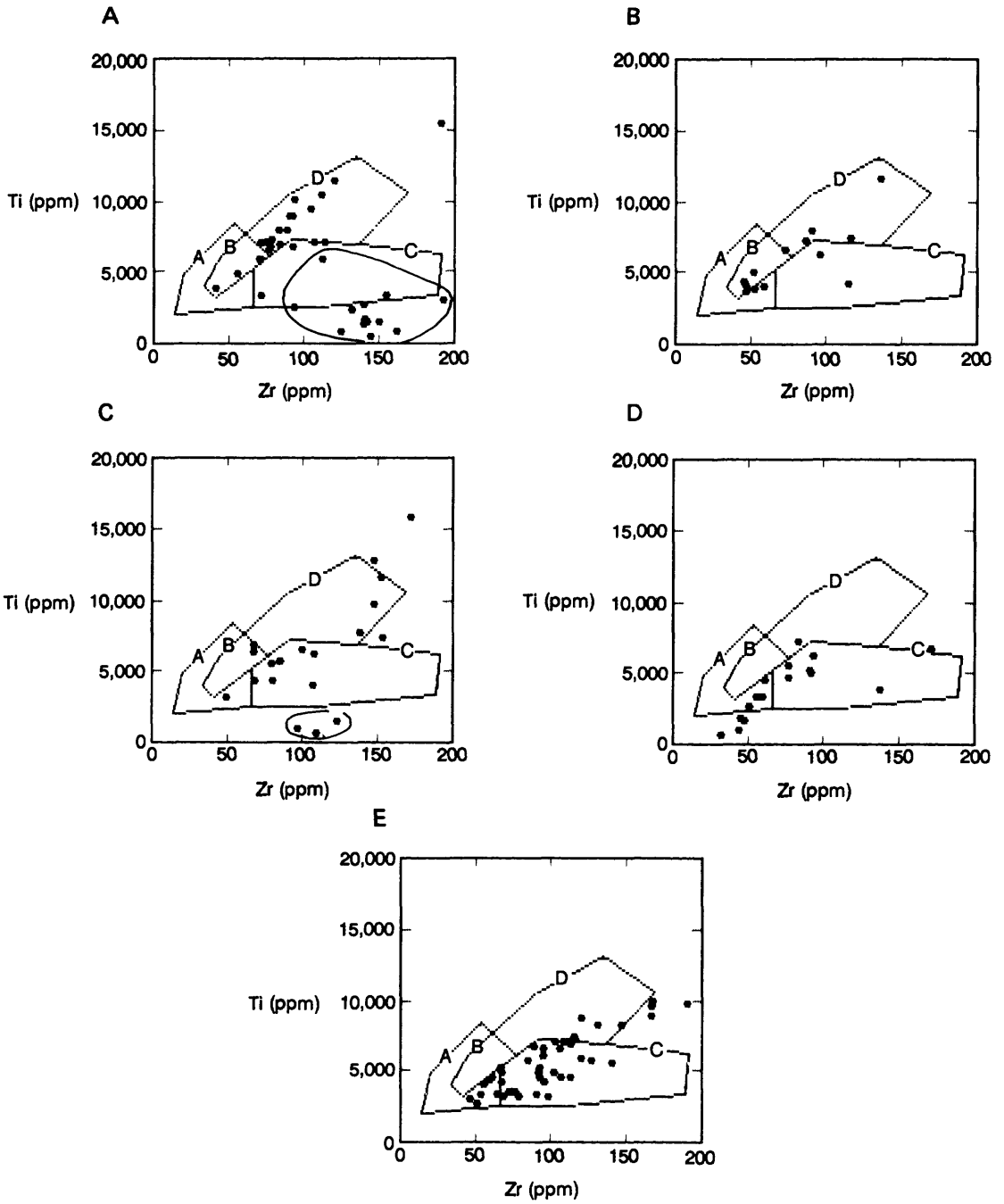

Figure 21--Compositional (Ti-Zr) diagrams for rocks of the Bi'r Tuluhah area: (A) metabasalt and metatuff, (B) amphibolite, (C) mafic dikes in serpentinite, (D) fine-grained diorite, and (E) Hulayfah group volcanic rocks. Fields are defined by Pearce and Cann (1973) as follows: Ocean-floor basalts (MORB), fields D and B; low-K tholeiites, fields A and B; calc-alkali basalts, fields C and B. Rhylotic-compositions are encircled in A and C.

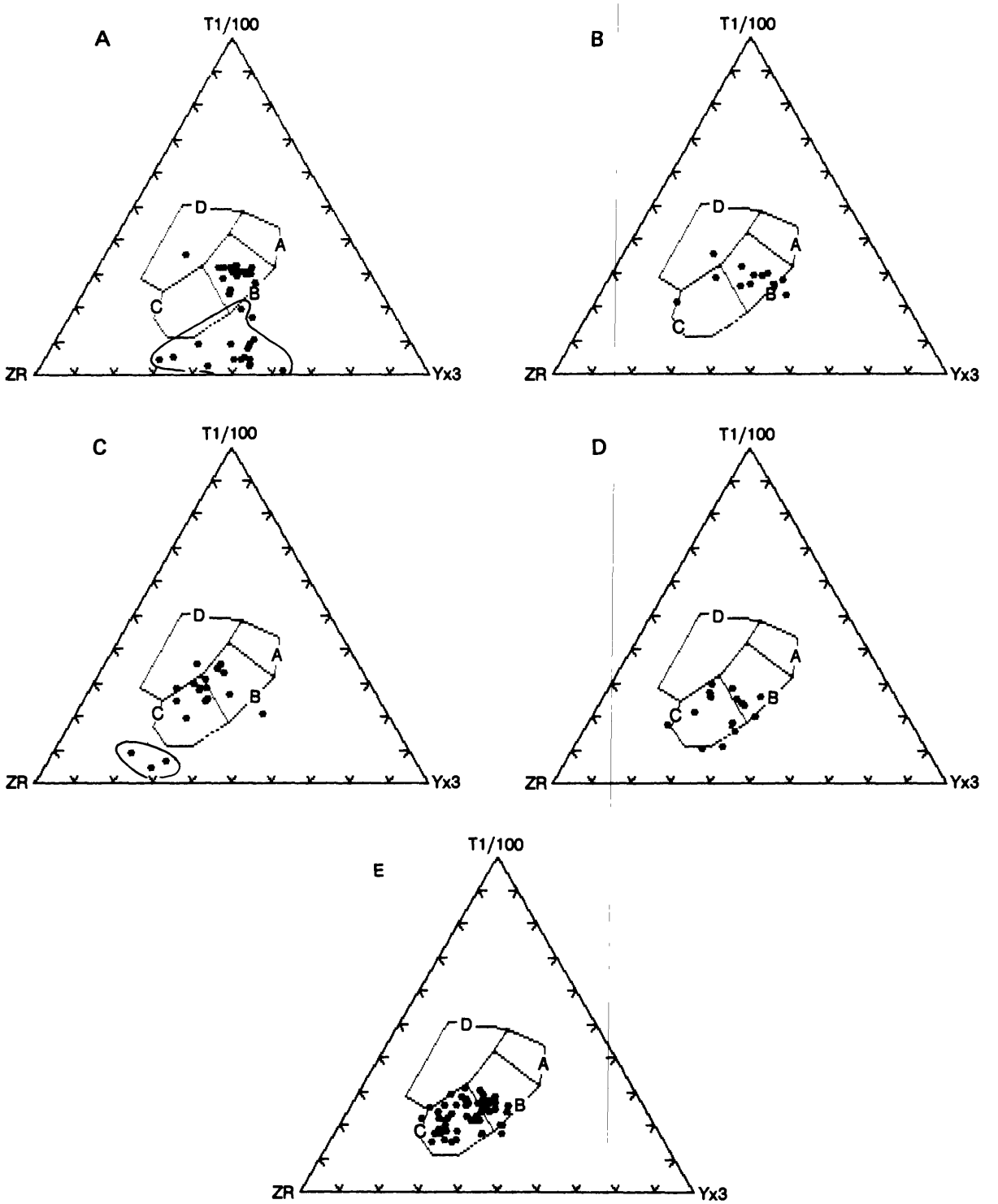

Figure 22--Zr-Ti-Y ternary diagrams for rocks of the Bi'r Tuluhah area: (A) metabasalt and metatuff, (b) amphibolite, (C) mafic dikes in serpertinite, (D) fine-grained diorite, and (E) Hulayfah group volcanic rocks. Fields are defined by Pearce and Cann (1973) as follows: oceanic-island basalts, field D; ocean-floor basalts, field B: low-K tholeiites, fields A and B; calc-alkali basalts, fields C and B. Rhyolitic compositions are encircled in A and C.

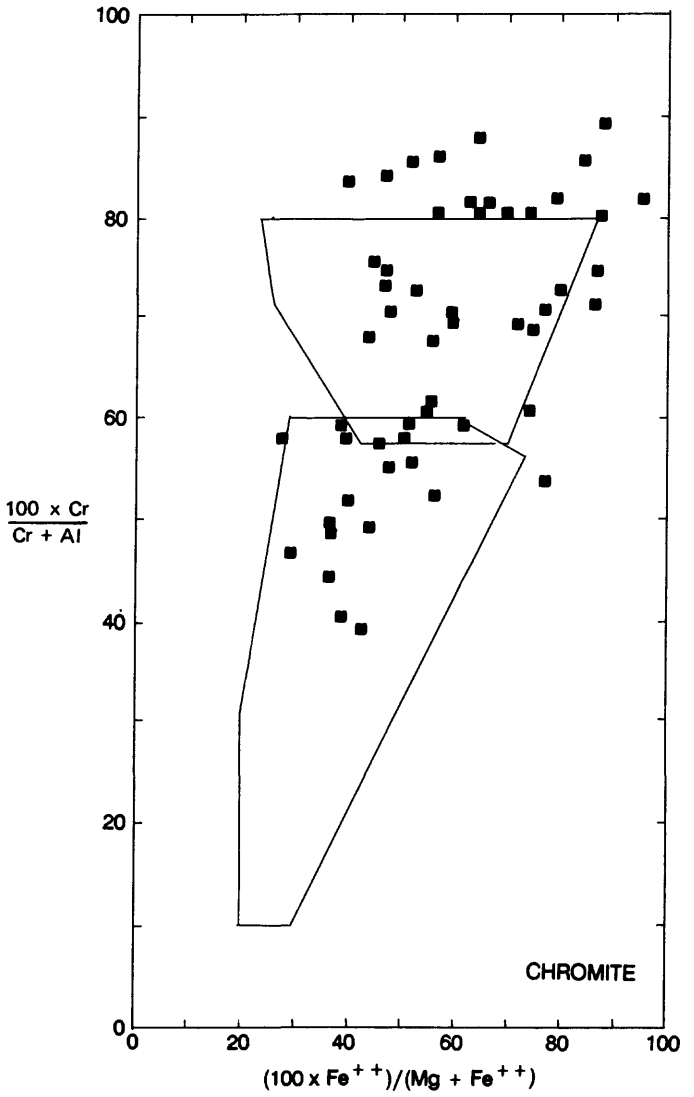

Figure 23--Plot of Cr-value, 100 x Cr/ (Cr + A1), versus Fe-value, 100 x Fe^{++}/ (Mg + Fe^{++}), for the average compositions of primary spinel in 56 serpentinite samples from the Nabitah fault zone. Fields derived from other investigations are indicated for reference: top, compositional range for cumulate peridotite in continental layered intrusions (Irvine, 1967); bottom, compositional range for abyssal peridotite (Dick and Bullen, 1984).

REGIONAL SYNTHESIS

TERRANES

The area displayed in figure 2 contains fragments of three geologically distinct terranes as defined by Stoeser and Camp (1984). The Hijaz terrane is located north of the Bi'r Umq suture and west of the Nabitah fault zone; the Asir terrane is located south of the Bi'r Umq suture and west of the Nabitah fault zone; and the Afif terrane is located east of the Nabitah fault zone. Although other geologic names have been applied to these regions (see, for example, Johnson, 1983), this terminology is adopted in this report because it has become entrenched in the literature.

NABITAH FAULTING

The remarkable convergence of data on the Nabitah fault zone from the Bi'r Tuluhah, Wadi Khadra, and Jabal al Qub areas allow some solid conclusions and reasonable inferences to be made about the tectonic evolution of the region (fig. 2).

In each of the three areas, the structure is dominated by subvertical north-trending strands of the Nabitah fault system. At Bi'r Tuluhah, the Nabitah fault system is represented by a 7-km-wide fault zone of juxtaposed tectonic slivers. At Wadi Khadra, the fault system is represented by anastomosing faults in a 5-km-wide phyllonite zone. At Jabal al Qub, the fault system is represented as anastomosing faults that bound horsts of serpentinite. In all three locations, the Nabitah fault zone separates rocks with different metamorphic histories. These observations support assertions (Schmidt and others, 1978; Stoeser and Camp, 1984) that the Nabitah fault zone is a major crustal break. Gonzalez (1974) and Caby (1983) preted the Nabitah fault zone to be a strike-slip feature. However, the concept that the Nabitah zone was a relict of a subduction or obduction zone has been more widely accepted by the geologic community (Schmidt and others, 1978; Camp, 1984; Stoeser and others, 1984; Stoeser and Camp, 1984; Agar, 1985; Stacey and Agar, 1985; Pallister and others, 1987). In this study, all structural data support the interpretation of Gonzalez (1974) and Caby (1983), and suggest that left-lateral strike-slip motion occurred on the fault system. Steeply plunging folds at Bi'r Tuluhah, Wadi Khadra, and Jabal al Qub are spatially associated with the Nabitah faults, suggesting strike-slip motion. Left-lateral displacement is suggested by drag folds on strands of the Nabitah fault system in these areas and by the orientations and asymmetrical folding of quartz veins in the Wadi Khadra phyllonite.

AFIF TERRANE

Nabitah Volcanic Arc

The region immediately east of the Nabitah fault zone is underlain by a composite batholith of granodiorite, diorite, and tonalite. One zircon age obtained from rocks of the Bi'r Tuluhah area indicates that granodiorite to dioritic intrusive activity occurred at 710 Ma. Motion on the Nabitah fault system appears to have been coincident with the intrusion of some of these rocks. At Bi'r Tuluhah, dikes in serpentinite were deformed to different degrees, suggesting emplacement during the deformation of the serpentinite in the Nabitah fault zone. Diorite and quartz-diorite intrusions at Bi'r Tuluhah truncate some strands of the Nabitah fault system, but are crosscut by other strands. Metadiorite at Jabal al Qub and granodiorite at Wadi Khadra have north-striking foliation and protoclastic texture that may have formed by intrusion during Nabitah faulting. The location and volume of the batholith (fig. 2) suggest that a major, north-trending calc-alkaline volcanic axis was active east of the Nabitah fault zone and contemporaneous with fault activity. This hypothetical volcanic axis is named the Nabitah volcanic arc in this report.

Rharaba Complex

On the basis of relationships in the Jabal al Qub area, gabbroic and ultramafic cumulus rocks of the Rharaba complex are interpreted to be components of the batholith east of the Nabitah fault zone. Analogy to cumulus gabbro and peridotite complexes in western North America

suggests that rocks of the Rharaba complex crystallized as cumulates in magma chambers beneath island-arc volcanic centers. According to this theory, exposures of the Rharaba complex should identify the paleo-axis of the Nabitah volcanic arc.

Ophiolitic Rocks of the Western Afif Terrane

Pre-batholithic rocks in this terrane are mainly roof pendants and septa composed of metamorphosed ophiolitic rocks. The Darb Zubaydah ophiolite appears to be a virtually intact model for these rocks. This ophiolitic section is situated within the Nuqrah belt, which is an exposure of volcanic and hypabyssal rocks that is essentially continuous from the ophiolite to the type locality near Nuqrah (fig. 2). Mapping by Delfour (1977, 1981) indicates that the same lithologies are present along the belt, although an ophiolitic section is apparently not preserved in most places. Thus, the rocks are interpreted to be approximately the same age. Compared to the rocks of the Darb Zubaydah ophiolite, the ophiolitic rocks in the Nabitah fault zone at Bi'r Tuluhah have similar metamorphic grade, lithologies, and geochemistry, suggesting that they were rifted from the ophiolitic terrane during Nabitah faulting. On the basis of petrologic similarities, the ophiolitic rocks at Wadi Khadra are also interpreted to be part of the same section; the occurrence of ophiolitic roof pendants between the Wadi Khadra and Bi'r Nifazi areas supports this inference and suggests that the ophiolitic rocks may have once been a continuous cover over the intervening batholith. The extreme deformation and dismemberment of the ophiolitic rocks in the Nabitah fault zone at Wadi Khadra further supports the hypothesis that Nabitah faulting disrupted and transported rocks from the ophiolitic terrane. The age of this pre-batholithic ophiolitic terrane appears to be approximately 800-850 Ma based on the radiometric age dates obtained from rocks of the Nuqrah and Bi'r Tuluhah areas.

The ophiolitic rocks appear to have formed in an island-arc environment. Thick sections of interbedded volcanoclastic rock, pillow basalt, volcanic wacke, and lahar present in the Darb Zubaydah ophiolite suggest that deposition of these rocks occurred near a volcanic center. Major- and trace-element abundances in the Darb Zubaydah volcanic rocks and fault-zone volcanic rocks at Bi'r Tuluhah are similar to those found in volcanic rocks from active island arcs in the western Pacific. The compositions of spinels found in the serpentinite are similar to those found in island arcs or ophiolites with island-arc affinities. No evidence was found for an ocean-ridge or back-arc-basin origin for these rocks.

Amphibolite of the Western Afif Terrane

Amphibolite crops out in roof pendants in the batholith, often associated with serpentinite. Serpentinized peridotite appears to have been thrust from west to east over amphibolite in the Jabal al Qub area. The same relation is suggested by the association and outcrop patterns of serpentinite and amphibolite in the Bi'r Tuluhah area where amphibolite typically crops out along the east side of serpentinite bodies. Indeed, this relationship was recognized repeatedly during reconnaissance of the peridotite massifs between Bi'r Tuluhah and Wadi Khadra (fig. 2). Observations such as the above have been interpreted to indicate obduction of the serpentinite protolith over the amphibolite (Pallister and others, 1987).

Although the evidence suggests that the serpentinite-amphibolite contact is tectonic, obduction is not consistent with all the data. Compared to obduction-related metamorphic rocks, "amphibolite-grade" assemblages near the Nabitah fault zone are significantly more extensive and indicate lower metamorphic temperatures. Malpas and Stevens (1979) observed that obduction-related metamorphism is typically confined to a narrow zone (<130 m) immediately beneath an overthrust sheet of ultramafic rocks and that the metamorphic grade in this zone ranges from greenschist to almandine- and pyroxene-amphibolite nearest the ultramafic rocks. In contrast, amphibolite with a vertical foliation crops out in a belt as much as 10 km wide in the Jabal al Qub area, and the presence of scattered amphibolite roof pendants to the north suggests that it must have been an extensive component of the pre-batholithic terrane. Near the Nabitah faults, the maximum metamorphic grade is epidote amphibolite; the same metamorphic-mineral

assemblages are found in metamorphosed dikes in the overlying serpentinite. The extent and grade of metamorphism argue for a regional thermal event rather than the contact-style metamorphism associated with obduction. The metamorphism may be related to early emplacement of the batholithic rocks east of the Nabitah fault zone. The tectonic significance of the serpentinite-amphibolite contact is unclear; without additional work, it is impossible to identify the mechanism as obduction or another process, such as intra-arc thrusting or subduction.

Hijaz Terrane

In the Bi'r Tuluhah area, the Hijaz is underlain by the Hulayfah group, which is composed of volcanic wacke and volcanic rocks ranging in composition from basalt to andesite. On the basis of the presence of shallow-water and subareal features and the compositions of the volcanic rocks, Delfour (1981) suggested that the Hulayfah group was deposited in an island-arc environment. Khattan (1983) concluded that the rocks of the Hulayfah group formed in an environment analogous to a moderately mature Cenozoic island arc. The present study indicates that the Hulayfah group is less metamorphosed than and geochemically distinct from nearby volcanic rocks within the Nabitah fault zone and in the Afif terrane. Available geochronologic data suggests that the age of the Hulayfah group may be about 740 Ma, or 50-100 m.y. younger than those rocks. These observations should discourage assignment of rocks from opposite sides of the Nabitah fault zone to the Hulayfah group.

The Hijaz terrane in the Wadi Khadra area is underlain by interbedded basalt and breccia unlike any rocks of the Hulayfah group found in the Bi'r Tuluhah area. These rocks may have been deposited along the scarp of the Nabitah fault zone.

Asir Terrane

In the Jabal al Qub area, the Asir terrane is underlain by interbedded basalt, andesite, rhyolite, and volcanic wacke, which are intruded by an 815-Ma tonalite pluton. Geochemical data are not available for these rocks, but their lithologic associations suggest that they were formed in the vicinity of an island arc. An age greater than 815 Ma for the volcanic and sedimentary rocks is significantly older than that of the volcanic rocks in the Hijaz terrane to the north. Similar observations constitute the basis for identification of the Bi'r Umq suture as a major plate boundary (Stoeser and Camp, 1984; Pallister and others, 1987).

Bi'r Umq Suture

The Bi'r Umq suture (fig. 2) is the eastern extension of the Port Sudan suture and one of the major plate boundaries of the Arabian Shield (Camp, 1984; Stoeser and Camp, 1984). Its intersection with the Nabitah fault zone is poorly exposed. Based on similar zircon ages obtained from plagiogranite at Bi'r Umq and Bi'r Tuluhah, Pallister and others (1987) suggest that the ophiolitic rocks found along the Nabitah suture and north of the Bi'r Umq suture may be a continuation of the Bi'r Umq suture that was rotated or transposed into a northerly trend. It should be noted, however, that there is evidence for left-lateral strike-slip motion on the Nabitah fault zone both to the north and south of the Bi'r Umq suture. This suggests that the Nabitah fault zone is a through-going structure with a consistent palinspastic history. Furthermore, geochronologic and geochemical data are also consistent with the derivation of the ophiolitic rocks at Bi'r Tuluhah from the Afif terrane. This does not rule out tectonic transport of fragments from the Bi'r Umq suture, but it demonstrates that it is not necessary to explain the age data. Also, structural relations at Wadi Khadra demonstrate that deformation, entrapment, and (presumably) transport of fragments of the Afif terrane occurred along the Nabitah fault zone. Based on these observations, the Nabitah fault zone is believed to truncate the Bi'r Umq suture.

Offset of the Asir Terrane and the Bi'r Umq Suture

Structural evidence for left-lateral, strike-slip motion on the Nabitah fault system is consistent with the apparent offset of >800-Ma volcanic rocks (fig. 2). At the latitude of Nuqrah and the Bi'r Tuluhah area, the Nabitah fault zone juxtaposes >800-Ma volcanic rocks to the east against <750-Ma volcanic rocks to the west. On the west side of the Nabitah fault, >800-Ma volcanic rocks

crop out south of the Bi'r Umq suture. If the Afif and Asir terranes were once a single terrane, their age distributions could be explained by transport of the Afif terrane northward relative to the Hijaz and Asir terranes along the Nabitah fault zone. This model suggests that the Bi'r Umq suture may be present in the Afif terrane, but it is offset to the north. It is tempting to speculate that ultramafic rocks located at lat 27.5° N. and long 42° E. (fig. 1) may be the northeastern expression of the Bi'r Umq suture. Another candidate (Pallister and others, 1987) for the Bi'r Umq suture is the Raha thrust fault: it trends northeast from lat 26° N. and long 42° E., and contains fragments of ultramafic rocks, gabbro, and listwaenite (Johnson and Williams, 1984).

TECTONIC MODEL

Considerable attention has been devoted to modeling the late Proterozoic tectonics of the Arabian Shield in terms of modern plate tectonics. With the exception of Caby (1983), however, no attempt has been made to explain left-lateral, strike-slip motion in the Nabitah fault zone. This section attempts to construct a model for the Arabian Shield as it may have appeared at the time Nabitah faulting was active. Such efforts are necessarily exercises in analogy. Consequently, the tectonics of two regions in which strike-slip faulting and calc-alkaline volcanism are presently active are discussed. These are Sumatra and the Japanese Islands north of Hokkaido. A third region, California, is also discussed because its geology has been well studied and, like the Arabian Shield, it contains a fossil tectonic environment in which strike-slip faulting appears to have played a major role. To facilitate comparison, all maps are presented at the same scale as figure 1, but the maps of Sumatra and the northern Japanese Islands have been rotated.

SUMATRA

The principal modern tectonic elements in the region of Sumatra are illustrated in figure 24, and the following description is abstracted from Hamilton (1979) unless specifically referenced otherwise.

The Indian plate is currently being subducted obliquely beneath Sumatra. An accretionary prism of highly deformed sedimentary rocks rests on the Indian plate east of the Java Trench (barbed line) and underlies the chain of small islands off the west coast of Sumatra. These islands, known as the Nias Islands, constitute a nonvolcanic forearc. A fore-arc basin, known as the Mentawai Trough, is situated between the Nias Islands and the Sumatran coast and is presently accumulating turbiditic sediments shed from Sumatra. Seismic-reflection profiles show that deformation of these sediments increases progressively toward the accretionary prism to the west. Western Sumatra is bowed upward into a geanticline upon which a narrow axis of active and recently volcanoes has formed. The Central Sumatran fault runs the length of Sumatra and is coincident with this volcanic axis. The Central Sumatran fault is an active, right-lateral, strike-slip feature, and there is a general agreement that it developed in response to oblique subduction of the Indian Plate (Beck, 1983; Huchon and Le Pichon, 1984). The trace of the Central Sumatran fault is locally obscured by Quaternary volcanic and sedimentary deposits. However, near the projection of the fault, Kastowo and Leo (1973) mapped windows in Quaternary deposits underlain by serpentinite and sheared serpentinite with mafic boudins. Hamilton (1979) suggests that the serpentinite may be a relict of an older subduction complex, but an origin by tectonic emplacement along a transform fault is also possible.

KURIL ARC

Kimura (1986) described the tectonics of the Japanese Islands north of Hokkaido (fig. 24) and concluded that many of the tectonic elements are the direct result of oblique subduction of the Pacific Plate. That author's observations are as follows: Chains of Quaternary volcanoes and volcanic islands located north of Hokkaido constitute the Kuril volcanic arc. These features, and large anticlines and smaller folds on the islands of

Etoroph and Urup, are arranged en echelon; they are oriented oblique to the Kuril Trench, but are nearly perpendicular to the velocity vector of the Pacific Plate. A nonvolcanic frontal arc (expressed at sea level by a chain of tiny islands) is developed to the east of the Kuril volcanic arc. A sediment-filled fore-arc basin is situated between these two arcs. A right-lateral strike-slip fault is located at the boundary of the fore-arc basin and volcanic arc. Bathymetric measurements indicate that northeast-trending grabens are presently active in the fore-arc basin. Magnetic anomalies located along the frontal arc are thought to be serpentinite diapirs. En echelon thrust faults are developed in northern Hokkaido. Kimura (1986) concluded that (1) the strike-slip faulting and orientation of the en echelon volcanic chains and fold belts are the result of oblique subduction, (2) diapiric rise of serpentinite is due to strike-slip faulting, (3) the development of grabens is due to tension in the fore-arc basin developed during its movement south, and (4) the thrust faults in Hokkaido resulted from collision of this oblique system with the Eurasian Plate.

California

A simplified geologic map of California showing Late Paleozoic to Early Cenozoic units and major structures is illustrated in figure 25. The Late Mesozoic Franciscan Melange Complex (Ernst, 1965) crops out along the northern California coast and is bordered to the east by marine sedimentary rocks of the Knoxville Formation (Hamilton, 1969). The boundary of these units is the Coast Range Thrust Fault, a locus of peridotite outcrops. The Knoxville Formation was deposited at the base of the Great Valley Sequence, a thick section of sedimentary rocks deposited in the Great Valley of California. These rocks range in age from Late Mesozoic to recent (Hackel, 1966). East of the Great Valley are the Late Mesozoic-Early Cenozoic granitic plutonic rocks of the Southern California Batholith. Late Paleozoic-Early Mesozoic ophiolitic rocks, island-arc volcanic rocks, amphibolite, serpentinite-matrix melange, and turbiditic sedimentary rocks crop out along the northwestern Sierra Nevada, where they are intruded by the batholith (Saleeby, 1982). These prebatholithic rocks are cut by swarms of north-trending faults (the Foothills Fault Zone). Exposures of ultramafic rock are abundant along these faults, which are strike-slip structures (based on steeply plunging fold axes) (Cebull, 1972).

Prebatholithic rocks in the northern Sierra Nevada formed during three distinct episodes (300-160 Ma) and involved the opening and closing of small basins (Saleeby, 1982). During Late Mesozoic to Early Cenozoic time, subduction off the California coast resulted in formation of the Franciscan Melange Complex (Ernst, 1965) in an accretionary prism, the deposition of the Great Valley Sequence in a fore-arc basin, and the intrusion of the Sierra Nevada Batholith as the plutonic core of an island arc (Hamilton, 1969). Deposition of the Great Valley Sequence continued for about 80 m.y. after cessation of Sierran plutonic activity, which suggests that fore-arc basins are long-lived features. Deformation of the prebatholithic rocks of the Sierra Nevada was interpreted in terms of transform tectonics resulting from oblique subduction, a theory supported by paleomagnetic data, displaced faunal belts, and melange development (Saleeby, 1983; Beck, 1983).

Application to Saudi Arabia

A simplified geologic map of the Arabian Shield modified from the lithostratigraphic compilation of Johnson (1983) is presented in figure 25. Stoeser and Camp (1984) divide the Arabian Shield into several terranes (or microplates) that are bounded by suture zones. The northwestern shield is underlain by the Midyan terrane, which is composed of island-arc rocks ranging in age from 700 to 600 Ma. To the south, the Midyan terrane is separated from the Hijaz terrane by the Yanbu suture (Y). The Hijaz terrane contains island-arc assemblages that range from 800 to 700 Ma in age. The Bi'r Umq suture (B) juxtaposes the Hijaz terrane with the Asir terrane to the south. The Asir terrane contains island-arc assemblages that range in age from >900 to 800 Ma in age. The Nabitah fault zone (N; Nabitah suture of Stoeser and Camp, 1984) lies athwart the Bi'r Umq suture and forms the western boundary of the Afif terrane. The Al Amar suture (A) forms the eastern boundary of the Afif terrane, east of which are the Abt schist and, at the easternmost projection of the Shield, the Ar Rayn terrane. Voluminous granitic rocks intrude all of these terranes and left-lateral Najd faulting has offset the

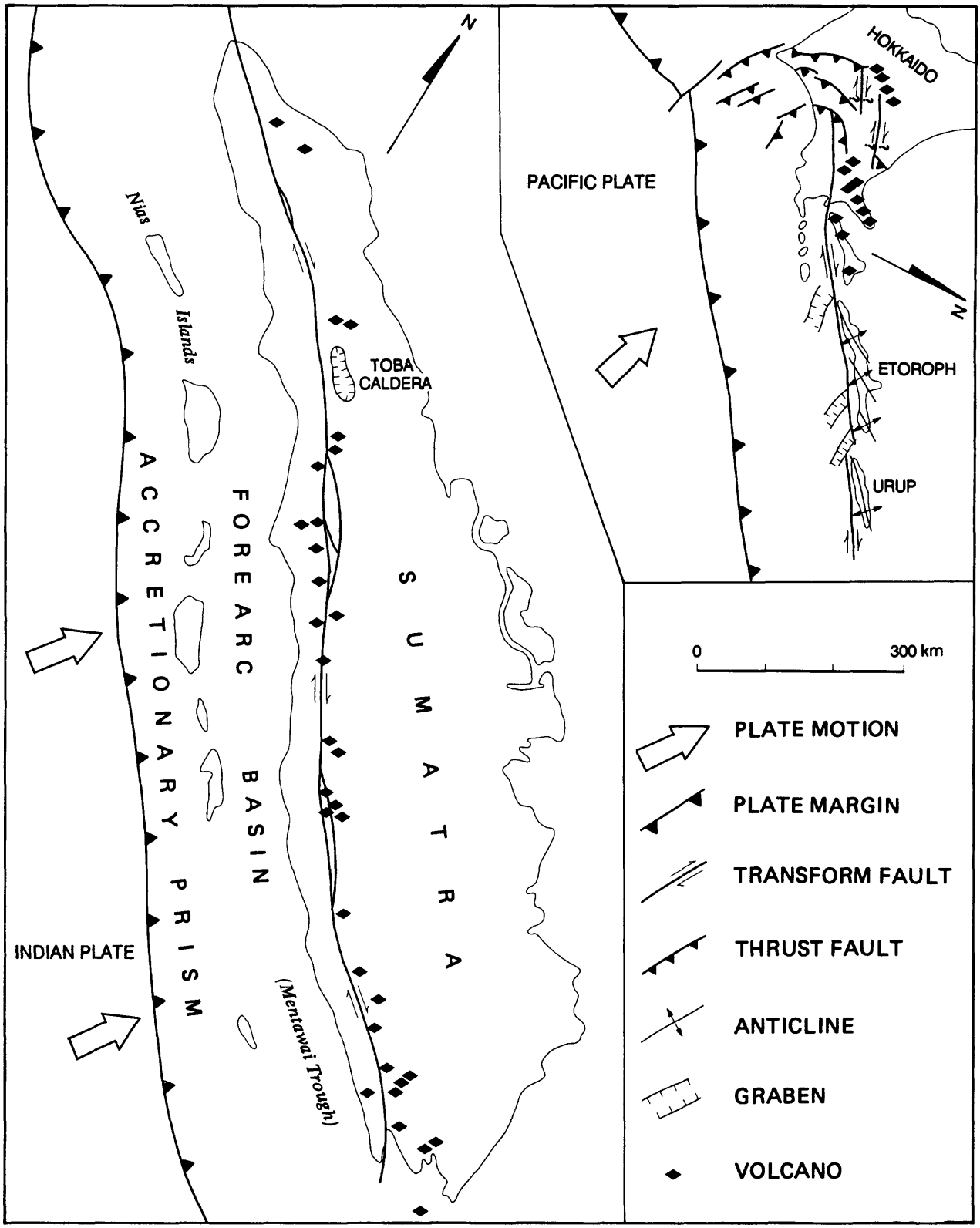

Figure 24--Maps illustrating the modern tectonic elements of Sumatra (Hamilton, 1979; Huchon and Le Pichon, 1984) and Japan north of Hokkaido (Kimura, 1986). The scale of both maps is identical to the scales of Figures 1 and 25. North has been rotated so that tectonic elements are approximately parallel. Barbed lines represent deep water axis for Java Trench off Sumatra and Kurli Trench north of Hokkaido.

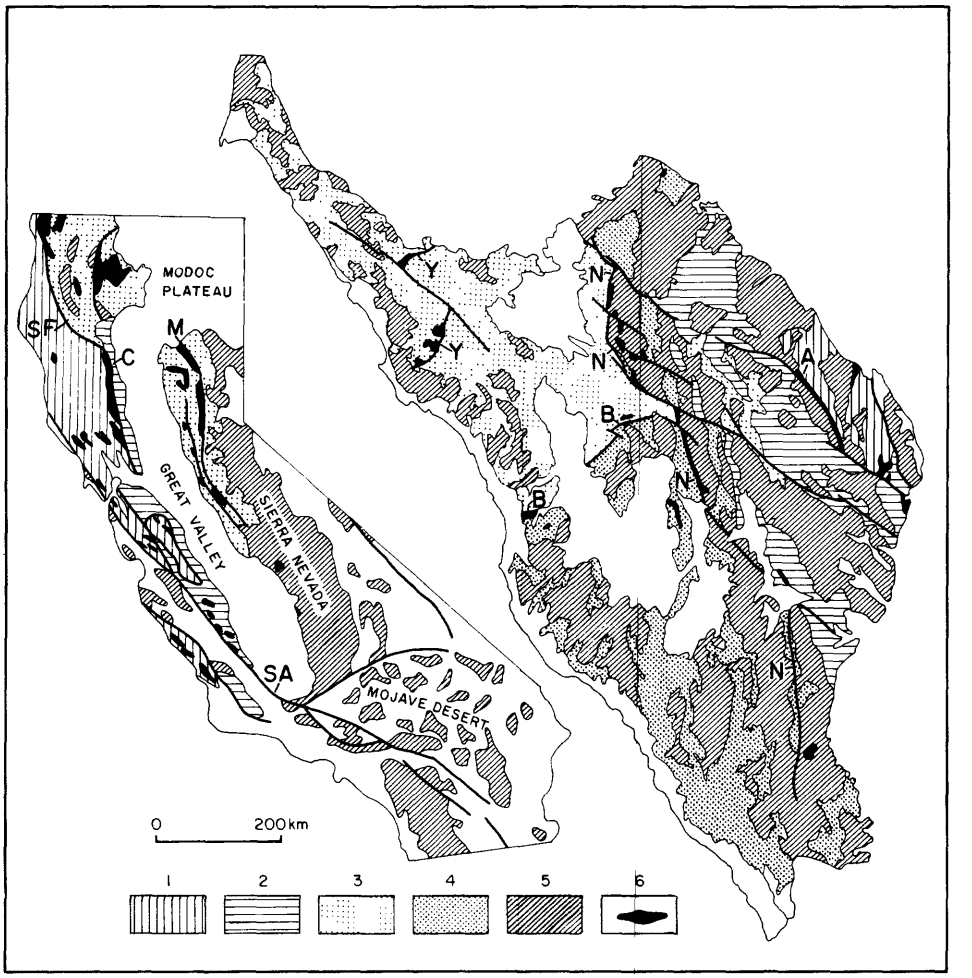

Figure 25–Maps illustrating analogous geologic and tectonic features in California (Bailey, 1966) and the Arabian Shield. Both maps are featured at identical scale to Figures 1 and 24. Faults are shown with heavy lines. California features: M, Melones Fault (part of the Foothills Fault Zone); C, Coast Range Fault; Sf, South Fork Mountain Thrust; SA, San Andreas Fault; pattern 1, Franciscan Formation: pattern 2, Great Valley Sequence; pattern 3, pre-Nevadan Paleozoic and Mesozoic volcanic and sedimentary rocks; pattern 4, not used; pattern 5, batholithic rocks of primarily Jurassic and Cretaceous age; pattern 6, ultramafic rocks. Arabian features: Y, Yanbu suture; B, Bi'r Umq suture; N, Nabitah fault zone; A, Al Amar suture; pattern 1, Abt schist; pattern 2, Murdama group; pattern 3, <800 Ma arc volcanic and sedimentary rocks; pattern 4, >800 Ma arc volcanic and sedimentary rocks; pattern 5, plutonic rocks; pattern 6, ultramafic rocks.

Nabitah fault zone and possibly the Al Amar Nabi suture.

The present investigation of the northern Nabitah fault zone found that strike-slip Nabitah faulting may have been contemporaneous with active arc volcanism on the Nabitah arc. The arc axis is inferred to be approximated by exposures of the Rharaba complexes in figure 2. Stoeser and Camp (1984) have emphasized the existence of a belt of locally deformed granodioritic to tonalitic rocks that parallels the Nabitah fault zone and constitutes their "Nabitah Zone". We suggest that the "Nabitah Zone" is the plutonic expression of the Nabitah arc and that the Nabitah fault zone is a transform fault analogous to the Central Sumatra

Fault or the Foothills Fault Zone. Nabitah faulting and volcanism were apparently active at about 710 Ma but must have occurred for some time before and after this date. On the basis of isotopic age dating of granitic rocks, Cole and Hedge (1986) suggest that a magmatic arc was active in this region between 700 to 670 Ma. An analogy to the Sierra Nevada batholith, where calc-alkaline plutonism was episodic between about 210 to about 80 Ma (Bateman and Wahrhaftig, 1966), would suggest that a similarly long span of time may be applicable to the Nabitah arc and fault zone.

The geology of Sumatra and California suggest that a genetically related accretionary prism should be found about 100-300 km from and parallel to the Nabitah arc. There is no evidence of the existence of such an accretionary prism west of the Nabitah fault zone. However, Schmidt and others (1978) have suggested that the Abt schist has many of the structural and petrologic characteristics of an accretionary prism. Significantly, the Abt schist parallels the Nabitah fault zone and its width is similar to that of the Franciscan Melange and the accretionary prism south of Sumatra. The distance from the Al Amar fault zone (the western limit of the Abt schist) to the Nabitah arc is about 200-250 km, which compares favorably with the separation of analogous features in California and Sumatra. The ultramafic rocks that are present along the Al Amar fault zone may be analogous to ultramafic rocks found along the Coast Range Thrust Fault in California.

The above hypothesis places the Nabitah fault zone behind the Nabitah arc relative to the proposed subduction zone. Although transform faults typically appear to be developed in the fore-arc region, there is some precedence for back-arc transform faulting. Figure 24 illustrates that the Central Sumatran Fault is locally situated behind the active arc. Furthermore, the same plate-boundary system may be traced northward into Burma where the active, right-lateral Sittang Fault is located behind the Cenozoic magmatic arc relative to the trench (Hamilton, 1979). Perhaps back-arc transform development, such as the Nabitah fault zone, indicates the pre-existence of an major crustal break.

Further analogy to Sumatra and California suggests that a fore-arc basin may be present between the Abt schist and the Nabitah arc. The Murdama group is presently in the appropriate geographic setting and is described by Wallace and Rowley (1984) as a thick sequence of interbedded sandstone, conglomerate, and shale that is locally interbedded with calc-alkaline volcanic rocks. Wallace and Rowley (1984) interpret the Murdama group to have formed near a volcanic arc, possibly in a back-arc-basin deposit. A fore-arc basin would be an equally appropriate location for Murdama deposition. Deposition of the Murdama group occurred between 670 and 655 Ma, but the beginning of Murdama deposition is not constrained and could have started earlier (Cole and Hedge, 1986). The range in ages relative to the proposed Nabitah arc is similar to that of the Great Valley Sequence as it relates to the Sierra Nevada Batholith (that is, contemporaneous with plutonic activity in time, but continuing for some time afterward).

Left-lateral, strike-slip motion on the Nabitah fault zone suggests that subduction involved an oblique component. If related subduction was indeed located in the region of the Abt schist, then the down-going plate was moving to the northwest relative to the Afif terrane. The model that emerges at this point suggests that the tectonic features discussed thus far are the mirror image of those in Sumatra, Japan, and California as presented in figures 24 and 25. Compared to published tectonic models, these speculations about the tectonism of the eastern Arabian Shield most closely resemble the conclusions of Schmidt and others (1978) who postulated westward-dipping subduction in the Al Amar region. However, oblique convergence is required in order for the present model to work.

Oblique subduction provides a model for the formation of F_1 folds of the Nabitah fault zone. Folding along gently dipping axes and stike-slip faulting both appear be the result of oblique subduction east of the Kuril arc (fig. 24; Kimura, 1979). This suggests that F_1 folding may have been related to the stress regime that caused Nabitah faulting. F_1 folding may have developed in zones where compressive stress from oblique subduction was not relieved by faulting; alternatively, it may have developed prior to faulting. Propagation of Nabitah faults and developing F_2 folds would locally cut, overprint, and destroy F_1 folds, but F_1 folds may have been preserved in fault blocks interiors. A corollary of this hypothesis is that, similar to the Kuril arc, F_1 fold axes were

perpendicular to the subducting plate's velocity vector. Based on the average orient-ation of F_1 at Bi'r Tuluhah and Jabal al Qub, this suggests that a subducting plate to the east was moving N. 30-45° E. relative to the over-riding Afif terrane.

The northern Arabian Shield thrust faults (fig. 1) may also be related to oblique subduction. The orientation of these features relative to the Nabitah fault zone and Nabitah arc is similar to thrust faults near the coast of Hokkaido (fig. 24). Northward motion of the Afif terrane may have been impeded by collision with the Hijaz terrane along the northeast projection of the Yanbu suture.

Oblique subduction may also explain the orientation of Najd faults. The Najd faults constitute a strikingly parallel system widly distributed over a large area (figs. 1 & 25). These faults commonly contain grabens of deformed Jibalah-group sedimentary rocks (Delfour, 1977), most abundant east of the Nabitah fault zone (Johnson, 1983). It is tempting to speculate that the Najd faults originally formed as normal faults like those east of the Kuril arc of Japan (fig. 24) and that the Jibalah-group rocks were deposited in the analogous grabens. The orientation of the Najd faults fits that theory if sinistral oblique subduction exists in the Al Amar area. If a subsequent shift in plate motions removed the oblique component from subduction, Nabitah faulting would end and the Najd faults would be in the appropriate orientation to become left-lateral strike-slip faults. Left-lateral motion on this fault system would deform the Jibalah-group rocks and be driven by the direct collision postulated by Schmidt and others (1978).

The proposed tectonic model of the eastern Arabian Shield does not explain large Murdama-group granitic intrusions and the Abt schist. Granitic intrusions are absent or rare in fore-arc basins and accretionary prisms. If the proposed model is correct, a second subduction zone located east of the exposed Shield may have been present, accounting for these intrusions. Although this is largely a "deus ex machina" solution, the presence of abundant 670-620-Ma granitic intrusions in the Ar Rayn terrane east of the Abt schist supports its use in the tectonic model.

IMPLICATIONS FOR GOLD MINERALIZATION

NABITAH ZONE

It is clear from the previous discussion that the Foothills Fault Zone of California is a potential analog to the Nabitah fault zone. As California has long been a major source of gold (Clark, 1966), a comparison of the two features might enhance our understanding of ore genesis in the central Arabian Shield.

The Nabitah Zone of Stoeser and Camp (1984) is recognized as a locus of auriferous quartz veins, which were sites for ancient gold mining (Smith and Johnson, 1986; Schmidt and others, 1978). A brief review of 14 sites (fig. 2) of early gold workings in the Al Hissu and southeast Nuqrah areas of the Nabitah fault zone was undertaken to help create a geologic model for use in future gold exploration. Of these, sites 1 through 13 were sampled and described during three weeks of field work in early winter, 1986. Area 14 is described by Brosset and Conraux (1978). The ancient gold workings at Al Obaid (area 3), Jabal Zarabin (area 5), Sukhaybarat (area 7), Mawan (area 8), and Umm Zarib (area 9) were first examined by Dirom (1946) and Schaffner (1955). The workings in the Al Hissu area were later visited and described by Duhamel and Petot (1972), whereas the workings in southeast Nuqrah were described by Aguttes and Chaumont (1974). Because of their small size and the low-lying terrain in which the workings are located, they can be easily overlooked from the ground. Also, the early miners typically obliterated any traces of the original material that was worked at the site, leaving only the tailings and quartz debris thinly scattered over the surrounding area. A summary of the geology of the sites is shown in table 1; geochemical data is shown in table 2.

Nine of the gold sites examined for this report are located in quartz diorite country rock

that is typically associated with granodiorite, or granite dikes. Area 7 (MODS 405, Table 1) is located in a granite stock, with the mineralization in the surrounding Murdama-group rocks (Smith and others, 1984). Areas 5, 8, 9, 11, and 12 (MODS 587, 397, 398, 4561, and 4559) are located within quartz diorite, granodiorite, and diorite intrusions at the western edge of the Murdama group (fig. 2). Areas 2, 6, and 10 (MODS 576, 295, and 392) are located in similar intrusives in a belt of south-trending assemblages of andesites and basalts 7-15 km wide (Letalenet and Bounny, 1977). Area 1, Jabal Jumaymah East (MODS 408), is located in granodiorite country rock at the western edge of the Murdama basin. Areas 3 and 4, Al Obaid and Jabal Burhah East (MODS 579 and 588), are in basalt country rock at the edge of the andesite and basalt assemblage. Area 13 is in listwaenite within the Nabitah fault zone, whereas area 14 is located in a schistose granite (Letalenet, 1979).

Three of the sites visited during the course of field work, areas 1, 7, and 8, (MODS 408, 405, and 397), have been studied extensively (Smith and others, 1984). Drilling results for Sukhaybarat al Gharbiyah, area 7 (MODS 405), indicate a reserve of 1,636 kg of gold (Smith and others, 1984). The results of drill-hole testing at Jabal Mawan, area 8 (MODS 397), show that the quartz veins in the area extend 30 m in depth, with no estimate of tonnage given (Aguttes and Chaumont, 1974). However, later calculations indicate that 5,475 kg of gold may be contained in the prospect (Smith and others, 1984). The small amount of mine debris found around the other workings indicates that most of the sites are too localized in area to be of great interest. An exception is area 9, Um Zarib (MODS 398), which is listed by Riofinex as having 1,458 kg of probable gold (Boyle and others, 1984). Area 13, located in the listwaenite, is of considerable interest as it contains ultramafic rocks, with no intrusives in the immediate vicinity and is the only such site that was visited. It is becoming increasingly clear that listwaenite can be a host rock for gold mineralization (Buisson and Leblanc, 1985). In fact, in the area of Bi'r Tawilah, just east of area 13, percussion drilling has revealed gold reserves of 97,500 tons with an average grade of 28.5 g/t (Smith and others, 1984) in a listwaenite host rock.

Although ancient mining activity resulted in the removal of much of the original mineralized rocks from the zones visited, some observations can still be made. The ancient workings fell into 3 major groups of orientations: N. 5-50° E., N. 65-85° W., and N. 10-30° W. These trends may indicate the orientation of the mineralization, since the workings would presumably follow the auriferous veins along strike. The northeast trend parallels the Nabitah fault zone and is the oldest. It is commonly cross-cut and offset in a left-lateral direction by quartz veins or dikes that trend west to northwest along the Najd fault system. These in turn are cut by veins and northwest-aligned dikes, which is evidently the youngest orientation. Economically, the northeast orientation appears to be the most important as 9 of the 13 sites examined had workings that followed this alignment. Iron-stained quartz veins parallel this orientation at 8 of the 13 sites. The gold is probably concentrated in quartz veins structurally controlled by northeast-trending faults and foliations. At Sukhaybarat ash Sharqiyah (MODS 406), east of area 7, drilling revealed a zone of mineralization of 2.8 million t at 3.12 g/t gold with extensions localized to the northeast (Clegg, 1985). At Jabal Mawan Southwest (area 8, MODS 397), the potential for inferred reserves of gold is more than three times that of the other sites listed (Smith and others, 1984); orientation here is also to the northeast. The west-northwest-oriented system has fewer and smaller workings; only three sites (areas 1, 7, and 9) had any major ancient workings with this orientation. Only Jabal Jumayah East (area 1) had workings associated with the west-northwest orientation; two other areas (5 and 6) were apparently prospected by ancient miners and found to be barren.

Foothills Fault Zone and the Mother Lode District

The Sierra Nevada province has long been a major source of gold in California (Clark, 1966). The main mineral belt, the Mother Lode, is a narrow 2-6-km-wide zone of auriferous quartz veins with a strike length of 180 km (Koschmann and Bergendahl, 1968). However, gold mineralization is more widely dispersed and can be 8-25 km from the main belt of lode mineralization (Koschmann and Bergendahl, 1968; see also fig. 26).

The gold-bearing region of the Mother Lode consists of two Paleozoic complexes, the Shoo Fly

and the Calaveras, and a zone of predominantly Mesozoic metavolcanic and metasedimentary rocks of island-arc affinity (Bohlke and Kistler, 1986). East of the Shoo Fly Complex are a series of late Jurassic and early Cretaceous plutons forming a northwest zone of intrusives, and early or middle Cretaceous plutons that form the core of the Sierra Nevada batholith and intersect the island-arc rocks in the south (Bohlke and Kistler, 1986). To the west of the island-arc rocks are sedimentary rocks of the Great Valley Sequence, within which are scattered granitic, gabbroic, and ultramafic rocks related to the island-arc rocks (Schweickert and Cowan, 1975). The Shoo Fly Complex is composed of continent-derived sandstone, siltstone, and shale. The Calaveras Complex is composed of oceanic and(or) island-arc-derived chert, argillite, and mafic-intermediate volcanic rocks (Bohlke and Kistler, 1986).

The island-arc rocks are separated from the Shoo Fly and Calaveras complexes by the major system of faults known as the Melones fault zone (Schweickert and Cowan, 1975). This narrow, northwest- to northeast-trending fault zone is the site of the major lode-gold mineralization (fig. 26). The zone itself is only 2-6 km wide; the very narrowness of the zone is important, as a similar zone of mineralization could be easily overlooked. Flanking the west side of the fault zone is a belt of ultramafic rocks. The gold-bearing quartz veins are commonly associated with the serpentine, although they are not found in the serpentine itself (Wisker, 1936). In some places, the most important control on gold mineralization is proximity to serpentinite (Cooke, 1947). The presence of carbonate and talc or mariposite is also a major control. Carbonate-rich areas have gold concentrations associated with them because the gold selectively replaced the carbonate in those areas affected by hydrothermal solutions (Cooke, 1947). The mariposite apparently formed from the solutions that reacted with chromite in the serpentinite. These solutions must have circulated through channels opened by fracturing of the country rocks. Other than proximity to serpentinite, the chemical composition of the country rocks does not limit or define the zones of high-grade gold mineralization (Johnston, 1940). There appear to be no discernable trends near high-grade ore zones and the change from barren to high-grade zones is abrupt; for this reason, assaying is not very useful as a prospecting method (Cooke, 1947).

The most significant orientation of the gold-bearing quartz veins is from north to northwest, following the strike of the minor fault zones paralleling the Melones fault zone (Coveny, 1981; Bohlke and Kistler, 1986). Two more orientations of gold mineralization are west-southwest to west-northwest (Wisker, 1936; Coveney, 1981). These quartz veins are smaller and more numerous. Quartz veins along the north-northwest alignment are associated with cross-cutting fault zones (Coveney, 1981). The third mineralization orientation is to the northeast (Logan, 1941), but it appears to be uncommon. Although it is barren of mineralization, this alignment is economically important because structural features along this strike tend to change the width and concentration of the vein quartz and gold (Johnston, 1940). These orientations are mirror images of the alignments reflected by the orientations of gold workings in Saudi Arabia relative to the Nabitah fault zone.

The Mother Lode's gold-bearing quartz veins are large, tabular, milky, and contain only minor sulphide staining (Koschmann and Bergendahl, 1968). In the Grass Valley district (fig. 26), sulfide-poor quartz veins are typically sheared and show a shear-banding structure (Johnston, 1940). The massive quartz veins of the area seldom have gold in them (Johnston, 1940). Pyrite, galena and sphalerite are commonly gold bearing, and galena in particular is regarded as a favorable indicator (Johnston, 1940). Although visible gold was once the main indicator for economic gold mineralization, it is rarely found today (Johnston, 1940).

The gold deposits of the Mother Lode have been classified as mesothermal in origin based on high gold-silver ratios (1-10), high CO_2 contents in the fluid inclusions, a homogenization temperature of 250-350° C, and an intermediate pH alteration zone (Nesbitt and others, 1986). The alteration products associated with the Mother Lode are (1) carbonatization, (2) silicification, and (3) sericitization. Also, pyrite, mariposite, albite, chlorite, talc, and graphite are formed (Nesbitt and others, 1986). Stable isotopic data also indicate a mesothermal origin for the Mother Lode gold deposits and suggests that the waters involved were originally meteoric but were modified isotopically during deep crustal circulation (Nesbitt and others, 1986).

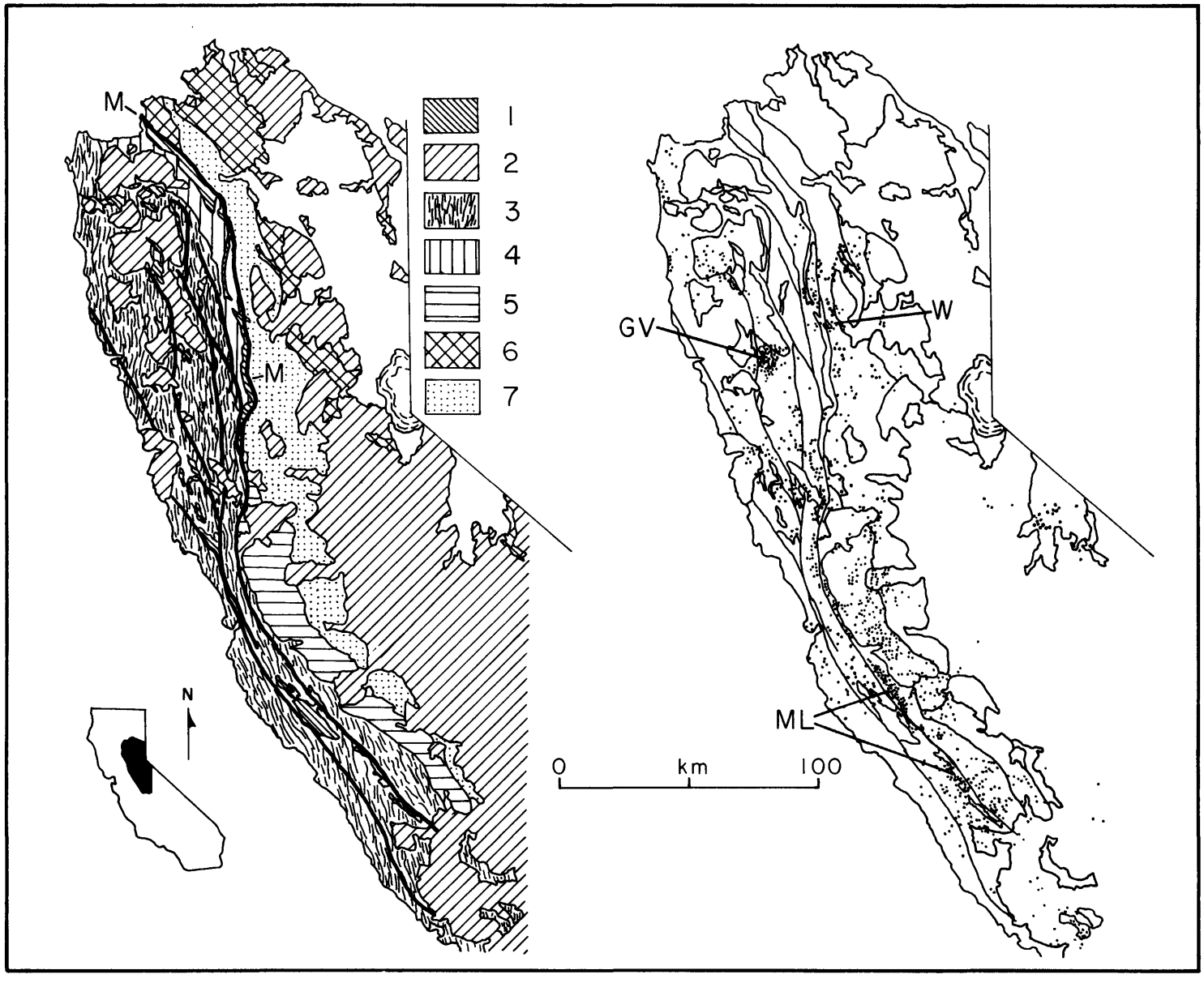

Figure 26--Simplified geologic maps of the northern Sierra Nevada mountains adapted from Bohlke and Kistler (1986) and showing the Foothills Fault Zone (heavy lines), the Melones Fault (M), gold mines (dots) and major lithologies. Lithologic symbols are: (1) serpentinized ultramafic rock; (2) Sierra batholith; (3) pre-batholithic ophiolitic, volcanic, and sedimentary rocks of island-arc affinity; (4) Calaveras Formation; (5) Calaveras Complex; (6) Shoo Fly Complex. Mining districts mentioned in the text are GV, Grass Valley; W, Washington; and ML, Mother Lode.

The heat source that drove water circulation in the Mother Lode may have been the Sierra Nevadan plutons. The flow of water may have been channeled by the serpentinite, which acted as impermeable barriers. This could explain the spatial association of gold-bearing veins and serpentinite. The gold mineralization in the Sierra Nevada is associated with fault zones that dip steeply to the east; this orientation would have allowed fluids to migrate upward from a great depth (Bohlke and Kistler, 1986). In contrast, shallow-dipping faults are barren of mineralization. These observations suggest that fault orientation could be significant in controlling mineralization along the Nabitah fault zone.

At this time, there is no agreement as to the ultimate source of the gold in the Mother Lode deposits. If the gold was derived from rocks of the Shoo Fly or Calaveras complexes then the probability of finding Mother Lode-type deposits along the Nabitah fault zone is diminished because there are no analogous formations nearby. However, if the gold was derived from the island-arc assemblages or the sub-Sierran mantle, then the chances of finding Mother Lode-type deposits along the Nabitah fault zone are better.

CONCLUSIONS

In both the Mother Lode district and the central Arabian Shield, the known gold deposits are commonly associated with granite plutons, or granodiorite intrusions (figs. 2 and 26). However, in the Mother Lode district, the major locus of lode-gold deposits is associated with the Melones fault zone and serpentine bodies. In the central Arabian Shield, the analogous setting is the Nabitah fault zone with its associated ultramafic rocks. This area is still relatively unexplored. Considering that the width of the main lode-gold-bearing zone in the Mother Lode district is only 2-6 km, it is possible that a mineralized zone of comparable size may have been overlooked along the Nabitah fault zone.

In the Mother Lode, the major auriferous quartz veins are milky and contain only minor sulphide. The massive quartz veins have little gold in them, but the quartz veins that are milky and have shear-bandings are the most likely to have high-grade gold ore. Because of the abrupt changes in grade from barren quartz to high-grade gold-bearing quartz (which appear in hand specimen to be the same), straightforward prospecting methods are not highly successful (Cooke, 1947). In Saudi Arabia, quartz veins that have sulphide stainings on them have been examined closely, but less has been done to investigate sulfide-poor quartz veins found along the Nabitah fault zone. In view of this, the following recommendations are made:

1. A preliminary study should be instituted to sample quartz veins near the Nabitah fault zone, focusing on areas of serpentinization and carbonate replacement.

2. Sheared quartz veins, with little sulfide mineralization, but located near zones of carbonate, should be sampled to determine the extent of gold enrichment.

3. Quartz veins trending N-N50E should be given priority over those trending east-west or northwest. Areas of cross-cutting quartz veins trending east-west or northwest should be examined as well.

4. Reconnaissance fluid-inclusion and stable-isotopic work should be carried out to determine if a mesothermal zone is in fact associated with the Nabitah fault zone.

DATA STORAGE

Field and laboratory data for this report, including petrographic descriptions, sample sites, and results of chemical analyses, are stored in Data-File USGS-DF-09-6 in the Jeddah office of the U.S. Geological Survey Saudi Arabian Mission.

One new file (MODS 4562) was added to the Mineral Occurrence Documentation System (MODS) data bank for the gold occurrence and Jabal al Qub. File MODS 4560 was added to the MODS data bank for the Jabal Mardah gossans.

ACKNOWLEDGMENTS

Major- and trace-element abundances reported in this report were determined by Mir Amjad Hussain and Abdul Malik Helaby, respectively. X-ray analysis and preparation of thin sections and samples for chemical analysis were performed by the petrography section of the U.S. Geological Survey Saudi Arabian Mission under the direction of Muhammed Naqvi. This manuscript was improved by reviews by J. Pallister and W. White.

This study was performed in accordance with a cooperative agreement between the U.S. Geological Survey (USGS) and the Saudi Arabian Ministry of Petroleum and Mineral Resources.

Table 1.—Characteristics of ancient gold mines in the vicinity of the Nabitah fault zone.

Area # (MODS)	Name (from BRGM) and location	Geologic setting	Mine description and status	Sample numbers	Chemical results
1 (408)	Jabal Jumaymah East (PC9) 25 18′ 40" N	Country rock: granodiorite with small intrusions of granite. Workings: parallel to and cross-cutting parallel diabase dikes. Dike Attitudes: north-south strike, 80 west dip. Mineralization: quartz veins with pyrite and galena. Milky-white quartz veins. Attitude: Barren qtz, N16E, 87W. Fe-stained quartz, N80W, 88S.	Three sets of small, elongated, shallow, filled-in pits located between two diabase dikes. Trend: western pits - aligned along N80W for 40 meters. eastern pits - aligned along N20E for 50 meters. Tailings: quartz with galena, pyrites and sphalerite. Visible gold. Status: Occurrence	Two backhoe trenches crosscutting dikes. Western trench composite samples: 221724 - 740. Eastern trench composite samples: 221741 - 749. 3 grab samples from tailings: 221532 - 534.	up to 12 ppm Au in qtz tailings; <1 ppm in dike rock.
2 (576)	Al Naysah South (RM19) 24 32′14" N 41 46′38" E	Country rock: foliated (N40E, 78W) qtz diorite. Workings: parallel to and cross-cutting granodiorite dikes, near a rhyolite dike. Dike Attitude: N40E, 84E, for both types. Mineralization: Quartz veins with pyrite, Fe-stained. Attitude: quartz vein-N40E, 78W.	Shallow, filled-in pits 250 meters east of a small trench. Trend: trench - N40E, 100 meters long. Pits - aligned along N20W for 65 meters. Tailings: quartz with some pyrite blebs. Visible gold. Status: Prospect	16 grab and rock chip samples: Grab: 221515, 517, 522, 537, 538, 541, 545. Chip: 221514, 516, 520, 521, 539, 540, 542, 543, 544. 221558 - pan sample, with visible gold.	0.3 - 4 ppm Au in qtz outcrop. nil in the dikes. 31 ppm Au in qtz tailings.
3 (579)	Al Obaid (RM22) 24 33′32" N 41 48′05" E	Country rock: foliated (N20E, 84W) basalt. Workings: within the basalt; no major dikes in the area. Mineralization: small quartz veins parallel to basalt foliation. Attitude: quartz are N20E, 84W.	Numerous small, shallow, filled-in pits. Trend: pits aligned N-S for 2000 meters. Tailings: finely crushed quartz with visible gold. Status: Occurrence	Three rock chip samples: 221518-quartz float 221519-basalt 221546-basalt 221559-pan sample with visible gold.	1 ppm Au in qtz float. nil in basalt.

Table 1.—Characteristics of ancient gold mines...(continued)

Area # (MODS)	Name (from BRGM) and location	Geologic setting	Mine description and status	Sample numbers	Chemical results
4 (588)	Jabal Burhah East (DV54) 24 45'00" N 41 53'20" E	Country rock: unfoliated basalt. Workings: cross-cutting small diabase dikes. Dike Attitude: N30W, 67E. Mineralization: milky-white quartz veins with Fe-staining on contacts with dikes. Attitude: qtz veins, N20E, 78W.	Three, small, shallow sets of pits. Trend: aligned N50E 150 meters. Tailings: milky-white quartz with no apparent mineralization. Status: Occurrence	Four rock chip samples: 221556-quartz 221585-dike float 221586-basalt 221587-andesite dike 221557-pan sample with visible gold.	No geochem assays.
5 (587)	Jabal Zarabin South 24 45'12" N 41 53'09" E	Country rock: foliated (N50W, 84W) quartz diorite. Workings: along contact of large quartz vein within quartz diorite. Mineralization: milky-white quartz with no alteration or Fe-staining. Attitude: quartz vein-N10W, 78E.	One set of small pits, probable prospecting pits. Trend: pits aligned along N30W for 100 meters. Tailings: none. Status: Occurrence	Three rock chip samples: 221590-andesite dike 221591-quartz 221592-basalt 221593-pan sample with visible gold.	No geochem assays.
6 295)	Jabal Umenupta 24 20'00" N 41 42'25" E	Country rock: foliated (N 8E, 76E) quartz diorite. Workings: along contact of diabase dike. Dike Attitude: strike N40W, 78W. Mineralization: no apparent mineralization.	One elongated trench, now filled-in, and quartz debris. Probable prospect pit. Trend: trench - N30W, for 75 meters. Tailings: no mine tailings, barren qtz. Status: Occurrence	221547-quartz	<0.1 ppm Au.

Table 1.—Characteristics of ancient gold mines...(continued)

Area # (MODS)	Name (from BRGM) and location	Geologic setting	Mine description and status	Sample numbers	Chemical results
7 (405)	Zukhaybarat al Gharbiyah 25 27'15" N 41 57'15" E	Country rock: unfoliated quartz diorite, containing foliated (N84W, 78W) granite roof pendants and cut by younger, unfoliated granite dikes. Workings: pits cross-cutting granite dikes. Dike Attitudes: strike N83W, 84W. Mineralization: quartz along contacts of granite dikes. Pyrite and galena in quartz, with visible gold. Attitude: quartz veins N26W, 80W.	One set of pits. Trend: pits aligned along N80W for 100 meters. Tailings: mixed granite and quartz containing pyrite, galena and visible gold. Status: Prospect	Five rock chip samples: 221548-diorite 221549-quartz and gold 221550-quartz and pyrite 221551-quartz and pyrite 221552-granite dike	0.5 ppm Au in granite dike. nil in quartz diorite 25 ppm Au in mine tailings.
8 (897)	Jabal Mawan Southwest 25 08'00" N 41 39'30" E	Country rock: unfoliated quartz diorite. Workings: pits parallel diabase dike. Dike Attitude: N10E, 84W. Mineralization: no quartz veins observed.	Numerous shallow, filled-in pits. Trend: pits aligned along N10E for 400 meters. Tailings: quartz, with pyrite and visible gold. Status: Prospect	Three rock chip samples: 221560-diabase dike 221561-quartz float 221562-quartz float 221563-pan sample with visible gold.	No geochem assays.

Table 1.--Characteristics of ancient gold mines...(continued)

Area # (MODS)	Name (from BRGM) and location	Geologic setting	Mine description and status	Sample numbers	Chemical results
9 (398)	Umm Zarib (Al Amirah) 25 07'36" N 41 41'48" E	Country rock: quartz diorite, with small granodiorite and gabrro dikes. Workings: cross-cutting granodiorite dikes. Dike Attitude: granodiorite, N10E, 84W. Mineralization: quartz veins east of workings containing pyrite and possible visible gold along contact of quartz diorite. Attitude: quartz veins, N60E, 83W. Attitude: quartz veins N26W, 80W.	Two parallel, aligned filled-in trenches, separated by 100 meters. Trend: N85W for 500 meters. Tailings: milky-white quartz, with no Fe-staining. Status: Prospect	Three rock chip samples: 221564-quartz diorite 221565-quartz tailings 221566-gabbro dike 221567-pan sample with visible gold.	(BRGM reports 6 ppm Au average)
10 (392)	Jabal Thuban North (RM14) 25 08'00" N	Country rock: foliated (N20E, 84E) quartz diorite intruded by gabbro dikes and later andesite dikes. Workings: parallel to and cross-cutting gabbro dikes, near andesite dike. Dike Attitude: N10W, 84W for earlier gabbro dikes, N55E, 80W for later andesite dikes. Mineralization: quartz veins containing epidote and Fe-stains. Attitude: quartz veins, N20E, 80W.	One small, shallow, filled-in, trench. Trend: aligned N55E for 25 meters. Tailings: quartz and epidote. Status: Prospect	Six rock chip samples: 221594-gabbro dike 221595-quartz diorite 221596-andesite dike 221597-quartz tailing 221598-gabbro dike 221599-quartz and epidote	quartz with 3.2 ppm Au.

Table 1.--Characteristics of ancient gold mines...(continued)

Area # (MODS)	Name (from BRGM) and location	Geologic setting	Mine description and status	Sample numbers	Chemical results
11 (4561)	Jabal Jumayah Central 25 16'40" N 41 40'00" E	Country rock: quartz diorite, cut by diabase dikes. Workings: sub-parallel to dikes. Dike Attitudes: N5E, 80W. Mineralization: small quartz veins without obvious sulphides. Attitudes: quartz veins, N70W, 84W.	Several shallow pits. Trend: aligned along N10E, for 25 meters. Tailings: quartz with Fe-staining and possible native silver. Status: Occurrence	Eight rock chip samples: 221568-quartz 221569-quartz diorite 221570-contact with dike 221571-diabase dike 221572-contact with dike 221573-quartz and gold 221574-quartz and galena 221575-quartz and galena	quartz diorite: nil.
12 (4559)	Jabal Jumayah Mid East 25 17'00" N 41 38'56" E	Country rock: quartz diorite, cut by gabbro dike. Workings: parallel to gabbro dike. Dike Attitude: N5E, 78E. Mineralization: no mineralization observed.	Shallow, filled-in trench. Trend: N5E, for 25 meters. Tailings: quartz with pyrite and chalcopyrite. Status: Occurrence	Five rock chip samples: 221576-gabbro dike 221577-granite dike 221578-gabbro dike 221579-quartz diorite 221589-quartz and pyrite	quartz diorite: nil.

Table 1.—Characteristics of ancient gold mines...(continued)

Area # (MODS)	Name (from BRGM) and location	Geologic setting	Mine description and status	Sample numbers	Chemical results
13 (4562)	Jabal al Qub 23 50'38" N 41 47'42" E	Country rock: serpentinite cut by tabular zones of listwaenite up to 50 meters wide and 100 meters long. Quartz zones invade and parallel listwaenite zones. Workings: quartz veins in listwaenite. Attitudes: listwaenite and quartz veins; N10W. Mineralization: Fe-stained quartz containing galena.	Three small, shallow pits and two shallow trenches up to 50 meters long. Trend: N10W Tailings: quartz Status: Occurrence	Eight rock chip, five grab samples: Rock: 221704-serp. 221705-list. 221706-list. 221707-quartz 221708-list. 221709-list. 221710-list. 221711-serp. Grab: 221713-quartz 221714-quartz 221715-quartz 221716-quartz 221717-list. 221716-pan sample with visible gold.	up to 0.36 ppm Au and 340 ppm Ag in the quartz.
14 (910) (915) (916) (917) (918) (919) (920) (2106) (2107)	Jabal al Hibr 9 different sites 23 40'00" - 23 45'00" N 42 05'00" - 42 10'00" E	Country rock: biotite granite, and gneiss, with small enclaves of metamorphosed mafic rocks. Mineralization: quartz veins with some sulphides. Attitudes: N40E to N60E, with secondary trend of N30W.	Nine quartz veins worked; mainly shallow, filled-in surface trenches. Trend: follows the strike of the quartz, N40E to N60E. Status: Occurrences	None	BRGM reports wide differences in Au values in area. High-37 ppm of Au.

Table 2.--Au-Ag geochemical values in ppm/ppb for selected samples from ancient mines of the Nabitah fault zone.

Area	Field No.	Rock type*	Au ppm	Au ppb	Ag ppm	Au/Ag Ratio
No. 1 Jabal Jumaymah						
(float)	221532	QR	8.4		10	0.84
(float)	221533	QR	1.64		4	0.41
(float)	221534	QR	12		10	1.20
	221722	AN	-	38	0.1	0.38
	221724	AN	0.15		0.4	0.38
	221725	AN	0.56		2.23	0.25
	221726	AN	0.15		0.10	1.50
	221727	QR	0.60		1.0	0.60
	221728	QR	0.90		4.5	0.20
	221729	QR	0.70		0.90	0.78
	221731	DR	0.10		0.14	0.71
	221732	DR		43	0.10	0.43
	221733	DR		71	0.13	0.55
	221734	DR		41	0.10	0.41
	221735	DR		52	0.10	0.52
	221736	DR		52	0.12	0.43
	221737	DR	0.10		0.16	0.63
	221738	DR	0.10		0.10	1.00
	221739	DR	0.15		0.12	1.25
	221740	DR	0.12		0.10	1.20
	221741	GR		63	0.10	0.63
	221742	GR		44	0.10	0.37
	221743	GR		46	0.12	0.38
	221744	AN		57	0.15	0.38
	221745	AN		68	0.15	0.45
	221746	GR		5	0.10	0.05
	221747	AN		16	0.10	0.16
	221748	GR		47	0.13	0.36
	221749	GR		54	0.17	0.32
No. 2 Al Naysah South						
	221514	QR		180	0.40	0.45
(float)	221515	QR	4		0.20	20.00
	221516	DR		92	0.10	0.92
(float)	221517	QR	8		1.50	5.30
	221520	RY		24	0.10	0.24
	221521	GD		27	0.10	0.27
	221514	QR		180	0.40	0.45
(float)	221515	QR	4		0.20	20.00
	221516	DR		92	0.10	0.92
(float)	221517	QR	8		1.50	5.30
	221520	RY		24	0.10	0.24

Table 2.--Au-Ag geochemical values in ppm/ppb...(continued)

Area	Field No.	Rock type*	Au ppm	Au ppb	Ag ppm	Au/Ag Ratio
No. 2 Al Naysah South						
	221521	GD		27	0.10	0.27
(float)	221522	QR	31.5		3.70	8.51
(float)	221538	QR	7.30		0.80	9.13
	221539	GD		16	0.12	0.13
(float)	221540	GD		7	0.20	0.06
	221541	QR	19.5		4.00	4.88
	221542	GD		68	0.14	0.49
	221543	RY		80	0.12	0.67
	221544	QR	0.30		1.20	0.25
(float)	221545	QR	7.00		0.70	10.00
No. 3 Al Obaid						
	221546	BA		18	0.20	0.09
No. 6 Jabal Umenupta						
	221547	QR		48	1.7	0.03
No. 7 Sukhaybarat Al Gharbiyah						
	221548	DR		23	0.12	0.19
	221550	QR	25.00		11	2.27
	221551	QR	1.06		0.70	1.50
	221552	QR	0.50		0.15	3.33
No. 10 Jabal Thuban						
	221598	GB		29	0.10	0.20
	221701	QR	3.20		0.10	32.00
No. 11 Jabal Jumayah Central						
	221570	DR		6	-	0.06
No. 12 Jabal Jumayah Mid East						
	221579	DR		14	0.10	0.14

* QR - quartz GD - granodiorite BA - basalt
AN - andesite RY - rhyolite GR - granite
DR - diorite GB - gabbro
Analysis by atomic absorption

REFERENCES

Agar, R. A., 1985, Stratigraphy and paleogeography of the Sirhan Group, Saudi Arabian Ministry for Mineral Resources Open-File Report DGMR-OF-05-16, 21 p.

Aguttes, J., and Chaumont, P., 1974, Geology and mineral exploration of the Jabal Mawan quadrangle: Bureau de Recherches Geologiques et Minieres Report 74 JED 11, 63 p.

Bailey, E. H., 1966, Geology of Northern California, California Division of Mines and Geology Bulletin 190, 508 p.

Bateman, P. C., and Wahrhaftig, C., 1966, Geology of the Sierra Nevada, in Geology of Northern California, E. H. Bailey, ed., California Division of Mines and Geology Bulletin 190, p. 107-169.

Beck, M. E., Jr., 1983, On the mechanism of tectonic transport in zones of oblique subduction, Tectonophysics, vol. 93, p. 1-11.

Blain, C. F., 1978, Mineralization and gossans in the Wadi Wassat-Wadi Qatan region, Kingdom of Saudi Arabia, U.S. Geological Survey Saudi Arabian Project Report 252, 34 p. USGS Open-File Report 79-671.

Bohlke, J. K., and Kistler, R. W., 1986, Rb-Sr, K-Ar, and stable isotope evidence for the ages and sources of fluid components of gold-bearing quartz veins in the Northern Sierra Nevada Foothills Metamorphic Belt, California: Economic Geology, vol. 81, pp. 296-322.

Boyle, D. McK., Badedah, S. S., and Saleh, V. T., 1984, A review and ranking of the mineral potential of auriferous quartz-vein occurrences in the Arabian Shield: Saudi Arabian Deputy Ministry for Mineral Resources Open-File Report RF-OF-04-7, 79 p.

Brosset, R., and Conraux, J., 1978, Geology and mineral exploration of the Jabal Abraq quadrangle, 23/42 A: Bureau de Recherches Geologiques et Minieres Technical Record 78-JED-1, 31 p.

Brown, G. F., Layne N. M., Jr., Goudarzi, G. H., and Maclean, W. H., 1963, Geologic map of the Northeastern Hijaz quadrangle, dom of Saudi Arabia: U.S. Geological Survey Miscellaneous Geologic Investigations Map I-205-A, scale 1:5000,000 (reprinted 1979, Saudi Arabian Directorate General of Mineral Resources Geologic Map GM-205-A, scale 1:500,000).

Buisson, G., and Leblanc, M., 1985, Gold in carbonatized ultramafic rocks from ophiolite complexes: Economic Geology, vol. 80, pp. 2028-2029.

Burns, L.E., 1985, The Border Ranges ultramafic and mafic complex, south-central Alaska: cumulate fractionates of island-arc volcanics, Canadian Journal of Earth Science, vol. 22, pp. 1020-1038.

Caby, R., 1982, Petrological and structural observations from the Nuqrah area and some remarks concerning the crustal history of the northern Najd Province, Saudi Arabia: Pan-African crustal evolution in Arabia and northeast Africa (Al-Shanti, A. M., ed.), Precambrian Research, vol. 16, pp. A11-A12.

Calvez, J. Y., Alsac, C., Delfour, J., Kemp, J., and Pellaton, C., 1983, Geological evolution of western, central and eastern parts of the northern Precambrian Shield, Kingdom of Saudi Arabia: Saudi Arabian Deputy Ministry for Mineral Resources Open-File Report BRGM-OF-03-17, scale 1:100,000.

Camp, V. E., 1984, Island arcs and their role in the evolution of the western Arabian Shield, Geological Society of America Bulletin, vol. 95, pp. 913-921.

Cebull, S. E., 1972, Sense of displacement along Foothills Fault System: New Evidence from the Melones Fault Zone, Western Sierra Nevada, California, Geological Society of America Bulletin, vol. 83, pp. 1185-1190.

Clark, W.B., 1966, Economic mineral deposits of the Sierra Nevada: California Division of Mines and Geology Bulletin 190, p. 209-214.

Clegg, I. H., 1985, A summarized compilation of prospects drilled by the DMMR and private sector, 1366-1404 (1936-1984): Saudi Arabian Deputy Ministry for Mineral Resources Open-File Report DM-OF-05-02, 130 p.

Cole, J. C., and Hedge, C. E., 1986, Geochronologic investigation of the Late Proterozoic rocks in the northeastern Shield of Saudi Arabia: Saudi Arabian Deputy Ministry for Mineral Resources Technical Record USGS-TR-05-5, 42 p. USGS Open-File Rpt 89-332.

Conraux, J., Delfour, J., and Eijkelboom, G., 1969, The Jabal Sayid prospect: Bureau de Recherches Geologiques et Minieres Report 69-JED-43, 50 p.

Cooke, H. R., 1947, The original Sixteen to One gold-quartz vein, Alleghany, California: Economic Geology, vol. 62, pp. 211-250.

Coveney, R. M., Jr., 1981, Gold quartz veins and auriferous granite at the Oriental Mine, Alleghany District, California: Economic Geology, vol. 76, pp. 2176-2199.

Delfour, J., 1977, Geology of the Nuqrah quadrangle, sheet 25E, Kingdom of Saudi Arabia: Saudi Arabian Directorate General of Mineral Resources Geologic Map GM-28, scale 1:250,000, 32 p.

Delfour, J., 1981, Geology of the Al Hissu quadrangle, sheet 24E, Kingdom of Saudi Arabia: Saudi Arabian Directorate General of Mineral Resources Geologic Map GM-58A, scale 1:250,000, 47 p.

Dick, H. J. B., and Bullen, T., 1984, Chromian spinel as a petrogenetic indicator in abyssal and alpine-type peridotites and spatially associated lavas, Contributions to Mineralogy and Petrology, vol. 86, pp. 54-76.

Dirom, G. A., 1946, Preliminary report on ancient gold mines, Nejd, Saudi Arabia: Saudi Arabian Deputy Ministry for Mineral Resources Open-File Report no. 23, 36 p.

Duhamel, M., and Petot, J., 1972, Geology and mineral exploration of the Al Hissu quadrangle, Bureau de Recherches Geologiques et Minieres Technical Record 72-JED-7, 57 p.

Ernst, W. G., 1965, Mineral paragenesis in Franciscan metamorphic rocks, Panoche Pass, California: Geological Society of America Bulletin, vol. 76, pp. 879-914.

Ewart, A., 1982, The mineralogy and petrology of Tertiary-Recent orogenic volcanic rocks in Andesites: Orogenic andesites and related rocks, R. S. Thorpe, ed., Wiley and Sons, New York.

George, R. P., 1978, Structural petrology of the Olympus ultramafic complex in the Troodos ophiolite, Cyprus: Geological Society of America Bulletin 89, pp. 845-865.

Gonzalez, Louis, 1974, Geology of the Jabal Ishmas Quadrangle, U.S. Geological Survey Saudi Arabian Project Report 186, 34 p. USGS Open-File Report 75-181.

Hackel, O., 1966, Summary of the Geology of the Great Valley, in Geology of Northern California, E. H. Bailey, ed., California Division of Mines and Geology Bulletin 190, pp. 217-252.

Hamilton, W., 1969, Mesozoic California and the underflow of the Pacific Mantle, Geological Society of America Bulletin, vol. 80, pp. 2409-2430.

Hamilton, W., 1979, Tectonics of the Indonesian Region, U. S. Geological Survey Professional Paper 1078, 345 p.

Hariri, M. M., 1985, A preliminary report on the Jabal Zalm ultramafic complex (22/42A), Saudi Arabian Deputy Ministry for Mineral Resources Open-File Report OF-05-25, 23p.

Huchon, Philippe and Le Pichon, Xavier, 1984, Sunda strait and central Sumatra fault geology, vol. 12(II), p. 668-672.

Irvine, T. N., and Baragar, W. R. A., 1971, A guide to the chemical classification of the common volcanic rocks, Canadian Journal of Earth Science, vol. 8, no. 5, p. 523-548.

Irvine, T. N., 1974, Petrology of the Duke Island ultramafic complex, southeastern Alaska, Memoirs of the Geological Society of America, no. 138.

Irvine, T. N., 1967, Chromian spinel as a petrogenetic indicator, Part 2: Petrologic applications, Canadian Journal of Earth Sciences, vol. 4, p. 71-103.

James, O. B., 1971, Origin and emplacement of the ultramafic rocks of the Emigrant Gap area, California, Journal of Petrology, vol. 12, p. 523-560.

Johnson, P. R., 1983, A preliminary lithofacies map of the Saudi Arabian Shield: Saudi Arabian Deputy Ministry for Mineral Resources Technical Record RF-TR-03-2.

Johnson, P. R., and Williams, P. L., 1984, Geology of the Jabal Habashi quadrangle, sheet 26F, Kingdom of Saudi Arabia: Saudi Arabian Deputy Ministry for Mineral Resources Open-File Report USGS-OF-04-10, 87 p.
USGS Open-File Report 85-3.

Johnston, W. D., Jr., 1940, The gold quartz veins of Grass Valley, California: U. S. Geological Survey Professional Paper PP 194, 101 p.

Kastowo, D., and Leo, G., 1973, Geologic map of the Padang Quadrangle, Sumatra, Geological Survey of Indonesia, scale 1:250,000.

Kattan, F. H., 1983, Geology of the Tuluhah belt north east Arabian Shield, M. Sc. Thesis, King Abdulaziz University, 110 p.

Kellogg, K. S., and Beckmann, G. E. C., 1984, Paleomagnetic investigation of upper Proterozoic rocks in the eastern Arabian Shield, Kingdom of Saudi Arabia, in A. M. Al Shanti, ed., Pan African Crustal Evolution of the Arabian-Nubian Shield: Faculty of Earth Sciences Bulletin (IGCP Publication 164), King Abdul Aziz University, pp. 483-500.

Kemp, J., Gros, Y., and Prian, J., 1982, Geologic map of the Mahd Adh Dhahab quadrangle, sheet 23E, Kingdom of Saudi Arabia: Saudi Arabian Directorate General of Mineral Resources Geologic Map GM-64A, scale 1:250,000, 47 p.

Kimura, G., 1986, Oblique subduction and collision: Forearc tectonics of the Kuril arc, Geology, vol. 14, p. 404-407.

Koschmann, A. H., and Bergendahl, M. H., 1968, Principle gold-producing districts of the United States: U. S. Geological Survey Professional Paper PP 610, pp. 53-84.

Leitch, E.C., 1984, Island arc elements and arc-related ophiolites, Tectonophysics, vol. 106, pp. 177-203.

Le Metour, J., Johan, V., and Tegyey, M.,1983, Geology of the ultramafic-mafic complexes in the Bi'r Tuluhah and Jabal Malhijah areas, Saudi Arabian Deputy Ministry for Mineral Resources Open-File Report BRGM-OF-03-40, 46 pp.

Letalenet, J., 1979, Geologic map of the Afif quadrangle, sheet 23F, Kingdom of Saudi Arabia: Saudi Arabian Directorate General of Mineral Resources Geologic Map GM-47 A, scale 1:250,000, 20 p.

Letalenet, J., and Bounny, I., 1977, Geology and mineral exploration of the Jabal As Sirhan quadrangle, sheet 23/42C, Kingdom of Saudi Arabia: Saudi Arabian Directorate General of Mineral Resources Open-File Report BRGM-77-JED-5, 32 p.

Logan, C. A., 1941, Mineral resources of Nevada County: California Journal of Mines and Geology, vol. 37, pp. 374-408.

Malpas, J., and Stevens, R. K., 1979, The origin and emplacement of the ophiolite suite with examples from western Newfoundland, in Ophiolites of the Canadian Appalachians and Soviet Urals, J. Malpas and R. W. Talkington, eds., Memorial University of Newfoundland, Department of Geology Report no. 8, pp. 21-43.

Marsh, B. D., 1982, The Aleutians, in Andesites: Orogenic andesites and related rocks, R.S. Thorpe, ed., John Wiley and Sons, New York, 724 p.

Myers, J. D., Marsh, B. D., and Sinha, K. A., 1985, Strontium isotopic and selected trace-element variations between two Aleutian volcanic centers (Adak and Atka): implications for the development of arc volcanic plumbing systems, Contributions to Mineralogy and Petrology, vol. 91, pp. 221-234.

Nesbitt, B. E., Murowchick, J. B., and Muehlenbachs, K., 1986, Dual origins of lode gold deposits in the Canadian Cordillera: Geology, vol. 14, pp. 506-509.

Pallister, J. S., Stacey, J. S., Fischer, L. B., and Premo, W. R., 1987, Precambrian ophiolites of Arabia: U-Pb geochronology, Pb isotopic characteristics, and implications for continental accretion: Saudi Arabian Deputy Ministry for Mineral Resources Open-File Report USGS-OF-07-10. USGS Open-File Report 88-606.

Pearce, J. A., and Cann, J. R., 1973, Tectonic setting of basic volcanic rocks determined using trace-element analyses, Earth and Planetary Science Letters, vol. 19, pp. 290-300.

Quick, J. E., 1981, Petrology and petrogenesis of the Trinity peridotite, an upper mantle diapir in the eastern Klamath Mountains, northern California, Journal of Geophysical Research, vol. 86, pp. 11837-11863.

Quick, J. E., and Helaby, A. M., 1988, XAP, a program for deconvolution and analysis of complex X-ray spectra, Saudi Arabian Directorate General of Mineral Resources Technical Record USGS-TR-08-3, 33 p. USGS Open-File Report 89-338.

Saleeby, J. B., 1980, Chronology of the structural and petrologic development of the southwest Sierra Nevada foothills, California: Summary, Geological Society of America Bulletin, Part 1, vol. 91, no. 6, pp. 317-320.

Saleeby, J. B., 1983, Accretionary tectonics of North American Cordillera, Annual Review Earth and Planetary Science, vol. 11, pp. 45-73.

Saleeby, J.B., 1982, Polygenetic ophiolite belt of the California Sierra Nevada: geochronological and tectonostratigraphic development, Journal of Geophysical Research, vol. 87, no. B3, pp. 1803-1824.

Schaffner, D. F., 1955, Preliminary report on Mawan (ancient gold workings): Saudi Arabian Deputy Ministry for Mineral Resources Open-File Report No. 52, 13 p.

Schweickert, R. A., and Cowan, D. S., 1975, Early Mesozoic tectonic evolution of the western Sierra Nevada, California: Geological Society of America Bulletin, vol. 86, pp. 1329-1336.

Schmidt, D. L., Hadley, D. G., and Stoeser, D. B., 1978, Late Proterozoic crustal history of the Arabian Shield, southern Najd Province, Kingdom of Saudi Arabia, U.S. Geological Survey Saudi Arabian Project Report 251. On file at the USGS Saudi Arabian Mission.

Shanti, M., 1985, Geologic investigation and rock geochemistry in the Nuqrah-As Safra and Jabal Sayid belts, Saudi Arabian Deputy Ministry for Mineral Resources Open-File Report BRGM-OF-05-23, 45 p.

Smith, E. A., Barnes, D. P., Johnson, P. R., Bognar, B., Garfield, L., and Scheibner, E., 1984, A review of the geology, mineralization, and mineral resource potential of the Kingdom of Saudi Arabia: Saudi Arabian Deputy Ministry for Mineral Resources Open-File Report RF-OF-05-1, vol. 1, 322 p.

Smith, E. A., and Johnson, P. R., 1986, Selected mineral occurrences of the Arabian Shield, showing their relationship to major Precambrian tectonostratigraphic entities, Saudi Arabian Deputy Ministry for Mineral Resources Technical Record RF-TR-06-1, scale 1:1,000,000, 143 p.

Snoke, A. W., Quick, J. E., and Bowman, H. R., 1981, Bear Mountains Igneous Complex, Klamath Mountains, California: an ultrabasic to silicic calc-alkaline suite, Journal of Petrology, vol. 22, no. 4, pp. 501-552.

Stacey, J. S., and Agar, R. A., 1985, U-Pb isotopic evidence for the accretion of a continental microplate in the Zalm region of the Saudi Arabian Shield, Journal of the Geological Society of London, vol. 142, pp. 1189-1203.

Stacey, J.S., and Stoeser D.B., 1983, Distribution of oceanic vs. continental leads in the Arabian-Nubian Shield: Contributions to Mineralogy and Petrology, vol. 84, pp. 91-105.

Stern, R. J., and Bibee, L. D., 1984, Esmeralda Bank: Geochemistry of an active submarine volcano in the Mariana Island Arc, Contributions to Mineralogy and Petrology, vol. 86, pp. 159-169.

Stoeser, D. B., Stacey, J. S., Greenwood, W. R., and Fischer, L. B., 1984, U/Pb zircon geochronology of the southern part of the Nabitah mobile belt and Pan-African continental collision in the Arabian Shield, Saudi Arabian Ministry for Mineral Resources Technical Record TR-04-5, 88 p.

Stoeser, D. B., and Camp, V. E., 1984, Pan-African Microplate accretion of the Arabian Shield, Saudi Arabian Deputy Ministry for Mineral Resources Report USGS-TR-04-17, 25 p.
Geological Society of American Bull. V 96, pp 817-826.

Stoeser, D. B., 1986, Distribution and tectonic setting of plutonic rocks of the Arabian Shield, Journal of African Earth Sciences, vol. 4, pp. 21-46.

Wallace, C. A., and Rowley, P. D., 1984, Reconnaissance study of the Murdama group, central and northern Murdama basin, Kingdom of Saudi Arabia [unpublished report].

Wisker, A. L., 1936, The gold-bearing veins of Meadow Lake district, Nevada County: California Journal of Mines and Geology, vol. 32, pp. 180-204.

APPENDIX A1.--Major- and trace-element abundances in volcanic rocks from the Darb Zubaydah ophiolite. [bdl, below detection limit; ---, not determined]

Entry	1	2	3	4	5	6	7	8
Sample No.	221238	221239	221240	221241	221242	221243	221245	221246
Analyses in weight percent								
Na_2O	3.5	3.3	3.6	4.2	3.8	---	2.6	3.1
MgO	4.5	5.2	4.0	1.8	1.9	---	1.6	1.1
Al_2O_3	17.1	15.5	19.1	15.6	17.2	---	14.8	16.8
SiO_2	52.5	52.2	55.0	66.1	66.1	---	68.2	70.7
K_2O	.9	.3	1.0	3.7	3.3	---	2.4	4.6
CaO	8.7	9.4	8.4	2.2	2.8	---	4.2	1.6
TiO_2	1.1	1.2	1.0	.8	.6	---	.7	.3
MnO	.2	.2	.1	.1	.1	---	.2	bdl
FeO	10.5	12.1	8.1	4.8	3.7	---	5.1	2.3
P_2O_5	.2	.1	.2	.2	.1	---	.3	bdl
Total	99.2	99.4	100.4	99.4	99.6	---	100.0	100.7
Analyses in parts per million								
Zn	130	100	110	86	65	22	110	57
Rb	32	16	35	70	78	110	76	120
Sr	460	830	460	310	190	110	240	170
Y	24	23	19	37	15	10	26	12
Zr	76	110	100	200	150	110	180	140
Nb	6	5	7	7	7	5	8	10
La	29	bdl	13	39	20	50	43	31
Nd	32	22	bdl	39	17	25	56	13
Ba	400	210	380	930	1050	940	520	1300
Ce	27	53	29	86	63	45	68	99

Entry	9	10	11	12	13	14	15	16
Sample No.	221247	221250	221252	221254	221255	221256	221257	221258
Analyses in weight percent								
Na_2O	4.4	3.7	2.4	5.5	1.1	5.3	1.5	2.5
MgO	6.0	6.4	1.5	3.9	1.8	3.4	1.5	5.8
Al_2O_3	18.8	19.1	13.3	17.3	11.8	14.9	10.5	17.0
SiO_2	48.7	50.1	66.6	52.9	74.6	60.1	75.3	47.0
K_2O	.3	.9	2.1	.5	5.6	.5	2.5	.4
CaO	10.0	8.5	8.2	7.8	3.0	7.6	6.5	17.1
TiO_2	1.0	1.0	.7	.9	.1	.8	.2	.6
MnO	.2	.1	.1	.2	bdl	.3	.1	.2
FeO	10.0	9.7	4.4	10.0	2.4	6.4	1.4	9.0
P_2O_5	.2	.1	.3	.2	.1	.2	.1	.1
Total	99.6	99.8	99.8	99.3	100.5	99.4	99.8	99.8
Analyses in parts per million								
Zn	100	94	60	110	92	98	77	110
Rb	12	28	39	22	180	17	59	11
Sr	480	330	250	470	220	260	200	390
Y	23	18	26	18	26	32	14	18
Zr	57	54	120	94	190	140	99	46
Nb	bdl	6	9	8	6	6	5	5
La	8	bdl	54	38	31	41	34	13
Nd	4	11	50	8	31	27	31	bdl
Ba	420	310	610	590	1200	260	810	150
Ce	29	bdl	43	49	63	46	39	13

APPENDIX A1.--Major- and trace-element abundances in volcanic rocks--(Continued).

Entry	17	18	19	20	21	22	23	24
Sample No.	221259	221263	221265	221266	221268	221269	221270	221283
				Analyses in weight percent				
Na_2O	2.9	1.6	.5	2.3	4.1	3.6	4.6	5.6
MgO	4.2	7.3	3.3	4.5	3.9	2.9	3.0	4.3
Al_2O_3	17.7	16.6	16.1	13.2	16.1	15.3	18.1	18.2
SiO_2	55.9	48.4	46.5	48.4	48.0	44.0	46.6	49.4
K_2O	.2	.1	bdl	.1	.2	.2	.2	.2
CaO	9.7	12.2	20.3	16.3	16.0	20.1	17.2	10.6
TiO_2	.8	1.7	1.4	2.2	1.5	1.8	1.6	1.4
MnO	bdl	.1	.2	.3	.2	.2	.2	.2
FeO	8.1	11.8	11.7	11.4	9.5	11.0	7.6	9.2
P_2O_5	.1	.2	.1	.3	.2	.2	.2	.1
Total	99.5	100.0	99.9	99.2	99.7	99.4	99.3	99.2
				Analyses in parts per million				
Zn	100	120	46	110	130	150	87	97
Rb	13	12	bdl	9	10	10	11	9
Sr	540	400	720	150	340	380	140	450
Y	24	32	27	36	27	30	29	29
Zr	87	92	74	110	83	100	75	85
Nb	7	bdl	bdl	bdl	bdl	bdl	bdl	6
La	bdl	bdl	bdl	bdl	11	9	2	2
Nd	60	27	8	26	9	bdl	26	13
Ba	150	47	53	42	120	120	75	170
Ce	35	17	9	22	7	18	10	bdl

Entry	25	26	27	28	29	30	31	32
Sample No.	221352	221353	221354	221355	221356	221357	221358	221359
*								
				Analyses in weight percent				
Na_2O	5.7	4.3	5.4	4.7	5.0	3.3	4.7	5.9
MgO	3.6	.6	3.7	3.3	3.9	6.0	2.6	2.9
Al_2O_3	17.7	15.3	17.8	16.9	18.4	18.7	17.7	17.3
SiO_2	52.5	72.3	52.9	58.3	53.5	49.7	59.2	56.1
K_2O	.3	2.3	.2	.4	.7	.6	.8	.3
CaO	10.5	3.0	11.0	6.6	8.3	10.4	6.3	5.7
TiO_2	1.4	.3	1.3	1.0	1.2	1.2	.7	1.2
MnO	.2	bdl	.2	.1	.1	.1	.1	.1
FeO	8.0	2.1	7.7	7.5	8.2	8.9	6.3	8.3
P_2O_5	.5	.2	.3	.3	.4	.3	.2	.3
Total	100.5	100.4	100.7	99.1	99.8	99.2	98.6	98.2
				Analyses in parts per million				
Zn	76	47	70	85	100	92	89	68
Rb	12	62	7	18	22	15	20	17
Sr	720	430	330	370	370	440	760	440
Y	23	8	30	27	26	32	27	21
Zr	120	140	110	120	120	110	160	120
Nb	11	7	7	8	8	7	8	6
La	25	21	25	28	1	bdl	14	bdl
Nd	34	bdl	30	24	29	32	23	26
Ba	180	1050	210	210	230	160	440	170
Ce	47	52	46	27	19	9	28	13

APPENDIX A1.--Major- and trace-element abundances in volcanic rocks--(Continued).

Entry	33	34	35	36	37	38	39	40
Sample No.	221360	221368	221369	221370	221372	221373	221374	221375
				Analyses in weight percent				
Na_2O	6.5	2.1	3.9	3.3	2.8	7.5	2.8	3.3
MgO	2.6	3.1	4.3	3.7	3.2	3.1	4.9	4.5
Al_2O_3	17.1	19.4	18.9	19.8	20.6	17.7	19.3	16.4
SiO_2	53.4	56.6	54.3	52.5	52.9	54.9	54.5	49.7
K_2O	1.3	1.4	.4	bdl	.2	.2	bdl	.1
CaO	9.8	9.2	9.7	11.9	12.2	6.1	9.5	10.6
TiO_2	1.2	.8	.7	.8	.6	1.4	.7	2.3
MnO	.2	.1	.2	.1	.1	.1	.1	.2
FeO	5.5	7.3	7.1	7.7	7.3	8.7	7.6	11.4
P_2O_5	.2	.2	.3	.1	.1	.3	.2	.3
Total	97.8	100.0	99.8	100.1	100.2	100.0	99.6	98.8
				Analyses in parts per million				
Zn	73	100	110	96	89	120	95	110
Rb	30	38	14	bdl	9	12	bdl	15
Sr	330	350	420	340	690	300	870	370
Y	20	17	19	17	15	34	13	39
Zr	89	76	94	83	66	100	59	150
Nb	6	6	7	6	5	bdl	bdl	bdl
La	45	13	18	5	12	bdl	11	15
Nd	58	17	14	13	27	bdl	23	40
Ba	1580	660	250	51	120	170	49	150
Ce	15	24	31	16	29	40	18	33

Entry	41	42	43
Sample No.	221376	221377	221378
		Analyses in weight percent	
Na_2O	3.6	5.0	2.2
MgO	4.8	2.8	3.0
Al_2O_3	17.9	14.5	16.1
SiO_2	51.7	64.3	53.7
K_2O	bdl	.1	.2
CaO	12.0	6.0	12.5
TiO_2	.7	.8	.7
MnO	.1	bdl	.2
FeO	8.2	5.6	11.0
P_2O_5	.3	.4	.2
Total	99.3	99.4	99.9
		Analyses in parts per million	
Zn	86	75	71
Rb	bdl	7	bdl
Sr	640	470	150
Y	18	33	22
Zr	53	170	68
Nb	bdl	6	bdl
La	5	51	12
Nd	22	31	11
Ba	60	110	210
Ce	29	81	31

APPENDIX A2.--Major- and trace-element abundances in hypabyssal rocks from the Darb Zubaydah ophiolite. [bdl, below detection limit; ---, not determined]

Entry	1	2	3	4	5	6	7	8
Sample No.	221285	221286	221287	221288	221289	221290	221291	221292
Analyses in weight percent								
Na_2O	3.5	1.5	2.7	2.7	4.0	1.1	1.9	3.4
MgO	7.6	3.8	4.6	9.0	5.4	10.9	10.4	5.4
Al_2O_3	16.9	18.1	20.7	17.1	14.9	17.2	14.1	16.4
SiO_2	50.8	40.4	50.0	48.8	51.1	50.0	51.3	49.6
K_2O	.6	2.5	1.4	.5	.3	.7	.4	.7
CaO	9.8	21.0	10.9	10.8	10.2	12.5	13.1	11.4
TiO_2	1.1	1.0	1.3	1.2	1.8	.3	.5	1.1
MnO	.1	.2	.1	.1	.2	.1	.1	.2
FeO	9.1	11.2	8.1	9.9	11.8	7.5	8.3	12.3
P_2O_5	.1	.1	.1	.1	.1	.1	bdl	.1
Total	99.7	99.7	99.8	100.4	99.8	100.4	99.9	100.5
Analyses in parts per million								
Zn	120	100	120	140	180	100	68	150
Rb	26	42	50	16	15	23	16	18
Sr	300	340	220	210	130	230	120	440
Y	28	21	24	28	41	9	15	29
Zr	120	48	95	98	140	32	48	69
Nb	bdl	4	6	bdl	bdl	5	6	6
La	35	bdl	bdl	bdl	bdl	13	6	23
Nd	31	bdl	21	6	27	9	3	31
Ba	190	440	210	84	130	150	75	500
Ce	20	22	34	20	34	16	bdl	25

Entry	9	10	11	12	13	14	15	16
Sample No.	221293	221294	221295	221296	221297	221298	221299	221300
Analyses in weight percent								
Na_2O	2.2	1.7	3.1	3.0	3.4	2.8	3.0	2.7
MgO	7.2	6.7	.9	1.0	.5	.6	.3	5.8
Al_2O_3	16.2	15.4	16.4	15.6	14.7	13.4	13.7	17.7
SiO_2	50.3	49.9	66.3	64.8	68.2	71.2	72.8	53.6
K_2O	1.5	1.3	2.2	1.5	1.4	3.0	4.7	.9
CaO	11.3	15.6	4.0	6.4	4.8	2.4	1.2	9.8
TiO_2	1.0	.6	.6	.6	.5	.3	.3	.9
MnO	.1	.1	.2	.2	.2	.1	.1	.1
FeO	9.8	8.9	5.9	6.2	5.5	4.9	3.7	7.6
P_2O_5	.3	.1	.1	.1	.1	bdl	5.9	.1
Total	99.9	100.3	99.7	99.4	99.3	98.8	105.7	99.2
Analyses in parts per million								
Zn	120	58	73	71	80	82	87	110
Rb	31	30	36	34	21	40	43	24
Sr	570	330	470	610	620	260	150	410
Y	26	19	56	45	54	48	58	19
Zr	76	50	210	180	190	210	230	87
Nb	6	7	6	7	8	7	bdl	6
La	10	5	245	18	15	16	224	11
Nd	25	10	28	37	22	bdl	53	15
Ba	1270	320	740	550	700	1340	2560	340
Ce	32	11	38	21	18	26	20	28

APPENDIX A2.--Major- and trace-element abundances in hypabyssal rocks--(Continued).

Entry	17	18	19	20	21	22	23	24
Sample No.	221301	221302	221303	221304	221305	221306	221307	221308
				Analyses in weight percent				
Na_2O	4.3	2.6	4.1	1.2	4.7	2.5	3.2	4.3
MgO	4.2	4.5	3.3	4.5	.3	.5	.4	4.7
Al_2O_3	15.9	15.6	14.5	17.0	13.9	14.1	12.7	16.5
SiO_2	57.6	55.8	56.0	51.2	69.6	70.0	73.8	54.6
K_2O	.3	.1	.6	.2	1.9	2.0	3.1	1.8
CaO	5.4	6.7	7.2	13.2	3.6	4.0	2.0	7.9
TiO_2	1.0	.9	1.2	1.0	.4	.4	.3	.7
MnO	.2	.3	.2	.2	.1	.1	.1	.2
FeO	10.8	11.2	10.2	11.7	4.4	5.0	4.4	8.5
P_2O_5	.2	.2	.2	.2	.2	.1	.2	.4
Total	100.0	97.9	97.6	100.4	99.1	98.7	100.2	99.7
				Analyses in parts per million				
Zn	150	140	72	110	93	140	82	93
Rb	bdl	bdl	17	13	26	44	51	48
Sr	310	330	330	140	210	460	210	710
Y	32	29	31	23	19	24	20	23
Zr	120	88	94	84	81	75	73	80
Nb	6	8	6	7	5	7	bdl	8
La	17	18	12	6	22	18	9	30
Nd	bdl	19	23	bdl	19	22	bdl	34
Ba	330	81	340	110	350	610	650	700
Ce	bdl	15	23	21	15	22	22	26

Entry	25	26	27	28	29	30	31	32
Sample No.	221309	221310	221311	221312	221313	221314	221333	221335
				Analyses in weight percent				
Na_2O	1.9	3.1	1.2	2.8	2.1	3.5	4.1	.8
MgO	1.1	6.1	7.3	7.2	5.9	6.6	4.7	3.4
Al_2O_3	13.8	15.7	14.8	15.2	17.3	15.7	14.4	16.1
SiO_2	66.3	52.0	50.0	50.0	49.2	51.3	57.2	53.1
K_2O	.5	1.0	.2	.3	.2	.3	.5	.3
CaO	8.1	10.6	14.6	11.8	11.7	10.6	6.0	14.0
TiO_2	.3	1.0	1.0	1.0	1.1	1.1	1.0	.6
MnO	.2	.2	.3	.2	.2	.1	.1	.2
FeO	6.9	10.5	10.7	11.2	11.9	10.9	11.7	11.6
P_2O_5	.2	.1	.1	bdl	.1	.2	.3	.1
Total	99.4	100.1	100.2	99.9	99.8	100.3	99.9	100.1
				Analyses in parts per million				
Zn	120	110	63	110	85	110	140	72
Rb	11	32	15	11	14	10	17	21
Sr	650	310	150	250	100	230	240	950
Y	20	24	24	22	30	26	32	10
Zr	64	66	66	69	90	74	94	50
Nb	5	7	5	bdl	7	bdl	6	4
La	bdl	11	bdl	bdl	8	2	49	bdl
Nd	7	2	bdl	36	27	28	bdl	bdl
Ba	140	240	110	290	44	110	270	92
Ce	30	9	3	22	22	10	33	17

APPENDIX A2.--Major- and trace-element abundances in hypabyssal rocks--(Continued).

Entry	33	34	35	36	37	38
Sample No.	221336	221337	221339	221346	221347	221348
			Analyses in weight percent			
Na_2O	2.7	.7	.8	3.7	1.6	6.0
MgO	4.4	2.5	9.8	3.9	3.7	.1
Al_2O_3	14.7	14.4	11.0	14.1	13.9	13.1
SiO_2	54.8	59.3	55.8	59.2	56.6	75.8
K_2O	.2	.3	.2	bdl	1.0	.2
CaO	9.1	11.9	12.4	5.1	7.5	1.5
TiO_2	.8	.4	.3	2.0	2.1	.3
MnO	.2	.2	.2	.1	.2	.1
FeO	13.3	10.4	8.8	11.3	12.6	2.0
P_2O_5	.2	.1	.1	.3	.3	.1
Total	100.2	100.2	99.4	99.7	99.5	99.2
			Analyses in parts per million			
Zn	110	81	53	150	110	53
Rb	bdl	11	11	bdl	21	9
Sr	290	83	110	96	120	380
Y	14	16	10	44	52	35
Zr	29	60	47	130	130	190
Nb	bdl	7	6	5	5	7
La	bdl	24	16	9	24	7
Nd	27	9	bdl	15	12	10
Ba	120	76	93	55	380	130
Ce	14	22	26	28	11	36

APPENDIX A3.--Major- and trace-element abundances in metabasalt and silicic metatuff in the Bi'r Tuluhah area
[bdl, below detection limit; ---, not determined]

Entry	1	2	3	4	5	6	7	8
Sample No.	206515	206520	206521	206529	206553	206555	206576	206577
Analyses in weight percent								
Na_2O	3.2	2.5	4.0	3.1	3.6	3.6	3.0	3.2
MgO	7.0	6.6	5.9	6.4	3.0	5.1	8.6	6.7
Al_2O_3	13.9	17.3	19.3	18.2	16.1	19.3	16.5	13.9
SiO_2	55.4	50.5	50.6	49.7	60.8	52.1	49.2	50.6
K_2O	.2	.1	.1	.7	.2	.7	.2	.3
CaO	9.2	10.0	9.1	13.0	6.9	10.7	11.7	8.7
TiO_2	1.0	1.1	1.0	.6	1.0	1.2	1.1	1.9
MnO	.3	.2	.2	.2	.3	.1	.2	.2
FeO	9.5	11.2	9.7	7.9	8.2	6.8	9.7	14.0
P_2O_5	bdl	bdl	bdl	bdl	bdl	bdl	bdl	bdl
Total	99.5	99.6	99.9	99.8	100.0	99.7	100.2	99.6
Analyses in parts per million								
Zn	130	130	130	100	150	97	100	160
Rb	13	11	9	21	9	20	9	17
Sr	89	370	350	280	260	220	160	180
Y	24	27	19	17	42	27	26	47
Zr	70	93	72	42	110	78	77	120
Nb	6	bdl	bdl	5	bdl	bdl	bdl	5
La	bdl	bdl	bdl	bdl	bdl	bdl	bdl	bdl
Nd	bdl	bdl	bdl	bdl	bdl	bdl	bdl	bdl
Ba	bdl	bdl	bdl	bdl	bdl	bdl	bdl	bdl
Ce	bdl	bdl	bdl	bdl	bdl	bdl	bdl	bdl

Entry	9	10	11	12	13	14	15	16
Sample No.	206592	206713	206715	206727	227031	227032	227033	227069
Analyses in weight percent								
Na_2O	2.2	2.7	3.0	2.0	3.9	5.2	2.4	3.4
MgO	7.7	7.2	5.8	8.4	7.9	6.1	9.9	8.6
Al_2O_3	17.1	16.5	13.7	15.8	15.2	16.8	13.6	16.0
SiO_2	48.1	49.3	49.1	48.2	50.0	52.7	49.7	51.2
K_2O	.1	.3	.3	.1	bdl	.1	.1	.1
CaO	12.9	13.8	11.9	13.3	9.5	9.6	10.3	8.7
TiO_2	1.2	.7	1.7	1.2	1.6	1.5	1.3	.8
CR_2O_3	bdl	bdl	bdl	bdl	bdl	bdl	bdl	bdl
MnO	.1	.2	.3	.1	.2	.1	.3	.1
FeO	10.5	8.9	13.7	9.8	10.9	7.8	11.5	10.7
P_2O_5	bdl	.1	.1	.1	bdl	bdl	bdl	bdl
Total	99.9	99.7	99.7	99.0	99.3	100.0	99.1	99.8
Analyses in parts per million								
Zn	110	86	160	71	120	110	58	84
Rb	12	10	9	8	10	8	13	9
Sr	180	150	320	150	160	140	90	77
Y	30	25	43	32	34	33	34	25
Zr	84	45	110	74	100	92	83	56
Nb	5	5	6	5	bdl	bdl	5	bdl
La	bdl	bdl	bdl	bdl	bdl	bdl	7	bdl
Nd	bdl	bdl	bdl	bdl	20	21	13	bdl
Ba	bdl	bdl	bdl	bdl	44	81	33	72
Ce	bdl	bdl	bdl	bdl	7	5	11	9

APPENDIX A3.--Major- and trace-element abundances in metabasalt and silicic metatuff--(Continued).

Entry	17	18	19	20	21	22	23	24
Sample No.	227070	227071	227073	227074	227077	227082	227086	227094
Analyses in weight percent								
Na_2O	1.2	2.5	2.7	3.0	2.9	3.9	1.6	.9
MgO	6.9	3.0	8.5	8.9	8.0	8.1	7.1	7.7
Al_2O_3	14.4	11.4	15.4	15.2	15.3	16.0	15.5	13.6
SiO_2	50.7	69.5	47.3	49.3	48.6	49.1	47.9	55.8
K_2O	.1	.2	.2	.2	.3	.1	.1	.2
CaO	15.3	4.7	12.9	12.7	11.2	10.1	15.4	11.3
TiO_2	.8	.6	1.3	1.1	1.5	1.2	1.1	.5
CR_2O_3	bdl	bdl	bdl	bdl	bdl	.1	.1	.1
MnO	.1	.4	.2	.1	.2	.2	.1	.2
FeO	9.2	5.9	9.9	9.3	11.0	10.5	10.0	9.3
P_2O_5	bdl	.3	.1	.1	.1	bdl	bdl	bdl
Total	98.8	98.4	98.5	100.0	99.1	99.2	98.7	99.5
Analyses in parts per million								
Zn	70	100	110	79	62	120	130	120
Rb	10	10	12	16	10	bdl	9	bdl
Sr	73	210	320	240	160	110	170	120
Y	16	62	29	23	32	30	29	30
Zr	49	160	89	77	90	72	75	72
Nb	bdl	15	8	bdl	9	bdl	bdl	bdl
La	bdl	58	bdl	bdl	9	18	bdl	bdl
Nd	8	56	4	33	21	bdl	17	2
Ba	67	90	39	49	89	33	11	21
Ce	13	89	bdl	2	11	3	21	bdl

Entry	25	26	27	28	29	30	31	32
Sample No.	227095	227034	227036	227037	227039	227041	227042	227043
Analyses in weight percent								
Na_2O	2.0	2.0	3.0	2.9	4.4	4.2	5.3	4.2
MgO	8.5	9.4	4.0	.8	5.8	4.5	3.0	.8
Al_2O_3	15.3	17.7	19.8	12.5	16.2	18.6	17.6	13.9
SiO_2	48.3	47.6	61.8	76.2	54.2	53.2	56.7	71.6
K_2O	.2	.1	3.1	2.2	.2	.2	.1	.2
CaO	13.7	6.7	2.2	2.4	3.9	7.0	5.7	3.2
TiO_2	1.2	2.6	.5	.1	1.7	1.2	1.2	.4
MnO	.2	.2	bdl	.1	.1	.2	.2	.1
FeO	10.5	12.6	4.9	2.1	11.3	9.6	9.1	4.0
P_2O_5	bdl	.3	bdl	bdl	.3	.3	.2	.1
Total	99.9	99.0	99.5	99.3	98.2	99.0	99.2	98.5
Analyses in parts per million								
Zn	110	170	94	78	160	110	110	88
Rb	88	9	35	25	bdl	7	9	12
Sr	510	340	200	190	140	100	230	120
Y	36	30	44	83	42	34	36	40
Zr	290	190	190	150	93	110	110	94
Nb	81	6	bdl	12	bdl	bdl	8	4
La	74	21	8	31	7	6	18	25
Nd	87	36	bdl	26	bdl	24	15	23
Ba	870	56	360	220	35	37	170	31
Ce	160	19	17	71	16	10	18	45

APPENDIX A3.–Major- and trace-element abundances in metabasalt and silicic metatuff--(Continued).

Entry	33	34	35	36	37	38	39	40
Sample No.	227044	227045	227047	227049	227050	227051	227052	227054
				Analyses in weight percent				
Na_2O	2.6	3.4	4.2	4.4	4.8	4.6	4.4	3.9
MgO	.6	bdl	.1	bdl	bdl	.4	.4	.1
Al_2O_3	12.5	12.0	13.5	12.2	14.1	14.2	12.4	12.2
SiO_2	75.6	76.5	72.5	76.9	71.9	71.4	73.9	76.1
K_2O	.7	2.5	.9	1.2	1.3	1.0	.7	.7
CaO	2.3	2.1	3.1	1.6	1.8	2.6	2.7	2.7
TiO_2	.2	.2	.2	.2	.2	.4	.4	.2
MnO	.2	bdl	.2	.1	.2	.3	.3	.2
FeO	2.3	2.6	3.7	2.6	3.7	4.5	3.9	3.3
P_2O_5	.1	.1	bdl	.1	.1	.1	.1	bdl
Total	97.0	99.5	98.3	99.3	98.3	99.6	99.3	99.4
				Analyses in parts per million				
Zn	87	88	140	110	130	140	140	120
Rb	14	34	17	20	26	19	15	18
Sr	100	120	160	140	160	130	140	130
Y	50	86	57	64	55	45	52	47
Zr	130	340	140	160	150	140	130	140
Nb	6	13	9	bdl	bdl	5	bdl	bdl
La	4	26	12	10	6	11	14	bdl
Nd	32	57	9	bdl	20	33	23	25
Ba	85	720	270	300	320	180	210	210
Ce	17	82	17	27	24	11	27	22

Entry	41	42	43
Sample No.	227055	227219	227224
		Analyses in weight percent	
Na_2O	4.3	4.9	5.3
MgO	.2	.5	.5
Al_2O_3	12.6	14.4	14.0
SiO_2	74.6	67.5	67.5
K_2O	.9	1.6	1.0
CaO	2.2	3.1	3.2
TiO_2	.3	.5	.6
MnO	.2	.1	.3
FeO	3.4	5.9	6.4
P_2O_5	.1	.1	.1
Total	98.7	98.8	99.0
		Analyses in parts per million	
Zn	110	140	130
Rb	18	31	21
Sr	100	180	280
Y	53	66	77
Zr	140	450	440
Nb	bdl	11	10
La	13	34	15
Nd	29	44	46
Ba	250	160	170
Ce	6	53	60

APPENDIX A4.--Major- and trace-element abundances in amphibolite in the Bi'r Tuluhah area.
[bdl, below detection limit; ---, not determined]

Entry	1	2	3	4	5	6	7	8
Sample No.	206500	206516	206518	206519	206527	206533	206536	206537
Analyses in weight percent								
Na_2O	3.4	3.9	5.4	3.8	2.8	2.9	3.8	2.8
MgO	7.7	7.9	.2	7.1	7.5	8.5	9.0	7.8
Al_2O_3	15.4	14.6	15.9	14.5	14.6	16.6	15.9	15.5
SiO_2	53.2	51.5	70.8	52.3	53.1	49.3	52.1	48.3
K_2O	.2	.4	3.7	.7	.4	.4	.3	.4
CaO	9.1	9.2	1.6	10.2	9.5	11.2	9.8	12.3
TiO_2	.7	.6	.5	.7	.7	1.1	.6	1.2
MnO	.2	.2	bdl	.2	.2	.2	.2	.3
FeO	10.2	10.6	1.6	9.8	10.5	10.0	9.0	10.6
P_2O_5	bdl	bdl	bdl	bdl	bdl	bdl	bdl	bdl
Total	100.0	98.9	99.8	99.3	99.3	100.3	100.7	99.2
Analyses in parts per million								
Zn	130	96	78	150	160	120	91	140
Rb	12	20	97	30	21	25	11	19
Sr	120	130	220	200	130	190	220	230
Y	25	25	26	22	24	29	18	30
Zr	59	47	280	47	45	73	53	86
Nb	5	7	10	bdl	4	6	bdl	9
La	bdl	bdl	bdl	bdl	bdl	bdl	bdl	bdl
Nd	bdl	bdl	bdl	bdl	bdl	bdl	bdl	bdl
Ba	bdl	bdl	bdl	bdl	bdl	bdl	bdl	bdl
Ce	bdl	bdl	bdl	bdl	bdl	bdl	bdl	bdl

Entry	9	10	11	12	13	14
Sample No.	206538	206541	206542	206611	206709	206724
Analyses in weight percent						
Na_2O	3.6	3.8	4.5	4.1	4.4	2.6
MgO	9.1	7.8	7.1	5.3	4.5	12.4
Al_2O_3	15.4	16.8	18.5	17.4	17.8	12.1
SiO_2	51.0	51.1	52.4	54.8	60.4	50.2
K_2O	bdl	.6	1.0	1.1	.9	.1
CaO	9.8	9.4	6.6	7.9	6.4	8.7
TiO_2	.8	1.3	1.0	1.2	.7	1.9
MnO	.3	.1	.2	.1	.1	.2
FeO	9.9	9.0	8.2	7.8	5.1	11.3
P_2O_5	bdl	bdl	bdl	.3	.3	.3
Total	100.0	99.9	99.4	100.0	100.8	99.8
Analyses in parts per million						
Zn	110	98	120	110	68	120
Rb	bdl	30	24	27	23	12
Sr	89	290	350	630	640	99
Y	22	26	28	24	14	25
Zr	52	90	96	120	120	140
Nb	6	10	5	8	7	21
La	bdl	bdl	bdl	bdl	bdl	bdl
Nd	bdl	bdl	bdl	bdl	bdl	bdl
Ba	bdl	bdl	bdl	bdl	bdl	bdl
Ce	bdl	bdl	bdl	bdl	bdl	bdl

APPENDIX A5.--Major- and trace-element abundances in diabase, gabbro, and plagiogranite dikes in serpentinite in the Bi'r Tuluhah area.
[bdl, below detection limit; ---, not determined]

Entry	1	2	3	4	5	6	7	8
Sample No.	206556	206569	206570	206571	206582	206583	206594	206624
Analyses in weight percent								
Na_2O	.3	.3	.6	4.4	4.4	3.6	6.8	3.3
MgO	3.0	4.2	8.2	5.3	4.6	9.4	2.4	7.9
Al_2O_3	25.1	16.7	17.1	17.8	18.8	18.4	19.2	18.3
SiO_2	40.5	47.7	46.4	54.9	57.7	48.5	57.3	49.1
K_2O	bdl	bdl	.1	1.0	.8	.6	.5	1.0
CaO	29.4	23.7	18.0	7.6	5.5	6.2	6.2	9.0
TiO_2	.5	.3	.4	1.3	1.0	2.1	.7	1.6
MnO	.1	.1	.2	.1	.2	.3	.2	.1
FeO	1.1	6.7	9.0	7.6	6.7	11.0	6.0	10.1
P_2O_5	bdl	bdl	bdl	.1	.1	7.8	.1	.2
Total	100.0	99.6	100.0	100.1	99.9	100.1	99.3	100.7
Analyses in parts per million								
Zn	17	66	87	120	120	120	120	100
Rb	9	11	8	19	20	15	19	25
Sr	140	58	20	500	380	410	560	550
Y	8	11	12	20	26	29	20	28
Zr	250	49	53	140	110	150	110	150
Nb	bdl	bdl	5	bdl	bdl	7	6	7
La	bdl	bdl	bdl	bdl	bdl	bdl	bdl	bdl
Nd	bdl	bdl	bdl	bdl	bdl	bdl	bdl	bdl
Ba	bdl	bdl	bdl	bdl	bdl	bdl	bdl	bdl
Ce	bdl	bdl	bdl	bdl	bdl	bdl	bdl	bdl

Entry	9	10	11	12	13	14	15	16
Sample No.	227105	227106	227107	227108	227109	227111	227112	227113
Analyses in weight percent								
Na_2O	4.2	5.9	6.8	6.8	7.6	3.1	bdl	3.9
MgO	8.2	8.5	.1	bdl	bdl	6.1	.8	10.4
Al_2O_3	16.2	15.9	14.9	14.6	14.9	18.6	24.9	15.2
SiO_2	50.9	55.6	73.1	74.1	72.7	46.8	44.5	50.2
K_2O	.2	.1	.2	.3	.2	.3	bdl	.2
CaO	10.8	7.0	2.5	1.8	1.8	11.0	27.7	9.2
TiO_2	1.1	.7	.3	.1	.2	.5	.2	1.1
MnO	.1	.1	bdl	.1	bdl	.2	bdl	.1
FeO	9.2	6.4	1.9	2.0	1.4	11.4	1.2	9.4
P_2O_5	.2	.1	.1	.1	.1	.1	.1	.2
Total	101.0	100.4	99.9	100.0	98.9	98.2	99.6	99.9
Analyses in parts per million								
Zn	92	75	39	53	24	76	45	120
Rb	bdl	bdl	8	8	10	bdl	bdl	bdl
Sr	340	600	210	220	200	520	42	410
Y	18	14	12	14	15	25	17	21
Zr	68	69	120	110	96	49	140	99
Nb	5	7	8	8	8	5	10	6
La	bdl	bdl	bdl	bdl	bdl	bdl	bdl	bdl
Nd	bdl	bdl	bdl	bdl	bdl	bdl	bdl	bdl
Ba	bdl	bdl	bdl	bdl	bdl	bdl	bdl	bdl
Ce	bdl	bdl	bdl	bdl	bdl	bdl	bdl	bdl

APPENDIX A5.--Major- and trace-element abundances in diabase, gabbro, and plagiogranite dikes--(Continued).

Entry	17	18	19	20	21	22	23
Sample No.	227114	227115	227116	227117	227119	227120	227123
				Analyses in weight percent			
Na_2O	3.8	4.7	5.7	3.6	4.2	4.1	6.2
MgO	6.3	7.8	7.8	5.1	7.3	5.7	4.5
Al_2O_3	16.3	15.2	15.2	18.5	16.3	13.9	16.8
SiO_2	48.2	51.9	55.7	52.9	53.0	47.3	53.8
K_2O	.6	.7	.4	.9	.7	.2	1.1
CaO	8.7	8.6	6.2	8.5	8.8	10.4	7.7
TiO_2	1.9	.9	.7	1.1	1.0	2.6	1.2
MnO	.1	.2	.1	bdl	.1	.2	.1
FeO	12.3	8.7	7.2	8.8	8.1	14.9	7.7
P_2O_5	.3	.2	.2	.1	.2	.4	.3
Total	98.5	98.8	99.3	99.5	99.7	99.8	99.5
				Analyses in parts per million			
Zn	130	89	70	120	97	150	92
Rb	16	14	10	16	bdl	8	21
Sr	530	760	550	660	390	290	590
Y	35	26	19	19	20	52	23
Zr	150	79	80	68	84	170	150
Nb	7	5	7	7	6	9	8
La	bdl	bdl	bdl	bdl	bdl	bdl	12
Nd	bdl	bdl	bdl	bdl	bdl	bdl	43
Ba	bdl	bdl	bdl	bdl	bdl	bdl	270
Ce	bdl	bdl	bdl	bdl	bdl	bdl	25

APPENDIX A6.--Major- and trace-element abundances in fine-grained diorite in the Bi'r Tuluhah area. [bdl, below detection limit; --- not determined]

Entry	1	2	3	4	5	6	7	8
Sample No.	206528	206544	206545	206565	206567	206568	206597	206610
				Analyses in weight percent				
Na_2O	3.0	3.8	3.1	4.1	5.2	bdl	4.8	3.5
MgO	8.1	9.2	5.9	3.5	5.6	bdl	8.4	8.5
Al_2O_3	15.9	14.7	13.5	16.0	15.4	bdl	13.5	15.7
SiO_2	49.5	54.8	59.2	63.6	59.2	bdl	57.0	53.9
K_2O	.5	.8	.4	1.0	bdl	bdl	.1	.8
CaO	11.4	7.8	7.9	5.3	6.1	bdl	8.8	7.7
TiO_2	1.2	1.0	.8	.6	.4	bdl	.3	.8
MnO	.1	.1	.1	.1	.2	bdl	.1	.2
FeO	9.9	7.2	8.7	4.9	7.6	bdl	7.5	8.6
P_2O_5	bdl	bdl	bdl	bdl	bdl	bdl	bdl	bdl
Total	99.6	99.4	99.7	99.2	99.7	bdl	100.5	99.7
				Analyses in parts per million				
Zn	91	91	110	120	68	110	110	140
Rb	18	25	19	15	10	20	12	12
Sr	260	450	240	490	38	540	33	520
Y	31	18	18	15	18	24	13	22
Zr	83	93	92	140	51	150	48	77
Nb	5	5	5	7	5	7	5	7
La	bdl	bdl	bdl	bdl	bdl	bdl	bdl	bdl
Nd	bdl	bdl	bdl	bdl	bdl	bdl	bdl	bdl
Ba	bdl	bdl	bdl	bdl	bdl	bdl	bdl	bdl
Ce	bdl	bdl	bdl	bdl	bdl	bdl	bdl	bdl

Entry	9	10	11	12	13	14	15
Sample No.	206818	227125	227127	227128	227129	227130	227151
				Analyses in weight percent			
Na_2O	4.2	6.2	5.8	4.3	4.0	4.3	5.1
MgO	8.8	4.6	8.0	8.5	8.5	3.8	6.3
Al_2O_3	13.0	16.2	14.4	13.7	16.0	18.0	17.9
SiO_2	57.7	58.6	57.1	57.0	52.1	56.6	52.0
K_2O	.4	.1	.1	bdl	.2	.9	.3
CaO	9.1	5.0	7.3	8.4	8.6	7.5	8.0
TiO_2	.1	.6	.3	.2	.6	1.1	.9
MnO	.1	.1	.1	.1	.1	.1	.2
FeO	4.9	8.2	7.2	7.5	8.7	7.1	9.0
P_2O_5	.1	.1	.1	bdl	.1	.3	.2
Total	98.2	99.8	100.4	99.5	98.9	99.7	99.9
				Analyses in parts per million			
Zn	78	110	54	83	87	95	74
Rb	8	bdl	bdl	8	bdl	17	15
Sr	96	82	140	56	280	410	480
Y	6	18	12	11	17	27	20
Zr	32	59	45	44	56	170	77
Nb	bdl	bdl	6	4	4	5	6
La	bdl	2	1	bdl	2	25	3
Nd	bdl	9	38	8	bdl	53	19
Ba	bdl	49	76	22	29	160	170
Ce	bdl	14	2	bdl	1	29	17

APPENDIX A6.--Major- and trace-element abundances in fine-grained diorite--(Continued).

Entry	16
Sample No.	227163
	Analyses in weight percent
Na_2O	3.0
MgO	7.4
Al_2O_3	15.9
SiO_2	54.2
K_2O	.5
CaO	9.4
TiO_2	.9
CR_2O_3	bdl
MnO	.2
FeO	7.8
P_2O_5	.1
Total	99.5
	Analyses in parts per million
Zn	83
Rb	14
Sr	350
Y	17
Zr	91
Nb	bdl
La	4
Nd	41
Ba	310
Ce	27

APPENDIX A7.—Major- and trace-element abundances in the Hulayfah-group volcanic rocks in the Bi'r Tuluhah area determined in this study.
[bdl, below detection limit; ---, not determined]

Entry	1	2	3	4	5	6	7	8
Sample No.	206546	206567	206601	206602	206603	206605	206839	227003
Analyses in weight percent								
Na_2O	4.2	5.2	3.3	4.0	2.7	4.0	2.8	2.6
MgO	6.6	5.6	10.0	4.9	4.8	8.5	4.5	10.6
Al_2O_3	17.9	15.4	14.2	16.8	15.1	16.9	15.8	12.2
SiO_2	53.8	59.2	54.5	58.5	55.8	51.9	57.6	54.6
K_2O	.8	bdl	.3	1.1	1.1	.9	.4	.1
CaO	6.9	6.1	8.9	6.7	8.2	8.5	9.3	13.0
TiO_2	.9	.4	1.1	1.0	1.4	1.5	.8	.7
MnO	.3	.2	.1	.1	.1	.1	.1	.1
FeO	8.4	7.6	7.7	6.6	10.3	7.3	6.6	6.6
P_2O_5	bdl	bdl	.1	.3	.1	bdl	.1	.1
Total	99.8	99.7	100.1	99.8	99.7	99.6	97.9	100.8
Analyses in parts per million								
Zn	120	68	86	130	69	110	92	52
Rb	23	10	10	24	40	24	17	bdl
Sr	380	38	330	390	210	350	410	600
Y	25	18	21	18	35	31	24	24
Zr	84	51	110	130	130	170	62	93
Nb	bdl	5	5	bdl	6	6	6	7
La	bdl	bdl	bdl	bdl	bdl	bdl	bdl	13
Nd	bdl	bdl	bdl	bdl	bdl	bdl	bdl	22
Ba	bdl	bdl	bdl	bdl	bdl	bdl	bdl	76
Ce	bdl	bdl	bdl	bdl	bdl	bdl	bdl	bdl

Entry	9	10	11	12	13	14	15	16
Sample No.	227006	227008	227009	227010	227011	227012	227013	227014
Analyses in weight percent								
Na_2O	3.0	3.9	3.9	4.5	3.9	5.4	4.1	5.8
MgO	12.4	1.9	4.5	1.9	5.4	2.9	2.8	5.8
Al_2O_3	13.2	18.2	16.6	15.8	15.9	14.8	14.2	16.1
SiO_2	55.1	60.6	53.4	59.7	52.7	60.4	60.8	55.4
K_2O	.4	2.0	.4	2.5	.4	.8	2.1	1.0
CaO	12.4	7.1	10.7	5.9	8.7	5.7	5.7	7.5
TiO_2	.5	.5	1.3	1.5	1.8	1.4	1.5	.8
MnO	bdl	bdl	.2	.1	.1	.1	.1	.1
FeO	4.1	4.9	8.6	7.0	9.8	7.5	8.1	7.4
P_2O_5	.1	.1	.2	.5	.4	.4	.3	.1
Total	101.2	99.2	99.7	99.3	99.2	99.5	99.6	99.8
Analyses in parts per million								
Zn	120	66	75	84	130	130	71	90
Rb	14	26	15	41	19	22	49	26
Sr	590	520	500	330	300	280	260	470
Y	16	15	35	55	49	61	61	26
Zr	68	98	210	380	220	320	310	100
Nb	bdl	bdl	bdl	11	bdl	8	12	5
La	bdl	6	36	48	25	37	39	5
Nd	15	bdl	bdl	42	19	39	52	bdl
Ba	110	500	23	470	200	220	340	200
Ce	20	10	37	81	10	82	71	30

APPENDIX A7.--Major- and trace-element abundances in the Hulayfah-group volcanic rocks--(Continued).

Entry	17	18	19	20	21	22	23	24
Sample No.	227015	227016	227017	227018	227019	227021	227022	227023
				Analyses in weight percent				
Na_2O	2.9	3.7	3.3	2.3	2.9	3.1	1.8	1.7
MgO	5.3	9.8	8.3	8.9	6.8	5.4	9.9	10.6
Al_2O_3	18.6	13.9	15.0	14.8	15.6	15.8	13.1	11.9
SiO_2	53.6	51.7	53.0	52.7	54.5	53.3	53.3	54.3
K_2O	.2	.4	.2	.3	.2	2.1	.6	.2
CaO	9.7	10.5	10.0	10.3	8.9	9.7	9.9	9.7
TiO_2	.8	.7	.9	.8	.6	1.2	.6	.5
MnO	.1	.2	.2	.1	.1	.1	.2	.2
FeO	8.4	9.0	8.9	8.8	8.4	7.5	9.0	9.7
P_2O_5	.1	.1	.1	.1	.1	.2	.1	.1
Total	99.7	100.0	99.8	99.0	98.2	98.4	98.3	98.9
				Analyses in parts per million				
Zn	91	57	110	88	91	100	140	99
Rb	8	18	10	10	12	43	22	9
Sr	220	260	190	140	160	590	110	110
Y	21	16	22	23	19	30	17	15
Zr	68	60	67	92	72	120	53	53
Nb	bdl	5	6	bdl	6	6	bdl	bdl
La	2	12	bdl	20	bdl	25	bdl	11
Nd	21	23	bdl	20	47	26	bdl	10
Ba	76	110	97	150	65	320	41	62
Ce	11	15	20	bdl	6	17	10	11

Entry	25	26	27	28	29	30	31	32
Sample No.	227024	227025	227027	227028	227029	227030	227177	227180
				Analyses in weight percent				
Na_2O	4.0	2.0	4.0	3.2	4.1	6.2	3.4	6.0
MgO	7.4	9.2	1.9	2.4	9.2	6.2	9.5	3.0
Al_2O_3	15.1	14.6	16.6	16.7	11.9	16.2	16.3	20.9
SiO_2	55.4	53.5	61.8	58.2	53.4	54.6	50.5	59.8
K_2O	.3	.4	.3	.9	.4	.5	.4	.9
CaO	7.9	9.9	6.5	7.6	11.3	6.9	9.0	4.5
TiO_2	.6	.7	.7	.9	.5	.7	1.4	.6
MnO	.2	.2	.1	.1	.2	.2	.1	bdl
FeO	7.8	8.8	6.3	7.8	8.9	8.5	8.3	3.4
P_2O_5	.1	bdl	bdl	.2	bdl	bdl	.3	.2
Total	98.7	99.2	98.3	98.0	99.9	99.9	99.3	99.3
				Analyses in parts per million				
Zn	41	110	67	80	120	92	68	70
Rb	12	20	11	20	15	15	13	17
Sr	180	130	270	160	150	450	370	890
Y	23	20	34	39	18	18	25	9
Zr	64	68	96	140	46	56	120	76
Nb	6	5	bdl	10	bdl	5	bdl	5
La	2	18	11	26	9	bdl	3	3
Nd	36	7	27	13	1	bdl	43	bdl
Ba	120	73	230	190	120	140	210	210
Ce	13	3	16	42	6	7	bdl	20

APPENDIX A7.--Major- and trace-element abundances in the Hulayfah-group volcanic rocks--(Continued).

Entry	33	34	35	36	37
Sample No.	227183	227184	227185	227195	227199
			Analyses in weight percent		
Na_2O	5.5	4.9	3.7	5.9	4.3
MgO	3.2	3.6	2.4	1.3	10.6
Al_2O_3	18.5	18.6	19.3	18.0	14.2
SiO_2	61.1	57.7	57.8	64.9	50.1
K_2O	.6	1.6	.8	.9	.4
CaO	5.1	4.4	8.0	4.9	11.1
TiO_2	.6	.8	.7	.5	1.2
MnO	.1	.1	.2	.1	.1
FeO	5.2	7.3	6.3	3.3	8.2
P_2O_5	.1	.2	.2	.1	bdl
Total	100.1	99.2	99.5	100.2	100.2
			Analyses in parts per million		
Zn	43	90	110	45	70
Rb	15	36	15	13	16
Sr	410	500	460	740	480
Y	10	19	18	12	19
Zr	90	110	110	78	110
Nb	5	bdl	4	bdl	6
La	11	19	6	11	10
Nd	10	32	7	7	bdl
Ba	220	360	290	240	190
Ce	23	47	23	30	5

APPENDIX A8.--Major- and trace-element abundances in the Hulayfah-group volcanic rocks in the Bi'r Tuluhah area reported by Kattan (1983)
[bdl, below detection limit; ---, not determined]

Entry	1	2	3	4	5	6	7	8
Sample No.	33043	33039	33040	33044	33042	33035	33045	33062
Analyses in weight percent								
SiO_2	52.2	52.2	52.8	54.2	56.8	57.7	57.8	51.6
TiO_2	1.4	1.1	1.7	1.6	1.4	1.1	1.2	1.6
Al_2O_3	18.4	16.8	17.9	18.7	16.1	14.7	16.2	16.9
Fe_2O_3	9.1	9.3	11.3	7.8	8.6	8.9	8.0	10.8
MnO	.1	.2	.1	.1	.1	.2	.1	.1
MgO	4.8	7.0	6.4	3.9	4.9	5.3	4.4	5.9
CaO	9.1	9.6	3.2	6.1	6.8	6.9	6.6	6.8
Na_2O	3.8	2.9	4.3	5.1	3.7	3.3	4.0	4.7
K_2O	.8	.6	1.9	2.1	1.2	1.4	1.5	1.5
P_2O_5	.2	.2	.3	.3	.3	.3	.3	.2
Total	100.0	100.0	100.0	100.0	100.0	99.9	100.0	100.0
Analyses in parts per million								
Nb	2	1	4	6	5	6	3	4
Y	27	23	37	30	40	42	38	36
Sr	407	468	398	493	441	282	427	302
Rb	13	4	42	23	20	34	21	31
Zr	147	89	167	190	255	242	217	166
Th	4	5	4	1	bdl	6	1	bdl

Entry	9	10	11	12	13	14	15	16
Sample No.	33059	33064	33061	33056	33054	33067	33060	33047
Analyses in weight percent								
SiO_2	51.7	52.0	52.1	56.6	57.4	57.8	60.3	51.5
TiO_2	1.0	1.7	1.2	1.2	1.2	1.0	1.7	1.2
Al_2O_3	15.0	14.6	17.8	14.9	16.4	15.4	15.0	15.8
Fe_2O_3	7.6	10.6	9.4	10.1	7.6	7.8	9.9	9.9
MnO	.1	.1	.1	.2	.1	.1	.2	.2
MgO	13.2	7.6	6.1	5.2	4.9	6.2	2.6	7.5
CaO	8.3	9.2	9.5	7.9	7.5	8.9	4.3	10.5
Na_2O	2.6	2.9	3.3	3.3	3.6	3.8	4.5	3.0
K_2O	.4	.9	.3	.4	1.0	1.0	1.1	.3
P_2O_5	.2	.4	.2	.2	.3	.2	.5	.2
Total	100.0	100.0	100.0	100.0	100.0	102.0	100.0	100.0
Analyses in parts per million								
Nb	bdl	7	bdl	1	2	1	5	1
Y	20	39	28	37	38	32	57	28
Sr	325	457	321	280	430	209	322	253
Rb	2	10	2	2	9	16	17	bdl
Zr	95	216	108	115	238	120	284	103
Th	1	5	4	bdl	bdl	bdl	2	bdl

APPENDIX A8--Major- and trace-element abundances in the Hulayfah-group volcanic rocks--(Continued).

Entry	17	18	19	20
Sample No.	33051	33003	33006	33005
			Analyses in weight percent	
SiO_2	51.9	53.1	56.7	57.4
TiO_2	1.2	1.1	.9	1.5
Al_2O_3	16.4	17.1	16.4	15.8
Fe_2O_3	8.5	8.8	7.8	8.4
MnO	.2	.1	.1	.1
MgO	9.4	6.3	6.0	4.3
CaO	8.2	9.5	8.8	7.5
Na_2O	3.3	3.5	3.0	3.7
K_2O	.8	.3	.3	1.0
P_2O_5	.2	.2	.2	.3
Total	100.0	100.0	100.0	100.0
			Analyses in parts per million	
Nb	1	1	1	8
Y	24	27	25	44
Sr	275	307	278	359
Rb	10	1	2	22
Zr	112	95	93	298
Th	bdl	1	2	1